Contents

List of Figures

Abstract

We will discuss a simple procedure to construct an arbitrarily close piecewise linear approximation of a circle and, in the limit, the circle itself. Beginning with a square, the inscribed circle may be better approximated by replacing each vertex of the square with a line tangent to the circle forming an octagon. By repeatedly applying this algorithm to the resulting figures, closer approximations may be obtained. First, we will adapt this procedure to Chaikin's algorithm, modifying it to produce rational curves in $\mathbb{R}^2$. Next, extending this method to $\mathbb{R}^3$, we will consider a cube to be a piecewise planar approximation of its inscribed sphere. Better approximations will be obtained by bevel-cutting each edge of the cube with a plane tangent to the sphere. In the limit, this process will yield the sphere itself.

Chapter 1

Introduction

In Computer Aided Geometric Design (CAGD) the representation of general shapes is a fundamental problem. Parametric B-spline surfaces, including Bézier patches, are often used by design systems to model free-form shapes. Two of the most commonly used regular shapes are the ellipsoid and the special case sphere. We would like representations of these to be easily defined, quickly generated, and mathematically accurate. Polynomial B-splines do not lend themselves to accurate representations of ellipsoids and spheres; we must resort to non-uniform rational B-splines (NURBS). Suppose we wanted to model a hemisphere. A straightforward method is to create a geodesic arc from the pole to the equator using a rational B-spline. Then form the surface by revolving this around the pole. This creates a bi-quadratic B-spline surface. However, the surface is degenerate since one of its edges collapses to a single point at the pole. There are many reasons we may want to calculate the surface normals of the hemisphere, including shading during rendering, but it is very difficult to calculate the normal at this degenerate pole. There are other tiling schemes [3] and we may resort to rational triangular Bézier patches. However, a rational quadratic Bézier patch is inadequate; we must use a rational quartic patch [8].

With the speed and memory of our current generation of graphics workstations, an old paradigm is regaining popularity – the surface based upon a mesh of control points with an arbitrary topology. These geometric methods, commonly called *corner-cutting*, *whittling*, or *woodcarvers* algorithms [4], are extensions of the NURBS techniques to an arbitrary mesh of control points. This arbitrary mesh, extended from the rectangular mesh of NURBS, allows great flexibility in the model's definition, and the simple geometric algorithm insulates the

user from the mathematical details. The current methods, initially developed by Doo and Sabin [5] [6] and Catmull and Clark [1] are based upon the subdivision rules for quadratic and cubic uniform B-spline surfaces respectively. The formulation allows us to specify an arbitrary underlying topology for a mesh structure and specifies a procedure so that the mesh can be successively refined to represent a closer and closer approximation to the surface. These surfaces, which have been shown to be tangent-plane continuous, can be modified by alternate subdivision masks [10] to represent surfaces with edges, darts, and cusps, giving a tremendous variety of surfaces possible.

We wish to add to these methods by specifying a method that works on a decidedly different geometrical paradigm, edge-cutting. We propose not to cut the corners but to bevel the edges to produce our surface. In this paper we develop a method to obtain piecewise planar approximations of ellipsoids and spheres by cutting the edges from rectangular prisms and cubes, respectively, and repeatedly applying the method to the results.

Chapter 2

Background

There is a common method used by sailboat builders to create a cylindrical wooden mast from a rectangular column. On a full-sized drawing of the column's cross-section, the desired cross-section of the finished mast is drawn (Figure 2.1).

Then, tangent lines to the finished shape are drawn so that the column's corners are removed. Using these tangent lines as a reference, marking gauges are constructed and used to transfer the reference lines to the faces of the column. Then the edges are removed by either sawing or planing to these reference lines, creating a new face for each of the original edges. This process is repeated on the new edges until the column is smooth enough for final sanding. The resulting mast may be circular if the original column is square. Any other oval shape may also be produced. From the two-dimensional drawings this corner-cutting method has been extruded to the three dimensions of the wooden column.

2.1 Chaikin's Algorithm

In 1974 G. M. Chaikin [2] presented his algorithm for generating curves from data points. Given a curve represented by the control points $\mathbf{P}_0$, $\mathbf{P}_1$, $\mathbf{P}_2$, and $\mathbf{P}_3$, this method generates a curve that is tangent to the lines $\overline{\mathbf{P}_1\mathbf{P}_2}$, and $\overline{\mathbf{P}_2\mathbf{P}_3}$ at the mid-point of each (Figure 2.2).

The curve is generated by dividing each line into three parts so that the ratio of the parts is $1 : 2 : 1$. Then, the corners are removed by connecting the new points adjacent to each corner. This process may be applied repeatedly until the desired smoothness is achieved. In the limit, the resulting curve will be made up of parabolic segments and is a

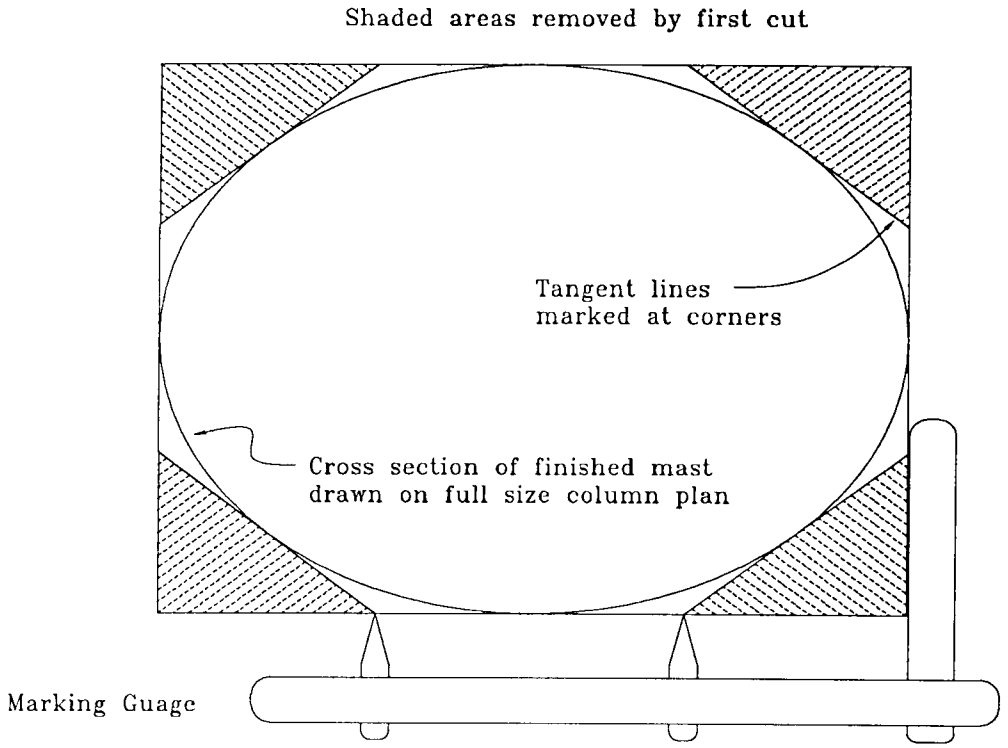

Figure 2.1: Cross-section of Wooden Mast

uniform quadratic B-spline.

2.2 Doo's Algorithm

A method to extend Chaikin's algorithm to three dimensions was presented by D. W. H. Doo [5] in 1978. Given a polyhedron composed of vertices and faces, new smaller faces are formed that result in a smoother polyhedron (Figure 2.3). In this method, the *centroid* of each face is found. New vertices are obtained by combining the centroid of a face with each vertex of that face using a weighting function. Given an n-sided polygonal face with vertices $\mathbf{P}_0, ..., \mathbf{P}_{n-1}$, the centroid, $\mathbf{C}$, is:

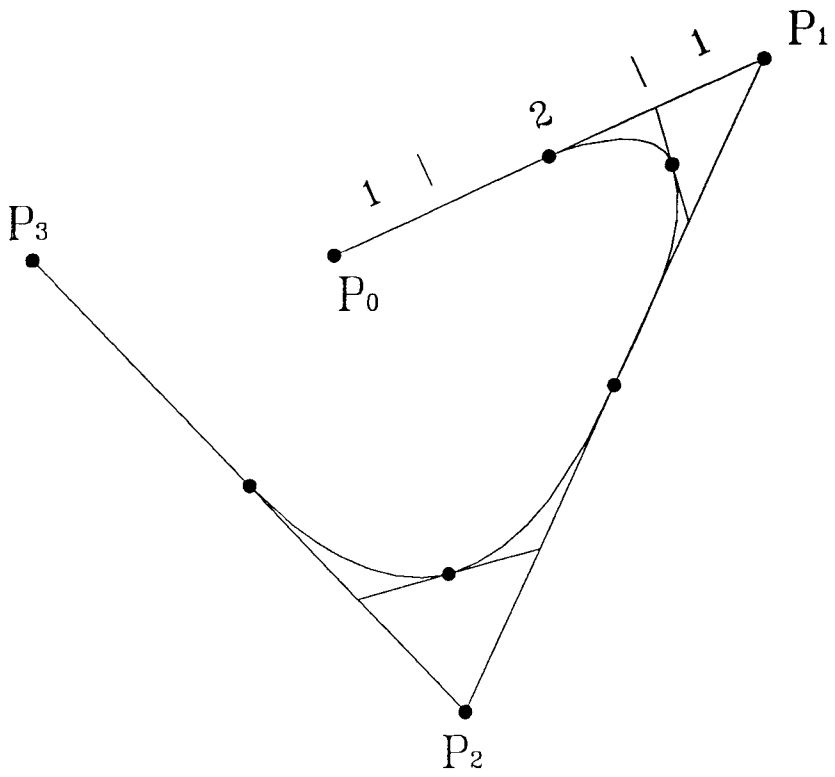

Figure 2.2: Chaikin's Algorithm

$$\mathbf{C} = \frac{1}{n} \sum_{i=0}^{n-1} \mathbf{P}_i$$

Each valence n vertex is replaced by n new points called *face points* . A new face point, $\mathbf{P}_r^{k+1}$, from a vertex, $\mathbf{P}_r^k$, is:[1]

$$\mathbf{P}_r^{k+1} = t\mathbf{P}_r^k + (1-t)\,\mathbf{C}_s^k$$

with the usual value for $t = \frac{1}{2}$. This results in three types of new faces:

[1] We will denote the *level* of refinement by the superscript k. The original control polygon or polyhedron is at level $k = 0$. After one refinement it is at level $k = 1$.

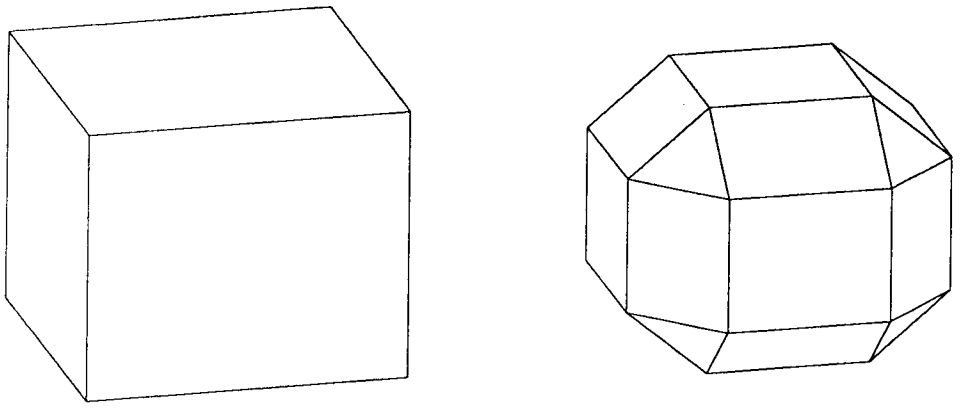

Figure 2.3: Doo's Algorithm Applied to a Cube

- Type **F** (formed by face): a new smaller face that replaces one of the original faces. This type of face will have the same number of edges as the original and will be smaller than the original.
- Type **V** (formed by vertex): A face that replaces each original vertex. These faces will have the same number of edges as the valence of the original vertex.
- Type **E** (formed by edge): A face that replaces an edge between two original faces. These will have four edges.

Using this method, new polyhedra are produced that are composed of all three types of faces. For each n-sided face a new, smaller n-sided face is produced. These faces always remain n-sided and gradually get smaller, converging to the centroid. Each vertex of valence m produces a new m-sided face that becomes a smaller m-sided face of Type **F**. Each edge between faces is replaced by a four-sided face that becomes a four-sided Type **F** face as it is processed. Doo demonstrated the resulting objects that are obtained when this method is applied to a cube using various weighting functions to define new vertex points.

2.3 Review of Conics as Rational Quadratic Curves

A fundamental result in CAGD is that conic sections can be written as rational quadratic curves. In this section we review much of this material, writing the conic section in *standard form* as a rational quadratic Bézier curve.[2] Although there are many different ways to define *conic sections*, we will define them as follows: a *conic section* in $\mathbb{R}^2$ is the perspective projection of a parabola in $\mathbb{R}^3$ onto a plane. Considering rotations and translations, this plane is usually considered to be the plane $w = 1$, and points on the parabola of the form $\begin{bmatrix} wx \\ wy \\ w \end{bmatrix}$ are usually associated with (projected to) the point $\begin{bmatrix} x \\ y \\ 1 \end{bmatrix}$ in the plane $w = 1$.

Suppose we are given a conic, $\mathbf{C}(t)$. Let $\mathbf{P}(t)$ be a corresponding parabola that projects to $\mathbf{C}(t)$. Since $\mathbf{P}(t)$ is a parabola, we can write it in Bézier form as

$$\mathbf{P}(t) = \mathbf{P}_0 B_{0,2}(t) + \mathbf{P}_1 B_{1,2}(t) + \mathbf{P}_2 B_{2,2}(t)$$

where $\mathbf{P}_i = \begin{bmatrix} x_i \\ y_i \\ w_i \end{bmatrix}$ are points in $\mathbb{R}^3$, and the $B_{i,2}$ are the quadratic Bernstein polynomials.

We can write $\mathbf{C}(t)$ as

$$\mathbf{C}(t) = \begin{bmatrix} x_c(t) \\ y_c(t) \\ 1 \end{bmatrix}$$

Clearly then, the parabola can be written as

$$\mathbf{P}(t) = \begin{bmatrix} w(t)x_c(t) \\ w(t)y_c(t) \\ w(t) \end{bmatrix}$$

where $w(t) = w_0 B_{0,2}(t) + w_1 B_{1,2}(t) + w_2 B_{2,2}(t)$, as this projects to $\mathbf{C}(t)$. Now, we can write

$$\sum_{i=0}^{2} \mathbf{P}_i B_{i,2}(t) = \begin{bmatrix} w(t)x_c(t) \\ w(t)y_c(t) \\ w(t) \end{bmatrix}$$

[2] Most of this section was adapted from pages 233-237 of [8].

$$= \begin{bmatrix} x_c(t)\left[\sum_{i=0}^{2} w_i B_{i,2}(t)\right] \\ y_c(t)\left[\sum_{i=0}^{2} w_i B_{i,2}(t)\right] \\ \left[\sum_{i=0}^{2} w_i B_{i,2}(t)\right] \end{bmatrix}$$

$$= \left[\sum_{i=0}^{2} w_i B_{i,2}(t)\right] \begin{bmatrix} x_c(t) \\ y_c(t) \\ 1 \end{bmatrix}$$

and, therefore, we can write the conic section as

$$\mathbf{C}(t) = \frac{\mathbf{P}_0 B_{0,2}(t) + \mathbf{P}_1 B_{1,2}(t) + \mathbf{P}_2 B_{2,2}(t)}{w_0 B_{0,2}(t) + w_1 B_{1,2}(t) + w_2 B_{2,2}(t)}$$

and if we set

$$\mathbf{p}_i = \begin{bmatrix} \frac{x_i}{w_i} \\ \frac{y_i}{w_i} \\ 1 \end{bmatrix}$$

then

$$\mathbf{C}(t) = \frac{w_0 \mathbf{p}_0 B_{0,2}(t) + w_1 \mathbf{p}_1 B_{1,2}(t) + w_2 \mathbf{p}_2 B_{2,2}(t)}{w_0 B_{0,2}(t) + w_1 B_{1,2}(t) + w_2 B_{2,2}(t)}$$

We call the points $\mathbf{p}_i$ the *control points* of the conic and the numbers w_i the ***weights*** of the corresponding vertices. Thus, the conic control polygon is the projection of the control polygon

$$\begin{bmatrix} x_i \\ y_i \\ w_i \end{bmatrix}$$

which is the control polygon of the 3d parabola, $\mathbf{P}$, that we projected into $\mathbf{C}$.

This form is called the *rational quadratic form* of a conic section. If all weights are equal, we obtain the non-rational conics (i.e., parabolas).

A Circle as a Rational Quadratic Bézier Curve

Consider the parametric equation

$$\begin{aligned} x(t) &= \tfrac{1-t^2}{1+t^2} \\ y(t) &= \tfrac{2t}{1+t^2} \end{aligned}$$

for $0 \leq t \leq 1$. We can show that this equation forms a quarter circle by calculating

$$\begin{aligned} x^2 + y^2 &= \left(\frac{1-t^2}{1+t^2}\right)^2 + \left(\frac{2t}{1+t^2}\right)^2 \\ &= \frac{1 - 2t^2 + t^4 + 4t^2}{(1+t^2)^2} \\ &= \frac{1 + 2t^2 + t^4}{(1+t^2)^2} \\ &= 1 \end{aligned}$$

Thus all points of the curve lie on the unit circle, and as t ranges between 0 and 1, the quarter circle in the first quadrant is traced.

This implies that the rational quadratic Bézier curve given by

$$\begin{aligned} \begin{bmatrix} 1B_{0,2}(t) + 1B_{1,2}(t) + 0B_{2,2}(t) \\ 0B_{0,2}(t) + 1B_{1,2}(t) + 2B_{2,2}(t) \\ 1B_{0,2}(t) + 1B_{1,2}(t) + 2B_{2,2}(t) \end{bmatrix} &= \begin{bmatrix} (1-t)^2 + 2(1-t)t + 0 \\ 0 + 2(1-t)t + 2t^2 \\ (1-t)^2 + 2(1-t)t + 2t^2 \end{bmatrix} \\ &= \begin{bmatrix} 1 - 2t + t^2 + 2t - 2t^2 \\ 2t - 2t^2 + 2t^2 \\ 1 - 2t + t^2 + 2t - 2t^2 + 2t^2 \end{bmatrix} \\ &= \begin{bmatrix} 1 - t^2 \\ 2t \\ 1 + t^2 \end{bmatrix} \end{aligned}$$

is a circle. The three control points that define this rational Bézier curve are

$$(\mathbf{P}_0, \mathbf{P}_1, \mathbf{P}_2) = \begin{bmatrix} 1 \\ 0 \\ 1 \end{bmatrix} \begin{bmatrix} 1 \\ 1 \\ 1 \end{bmatrix} \begin{bmatrix} 0 \\ 2 \\ 2 \end{bmatrix}$$

This translates into the projected control points

$$\begin{bmatrix} 1 \\ 0 \\ 1 \end{bmatrix} \begin{bmatrix} 1 \\ 1 \\ 1 \end{bmatrix} \begin{bmatrix} 0 \\ 1 \\ 1 \end{bmatrix}$$

with $w_0 = 1$, $w_1 = 1$ $w_2 = 2$.

Reparameterizing the Curve into Standard Form

We can put this circle into an alternate form, called *standard form*, with $w_0 = w_2 = 1$. To do this, we make a parameter change[3] replacing t by

$$\frac{\hat{t}}{\rho(1-\hat{t})+\hat{t}}$$

and $(1-t)$ by

$$\frac{\rho(1-\hat{t})}{\rho(1-\hat{t})+\hat{t}}$$

Simplifying the equation of the conic after this reparameterization, we obtain

$$\mathbf{C}(\hat{t}) = \frac{\rho^2 w_0 \mathbf{p}_0 B_{0,2}(\hat{t}) + \rho w_1 \mathbf{p}_1 B_{1,2}(\hat{t}) + w_2 \mathbf{p}_2 B_{2,2}(\hat{t})}{\rho^2 w_0 B_{0,2}(\hat{t}) + \rho w_1 B_{1,2}(\hat{t}) + w_2 B_{2,2}(\hat{t})}$$

where the $\mathbf{p}_i$ are the projected control points of the rational quadratic above. If

$$\rho = \sqrt{\frac{w_2}{w_0}}$$

then the equation of the circle can be rewritten as

$$\mathbf{C}(\hat{t}) = \frac{w_2 \mathbf{p}_0 B_{0,2}(\hat{t}) + \sqrt{\frac{w_2}{w_0}} w_1 \mathbf{p}_1 B_{1,2}(\hat{t}) + w_2 \mathbf{p}_2 B_{2,2}(\hat{t})}{w_2 B_{0,2}(\hat{t}) + \sqrt{\frac{w_2}{w_0}} w_1 B_{1,2}(\hat{t}) + w_2 B_{2,2}(\hat{t})}$$

In our case, $\rho = \sqrt{2}$, $w_0 = w_1 = 1$, and $w_2 = 2$, and we obtain

$$\mathbf{C}(t) = \frac{2\mathbf{p}_0 B_{0,2}(\hat{t}) + \sqrt{2}\mathbf{p}_1 B_{1,2}(\hat{t}) + 2\mathbf{p}_2 B_{2,2}(\hat{t})}{2B_{0,2}(\hat{t}) + \sqrt{2}B_{1,2}(\hat{t}) + 2B_{2,2}(\hat{t})}$$

After dividing all the weights by 2 (which divides both numerator and denominator by 2 and makes no change in the curve), we obtain

$$\mathbf{C}(t) = \frac{\mathbf{p}_0 B_{0,2}(t) + \frac{\sqrt{2}}{2}\mathbf{p}_1 B_{1,2}(t) + \mathbf{p}_2 B_{2,2}(t)}{B_{0,2}(t) + \frac{\sqrt{2}}{2} B_{1,2}(t) + B_{2,2}(t)}$$

which is in standard form.

Therefore, we can write our quarter circle as a rational quadratic curve with projected control points

$$\begin{bmatrix} 1 \\ 0 \\ 1 \end{bmatrix} \begin{bmatrix} \frac{\sqrt{2}}{2} \\ \frac{\sqrt{2}}{2} \\ \frac{\sqrt{2}}{2} \end{bmatrix} \begin{bmatrix} 0 \\ 1 \\ 1 \end{bmatrix}$$

[3] See Farin [8], page 236.

Chapter 3

Two Dimensions

3.1 Constructing a Circle from a Square

We will present a method to construct a sphere by refining a cube. To lay a foundation for this we will examine the two-dimensional case. This will give us insight into the three-dimensional case. The procedure we will use is a generalization of a simple algorithm that creates a circle from a square by first cutting off the corners of the square and successively cutting the corners of the resulting objects. This algorithm can be easily defined if we start with a basic square of side length 2 shown in Figure 3.1. We inscribe a circle in the square, which will have radius 1.

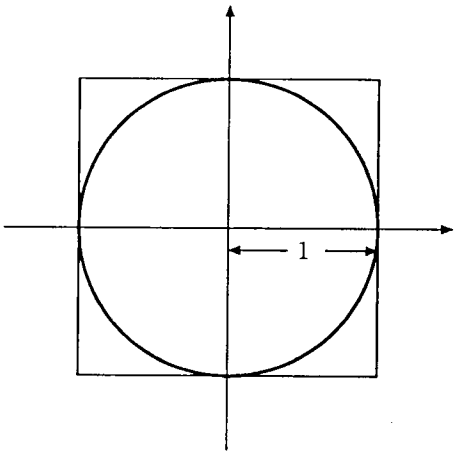

Figure 3.1: Circle Inscribed in a Square

This square has four sides, each of which is tangent to the circle, and each has its midpoint on the circle. Our refinement procedure will iteratively produce polygons that have a similar structure: after the kth iteration the polygon will have 2^{k+2} sides, each of which has its midpoint on the circle. We can illustrate this procedure by showing the results of successive applications of the refinement. We begin by cutting off the four corners of the square.

Consider an arc of the circle between two consecutive points where the square and circle coincide. We construct the tangent line to this arc at the midpoint of the arc. Using this tangent line as a cutting plane, we can cut off the corner and construct a new polygonal shape where the corner of the square has been removed (Figure 3.2).

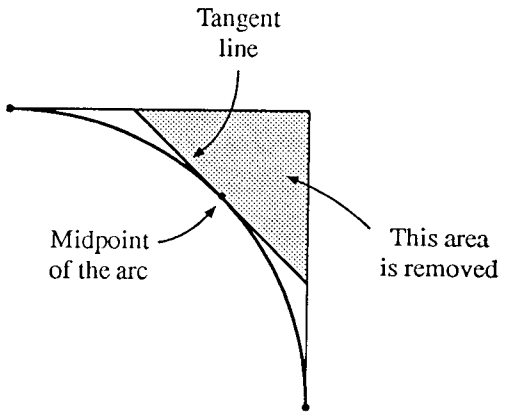

Figure 3.2: Corner of the Square

If we do this process for each of the four quadrants, we obtain the new polygonal shape shown in Figure 3.3 with the circle inscribed in it.

We have doubled the number of segments in the approximating polygon – square to octagon. We now perform a similar geometric operation on this figure (Figure 3.4). Consider the arc of the circle between successive points on the control polygon that are tangent to the circle. Construct the tangent line to the midpoint of this arc.

Cut off the indicated region using the plane of the tangent line as the cutting plane. If we do this for each of the eight circle segments between successive points where the circle and octagon intersect, we obtain a new polygonal shape which is shown in Figure 3.5:

This polygon has sixteen edges each tangent to the circle. Each of the edges has its midpoint on the circle.

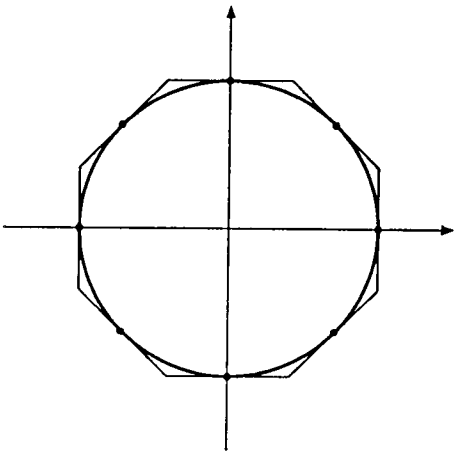

Figure 3.3: Square Refined to Octagon

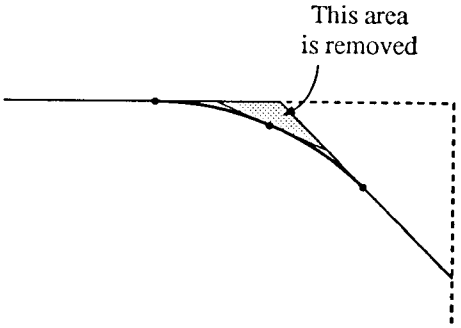

Figure 3.4: Corner of the Octagon

The general idea with this algorithm is to continue this process indefinitely. Visually, the polygons generated can be seen to be converging to a circle, and it is easily seen that geometrically this is also the case. In general, we are creating, with each iteration of this algorithm, a polygon for which all edges are tangent to the circle. In the kth iteration, the polygon will have 2^{k+2} edges, and the midpoint of each edge will be a point on the circle.

3.2 Defining the Algorithm Geometrically

3.2.1 First Method

Consider a control polygon (Figure 3.6) that represents a square containing the four control points $\mathbf{P}_0 = (-1,-1)$, $\mathbf{P}_1 = (-1,1)$, $\mathbf{P}_2 = (1,1)$ and $\mathbf{P}_3 = (1,-1)$.

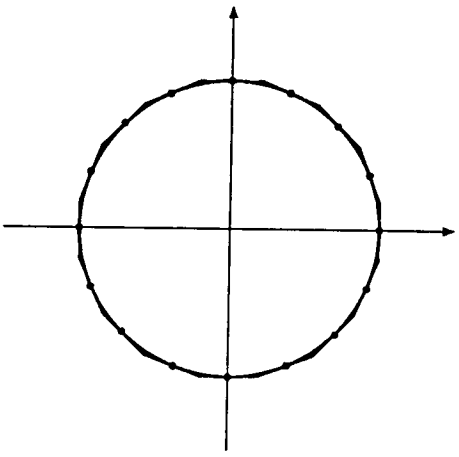

Figure 3.5: Sixteen-sided Polygon

Using the general outline of the algorithm given in section 3.1 above, generate a refinement of this control polygon by defining a new set of control points

$$\left\{\mathbf{P}_0^1, \mathbf{P}_1^1, \mathbf{P}_2^1, \mathbf{P}_3^1, \mathbf{P}_4^1, \mathbf{P}_5^1, \mathbf{P}_6^1, \mathbf{P}_7^1\right\}$$

where for $0 \leq i \leq 3$,

- each of the control points $\mathbf{P}_{2i}^1$ and $\mathbf{P}_{2i+1}^1$ is on the line segment $\overline{\mathbf{P}_i^1\mathbf{P}_{i+1}^1}$, and
- the line $\overline{\mathbf{P}_{2i-1}^1\mathbf{P}_{2i}^1}$ is tangent to the circle at the point where the line from the center of the circle to $\mathbf{P}_i$ intersects the circle.[1]

For example, examine the upper right-hand quadrant of the polygon in Figure 3.7:

In calculating the exact position of $\mathbf{P}_3^1$ on the line $\overline{\mathbf{P}_1\mathbf{P}_2}$, we can see that $d_1 = 2 - \sqrt{2}$, and the point $\mathbf{P}_3^1$ is defined by

$$\begin{aligned}
\mathbf{P}_3^1 &= \left(1 - \frac{2-d_1}{2}\right)\mathbf{P}_1 + \frac{2-d_1}{2}\mathbf{P}_2 \\
&= \frac{d_1}{2}\mathbf{P}_1 + \left(1 - \frac{d_1}{2}\right)\mathbf{P}_2 \\
&= \left(1 - \frac{\sqrt{2}}{2}\right)\mathbf{P}_1 + \frac{\sqrt{2}}{2}\mathbf{P}_2 \\
&= t_0\mathbf{P}_1 + (1-t_0)\mathbf{P}_2
\end{aligned}$$

[1] We note that our subscripts are all written modulo 8.

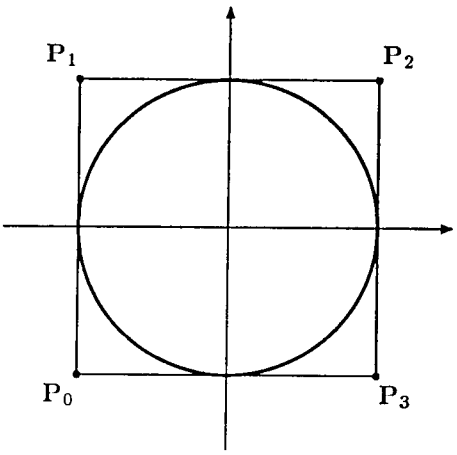

Figure 3.6: Inscribed Circle: Method One

where $t_0 = 1 - \frac{\sqrt{2}}{2}$. By symmetry $\mathbf{P}_4^1$ is defined by

$$\mathbf{P}_4^1 = (1 - t_0)\,\mathbf{P}_2 + t_0\mathbf{P}_3$$

Considering, then, all four corners of the square, we can see that the refinement can be described as

$$\begin{aligned} \mathbf{P}_{2i}^1 &= (1 - t_0)\,\mathbf{P}_i + t_0\mathbf{P}_{i+1} \\ \mathbf{P}_{2i+1}^1 &= t_0\mathbf{P}_i + (1 - t_0)\,\mathbf{P}_{i+1} \end{aligned}$$

and we obtain the new control polygon that is shown in Figure 3.8:

For the next refinement we calculate the control polygon, $\{\mathbf{P}_i^2 : 0 \leq i < 16\}$. An example that illustrates this case is given in Figure 3.9:

Here we have that

$$\begin{aligned} \mathbf{P}_5^2 &= t_1\mathbf{P}_2^1 + (1 - t_1)\,\mathbf{P}_3^1 \\ \mathbf{P}_6^2 &= (1 - t_1)\,\mathbf{P}_3^1 + t_1\mathbf{P}_4^1 \end{aligned}$$

where

$$t_1 = \frac{d_2}{l}$$

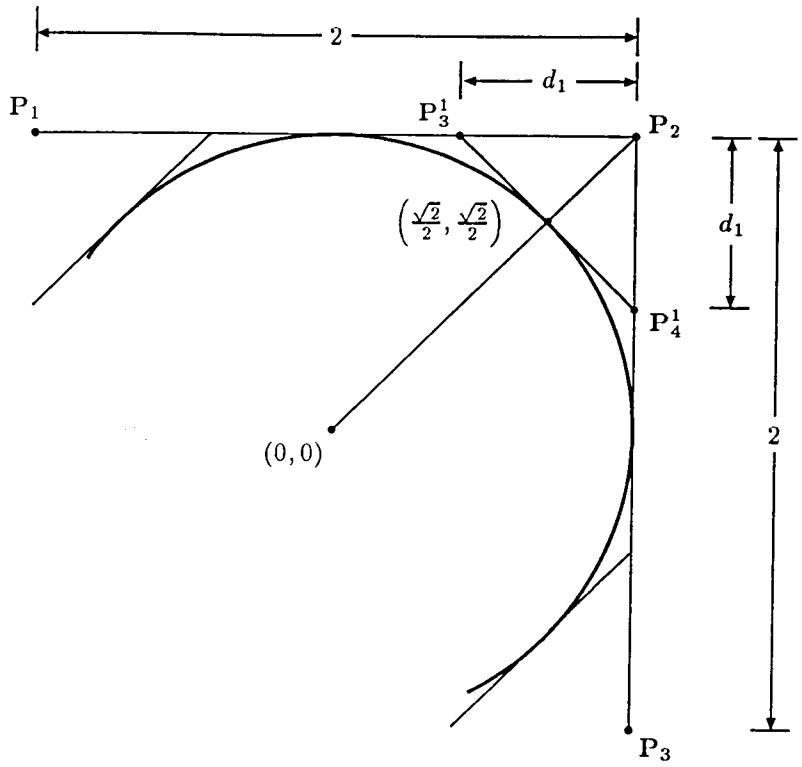

Figure 3.7: Upper Right-hand Quadrant

and l is the length of an edge of the octagon, that is

$$\begin{aligned} l &= 2 - 2d_0 \\ &= 2 - 2(2 - \sqrt{2}) \\ &= 2(\sqrt{2} - 1) \end{aligned}$$

and

$$\begin{aligned} d_1 &= \frac{l}{2} - \tan\frac{22.5°}{2} \\ &= \frac{2(\sqrt{2}-1)}{2} - \tan\frac{22.5°}{2} \end{aligned}$$

We can then calculate that $t_1 \approx 0.25989$, which enables us to calculate the control polygon in Figure 3.10.

To generate the general value of t_i, we refer to Figure 3.11, which illustrates an arc of the circle subtending an angle of 2θ.

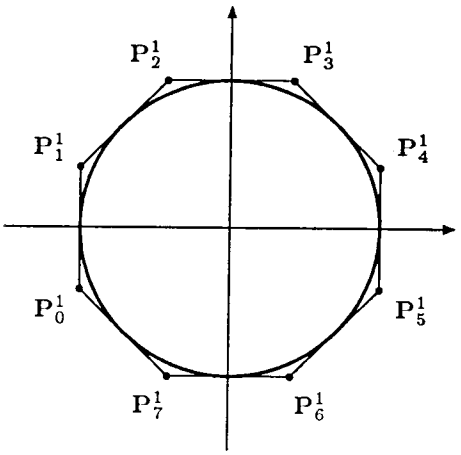

Figure 3.8: Control Polygon at Level $k = 1$

In Figure 3.11 point $\mathbf{P}$ is at the intersection of two tangent lines, each tangent to the circle at the endpoints of the arc subtending an angle of θ. $\mathbf{P}$ therefore lies on the line that is the bisector of the angle θ, and to calculate $\mathbf{P}$ from $\mathbf{P}_0$ and $\mathbf{P}_1$, we form

$$\mathbf{P} = \mathbf{P}_0 + t_\theta(\mathbf{P}_1 - \mathbf{P}_0)$$

where

$$t_\theta = \frac{tan\theta - \tan\frac{\theta}{2}}{2\tan\theta}$$

Simplifying t_θ, we obtain

$$\begin{aligned} t_\theta &= \frac{tan\theta - \tan\frac{\theta}{2}}{2\tan\theta} \\ &= \frac{1}{2}\left(1 - \frac{\tan\frac{\theta}{2}}{\tan\theta}\right) \\ &= \frac{1}{2}\left(1 - \frac{\frac{\sin\theta}{1+\cos\theta}}{\frac{\sin\theta}{\cos\theta}}\right) \\ &= \frac{1}{2}\left(1 - \frac{\cos\theta}{1+\cos\theta}\right) \\ &= \frac{1}{2}\left(\frac{1}{1+\cos\theta}\right) \end{aligned}$$

Initially in our refinement $\theta = \frac{\pi}{4}$, and substituting this into our formula for t_0, we have

$$t_0 = t_{\frac{\pi}{4}} = \frac{1}{2}\left(\frac{1}{1+\cos\frac{\pi}{4}}\right)$$

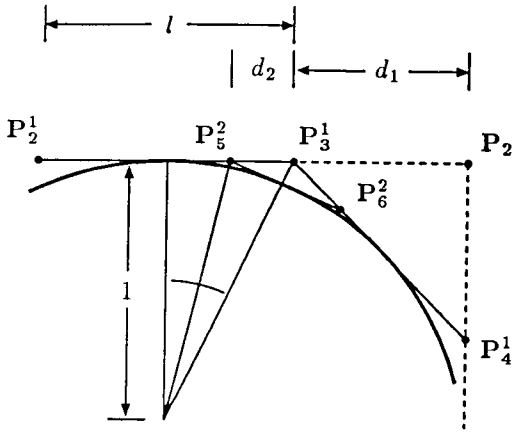

Figure 3.9: Quadrant Refined to Level $k = 2$

$$\begin{aligned} &= \frac{1}{2}\left(\frac{1}{1+\frac{\sqrt{2}}{2}}\right) \\ &= \left(\frac{1}{2+\sqrt{2}}\right) \\ &= \left(1-\frac{\sqrt{2}}{2}\right) \end{aligned}$$

as before. Continuing this, we obtain

$$t_1 = t_{\frac{\pi}{8}} = \frac{1}{2}\left(\frac{1}{1+\cos\frac{\pi}{8}}\right) \approx 0.25989$$

and in general

$$t_k = t_{\frac{\pi}{2^{k+2}}} = \frac{1}{2}\left(\frac{1}{1+\cos\left(\frac{\pi}{2^{k+2}}\right)}\right)$$

We note that $t_k \to \frac{1}{4}$ as $k \to \infty$. Thus, the value of t is based on the level of refinement. Subdivision schemes that incorporate the level of refinement into the algorithm are known as *non-stationary* schemes. [7]

If the initial control polygon is written as $\{\mathbf{P}_0^0, \mathbf{P}_1^0, \mathbf{P}_2^0, \mathbf{P}_3^0\}$ then the elements of the kth control polygon can be written as

$$\begin{aligned} \mathbf{P}_{2i}^k &= t_{k-1}\mathbf{P}_i^{k-1} + (1-t_{k-1})\mathbf{P}_{i+1}^{k-1} \\ \mathbf{P}_{2i+1}^k &= (1-t_{k-1})\mathbf{P}_i^{k-1} + t_{k-1}\mathbf{P}_{i+1}^{k-1} \end{aligned}$$

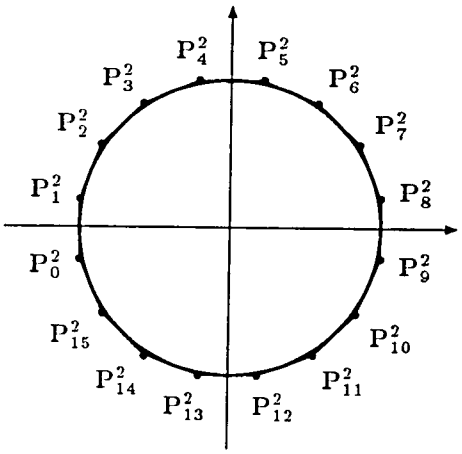

Figure 3.10: Complete Level $k = 2$ Control Polygon

3.2.2 Second Method

In this section, we adapt the algorithm presented in section 3.2.1 to make it somewhat simpler to analyze for our "non-circle" cases. In this adaptation, we represent the points that are tangent to the circle as additional control points in the control polygon.

In the initial case of the square, we now have eight control points in Figure 3.12. This may not look like a big change, but it will enable us to analyze the circle in pieces. In particular, each piece is defined by three control points, two of which are tangent to the circle. Take, for example, Figure 3.13, where we have an initial set of control points $\{\mathbf{P}_0, \mathbf{P}_1, \mathbf{P}_2\}$, and the generated refinement, $\{\mathbf{P}_0^1, \mathbf{P}_1^1, \mathbf{P}_2^1, \mathbf{P}_3^1, \mathbf{P}_4^1\}$.

In this case the refinement algorithm generates a new point tangent to the curve ($\mathbf{P}_2^1$), and two new control points, ($\mathbf{P}_1^1$ and $\mathbf{P}_3^1$). By symmetry we have

$$\begin{aligned}
\mathbf{P}_0^1 &= \mathbf{P}_0 \\
\mathbf{P}_1^1 &= (1 - t_\theta)\mathbf{P}_0 + t_\theta \mathbf{P}_1 \\
\mathbf{P}_2^1 &= \frac{1}{2}\mathbf{P}_1^1 + \frac{1}{2}\mathbf{P}_3^1 \\
\mathbf{P}_3^1 &= t_\theta \mathbf{P}_1 + (1 - t_\theta)\mathbf{P}_2 \\
\mathbf{P}_4^1 &= \mathbf{P}_2
\end{aligned}$$

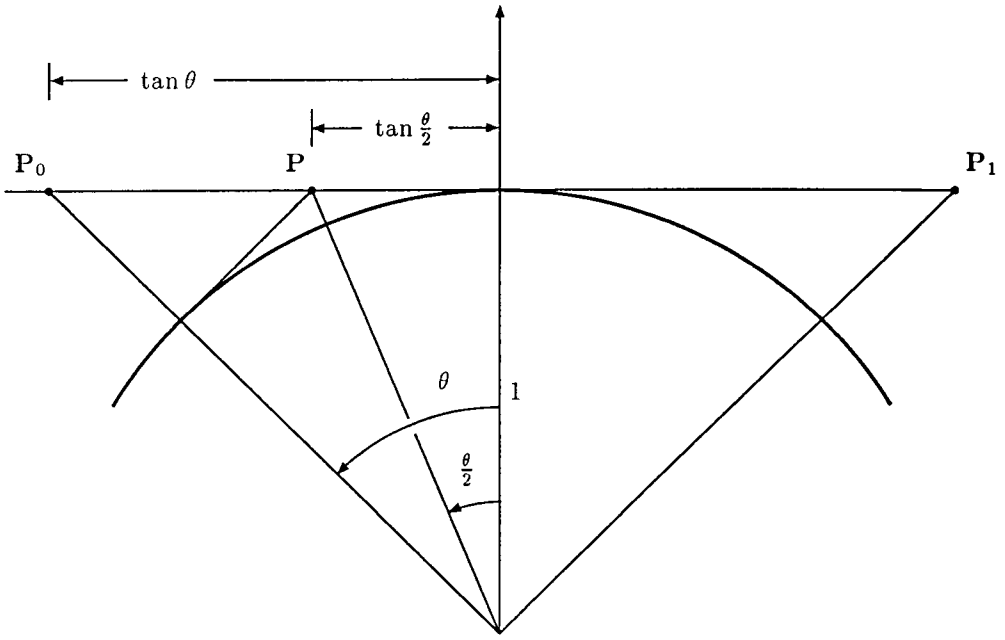

Figure 3.11: Calculating t_θ

where

$$t_\theta = \frac{\tan\frac{\theta}{2}}{\tan\theta} = \frac{\frac{\sin\theta}{1+\cos\theta}}{\frac{\sin\theta}{\cos\theta}} = \frac{\cos\theta}{1+\cos\theta}$$

Again, we initialize our iteration with $\theta = \frac{\pi}{4}$ and proceed with $\theta = \frac{\pi}{2^{k+2}}$ for $k = 1, 2, 3, 4, \ldots$

Consider the length of the arc from point $\mathbf{P}_0$ to $\mathbf{P}_2$ (Figure 3.11). The point $\mathbf{P}_2^1$ is at the midpoint of this arc. Additionally, it lies on the line $\overline{\mathbf{P}_1\mathbf{P}_c}$ where $\mathbf{P}_c$ is the center of the arc. After one refinement we have replaced point $\mathbf{P}_1$ with the edge $\overline{\mathbf{P}_1^1\mathbf{P}_3^1}$. When we consider the arc from $\mathbf{P}_2^1$ to $\mathbf{P}_4^1$, we notice that it is bisected by the line $\overline{\mathbf{P}_3^1\mathbf{P}_c}$. In general, when we refine our control polygon from level k to level $k+1$, we halve the arc length between adjacent control points on the arc. Additionally, if control points $\mathbf{P}_i^k$ and $\mathbf{P}_{i+2}^k$ lie on the arc, the line $\overline{\mathbf{P}_{i+1}^k\mathbf{P}_c}$ bisects the arc from $\mathbf{P}_i^k$ to $\mathbf{P}_{i+2}^k$ and bisects the line $\overline{\mathbf{P}_i^k\mathbf{P}_{i+2}^k}$. From the definition of a radian it follows that we halve the angle between the radii to adjacent control points on the arc when we halve the arc length between them.

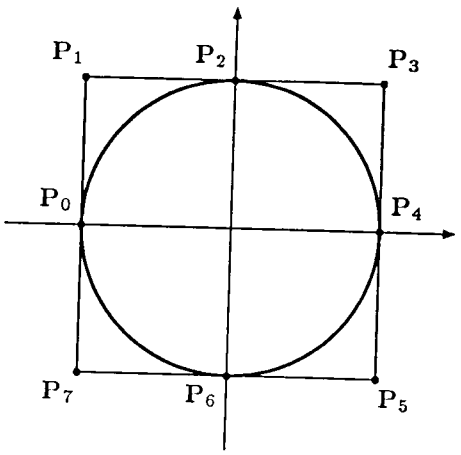

Figure 3.12: Inscribed Circle: Method Two

Consider the ratio of t_θ to $1 - t_\theta$.

$$\begin{aligned}
\frac{t_\theta}{1-t_\theta} &= \frac{\frac{\cos\theta}{1+\cos\theta}}{1-\frac{\cos\theta}{1+\cos\theta}} \\
&= \frac{\frac{\cos\theta}{1+\cos\theta}}{\frac{1+\cos\theta}{1+\cos\theta}-\frac{\cos\theta}{1+\cos\theta}} \\
&= \frac{\frac{\cos\theta}{1+\cos\theta}}{\frac{1}{1+\cos\theta}} \\
&= \cos\theta
\end{aligned}$$

We will call the ratio of t to $1-t$, the *parametric ratio.* As the object is refined, the ***standard parametric ratio*** of t_k to $1 - t_k$ is

$$\frac{t_k}{1-t_k} = \cos\frac{\pi-\alpha}{2^{k+1}} \tag{3.1}$$

for $k = 0, 1, 2, 3, ...$, where α is the interior angle[2] between the original (level $k = 0$) adjacent edges. For the square, $\alpha = \frac{\pi}{2}$.

The general case can be written as

$$\begin{aligned}
\mathbf{P}_{2i}^{k} &= \mathbf{P}_{i}^{k-1} \\
\mathbf{P}_{2i+1}^{k} &= (1-t_{k-1})\mathbf{P}_{i}^{k-1} + t_{k-1}\mathbf{P}_{i+1}^{k-1}
\end{aligned}$$

[2]The smaller of the two angles formed by two rays emanating from a point

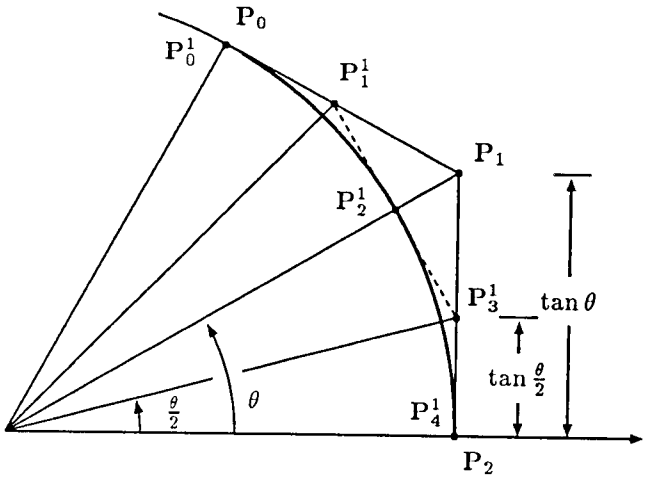

Figure 3.13: Calculating the Arc of a Circle

$$\begin{aligned} \mathbf{P}_{2i+2}^k &= \frac{1}{2}\mathbf{P}_{2i+1}^n + \frac{1}{2}\mathbf{P}_{2i+3}^n \\ \mathbf{P}_{2i+3}^k &= t_{k-1}\mathbf{P}_{i+1}^{k-1} + (1-t_{k-1})\mathbf{P}_{i+2}^{k-1} \\ \mathbf{P}_{2i+4}^k &= \mathbf{P}_{i+2}^{k-1} \end{aligned}$$

$$t_k = \frac{\cos\frac{\pi}{2^{k+2}}}{1+\cos\frac{\pi}{2^{k+2}}}$$

We note that $t_k \to \frac{1}{2}$ as $k \to \infty$.

3.3 Chaikin's Algorithm on Rational Curves

The procedure described in section 3.2.2 may be thought of as an adaptation of Chaikin's algorithm (section 2.1) so that rational curves may be produced. Chaikin's algorithm may be modified so that it will interpolate the end points by use of phantom control points to replace the end points. We will consider a variation of Chaikin's algorithm that interpolates the end points and modify this so that rational curves may be produced . Consider an original ($k = 0$) control polygon of n points

$$\{\mathbf{P}_0, \mathbf{P}_1, ..., \mathbf{P}_{n-2}, \mathbf{P}_{n-1}\}$$

where points $\mathbf{P}_0$ and $\mathbf{P}_{n-1}$ are tangent to the curve and all other points are *non-tangent* points (Figure 3.14). To refine the polygon to level $k+1$ the modified algorithm is:

1. At level $k+1$ insert a *new tangent point* at the midpoint of each edge that is bounded by two level k non-tangent points. For example, to process the level $k = 0$ control polygon, we insert a level $k+1$ new tangent point at the midpoint of every edge except $\overline{\mathbf{P}_0\mathbf{P}_1}$ and $\overline{\mathbf{P}_{n-2}\mathbf{P}_{n-1}}$. The resulting control polygon is

$$\{\mathbf{P}^1_0, \mathbf{P}_1, \mathbf{P}^1_3, \mathbf{P}_2, \mathbf{P}^1_6, ..., \mathbf{P}^1_{3(n-4)}, \mathbf{P}_{n-3}, \mathbf{P}^1_{3(n-3)}, \mathbf{P}_{n-2}, \mathbf{P}^1_{3(n-2)}\}$$

   where

$$\begin{aligned} \mathbf{P}^1_0 &= \mathbf{P}_0 \\ \mathbf{P}^1_{3(n-2)} &= \mathbf{P}_{n-1} \\ \mathbf{P}^1_{3i} &= \frac{1}{2}(\mathbf{P}_i + \mathbf{P}_{i+1}) \end{aligned}$$

   and points $\mathbf{P}^1_0$, $\mathbf{P}^1_{3(n-2)}$, and $\mathbf{P}^1_{3i}$ are tangent to the curve.
   Generally, we use the *midpoint method* to define new tangent points. The midpoint method is defined as:

$$\mathbf{P}^{k+1}_{3i} = \frac{1}{2}\left(\mathbf{P}^k_i + \mathbf{P}^k_{i+1}\right)$$

   That is, the new tangent point is at the midpoint of the new edge.

2. Separate the level k control polygon into parts that contain three points: tangent point, non-tangent point, tangent point. Our original control polygon would be separated into:

$$\{\mathbf{P}^1_0, \mathbf{P}^0_1, \mathbf{P}^1_3\}$$

$$\{\mathbf{P}^1_3, \mathbf{P}^0_2, \mathbf{P}^1_6\}$$

$$...$$

$$\{\mathbf{P}^1_{3(n-4)}, \mathbf{P}^0_{n-3}, \mathbf{P}^1_{3(n-3)}\}$$

$$\{\mathbf{P}^1_{3(n-3)}, \mathbf{P}^0_{n-2}, \mathbf{P}^1_{3(n-2)}\}$$

   We now have $n-2$ control polygons each of which contains three points and is tangent to the curve at its end points.

3. Replace every non-tangent level k point, $\mathbf{P}_i^k$, with two new non-tangent level $k+1$ points, $\mathbf{P}_{3(i-1)+1}^{k+1}$ and $\mathbf{P}_{3(i-1)+2}^{k+1}$ at, the midpoints of the edges adjacent to $\mathbf{P}_i^k$.

$$\begin{aligned}\mathbf{P}_{3(i-1)+1}^{k+1} &= \frac{1}{2}\left(\mathbf{P}_i^k + \mathbf{P}_{3(i-1)}^{k+1}\right)\\ \mathbf{P}_{3(i-1)+2}^{k+1} &= \frac{1}{2}\left(\mathbf{P}_i^k + \mathbf{P}_{3i}^{k+1}\right)\end{aligned}$$

Continuing with our example, we would replace $\mathbf{P}_1^0$ with $\mathbf{P}_1^1$ and $\mathbf{P}_2^1$ at the midpoints of $\overline{\mathbf{P}_0\mathbf{P}_1}$ and $\overline{\mathbf{P}_1\mathbf{P}_3^1}$. Our completed level $k+1$ control polygons would be

$$\{\mathbf{P}_0^1, \mathbf{P}_1^1, \mathbf{P}_2^1, \mathbf{P}_3^1\}$$

$$\{\mathbf{P}_3^1, \mathbf{P}_4^1, \mathbf{P}_5^1, \mathbf{P}_6^1\}$$

$$\ldots$$

$$\{\mathbf{P}_{3(n-4)}^1, \mathbf{P}_{3(n-4)+1}^1, \mathbf{P}_{3(n-4)+2}^1, \mathbf{P}_{3(n-3)}^1\}$$

$$\{\mathbf{P}_{3(n-3)}^1, \mathbf{P}_{3(n-3)+1}^1, \mathbf{P}_{3(n-3)+2}^1, \mathbf{P}_{3(n-2)}^1\}$$

For example, in Figure 3.14 we are given the control points $\{\mathbf{P}_0, \mathbf{P}_1, \mathbf{P}_2, \mathbf{P}_3\}$ and may generate a curve that is tangent to $\overline{\mathbf{P}_0\mathbf{P}_1}$ at $\mathbf{P}_0$, to $\overline{\mathbf{P}_2\mathbf{P}_3}$ at $\mathbf{P}_3$, and to $\overline{\mathbf{P}_1\mathbf{P}_2}$ at its midpoint. We start by adding a new tangent point $(\mathbf{P}_3^1)$ at the midpoint of $\overline{\mathbf{P}_1\mathbf{P}_2}$ then divide the control polygon into two parts, $\{\mathbf{P}_0^1, \mathbf{P}_1, \mathbf{P}_3^1\}$ and $\{\mathbf{P}_3^1, \mathbf{P}_2, \mathbf{P}_6^1\}$. For each half we replace the corner points, $\mathbf{P}_1$ and $\mathbf{P}_2$, with two new points that are at the midpoints of the adjacent lines. So we have

$$\begin{aligned}\mathbf{P}_0^1 &= \mathbf{P}_0\\ \mathbf{P}_1^1 &= (1-t)\,\mathbf{P}_0 + t\mathbf{P}_1\\ \mathbf{P}_2^1 &= (1-t)\,\mathbf{P}_3^1 + t\mathbf{P}_1\\ \mathbf{P}_3^1 &= (1-t)\,\mathbf{P}_1 + t\mathbf{P}_2\\ \mathbf{P}_4^1 &= (1-t)\,\mathbf{P}_3^1 + t\mathbf{P}_2\\ \mathbf{P}_5^1 &= (1-t)\,\mathbf{P}_3 + t\mathbf{P}_2\\ \mathbf{P}_6^1 &= \mathbf{P}_3\end{aligned}$$

where

$$t = \frac{1}{2}$$

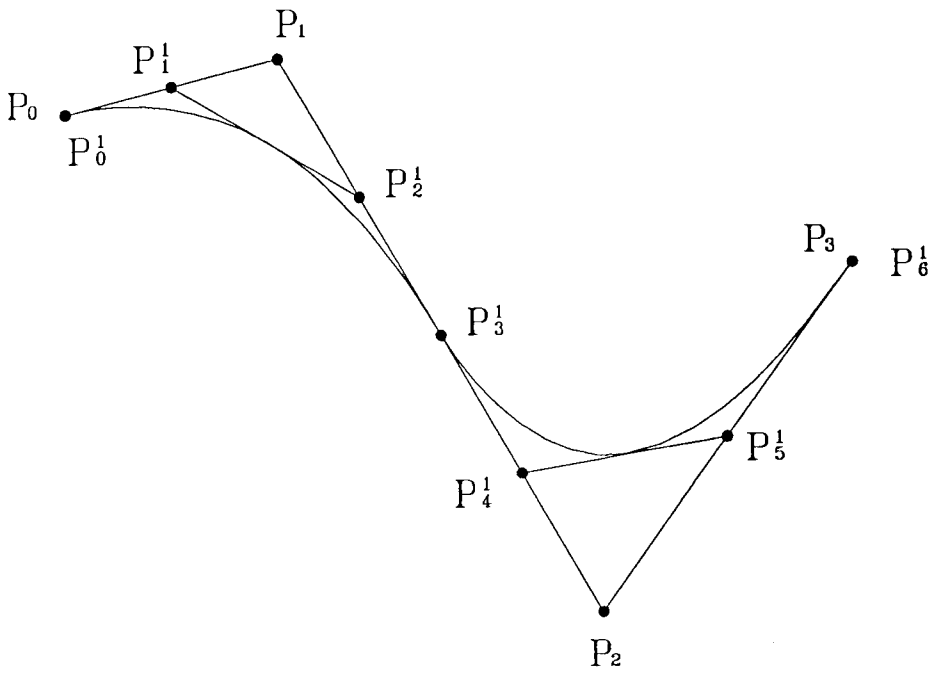

Figure 3.14: End-point Interpolating Chaikin's

These new points are: $\mathbf{P}_1^1$, $\mathbf{P}_2^1$ to replace $\mathbf{P}_1^0$ and $\mathbf{P}_4^1$, $\mathbf{P}_5^1$ to replace $\mathbf{P}_2^0$. The separated level $k+1$ control polygons are $\{\mathbf{P}_0^1, \mathbf{P}_1^1, \mathbf{P}_2^1, \mathbf{P}_3^1\}$ and $\{\mathbf{P}_3^1, \mathbf{P}_4^1, \mathbf{P}_5^1, \mathbf{P}_6^1\}$. This process may be repeated until a piecewise linear approximation of sufficient smoothness is obtained, and, in the limit, a piecewise parabolic curve is generated.

Suppose we wanted to use a Chaikin-like algorithm to produce a curve that is, in the limit, piecewise circular arcs. Considering the example above, we will show that arcs of circles may be generated provided the original control polygon satisfies

$$\left|\overline{\mathbf{P}_0\mathbf{P}_1}\right| + \left|\overline{\mathbf{P}_2\mathbf{P}_3}\right| = \left|\overline{\mathbf{P}_1\mathbf{P}_2}\right|$$

Until now, we have used the midpoint method to define new tangent points. At the initial level, however, we cannot necessarily do this and produce circular arcs. In Figure 3.15 we

have two points on a circle, $\mathbf{P}_0$ and $\mathbf{P}_1$, that are not opposite each other. The lines tangent to the circle at these points will intersect at a point $\mathbf{P}_p$.

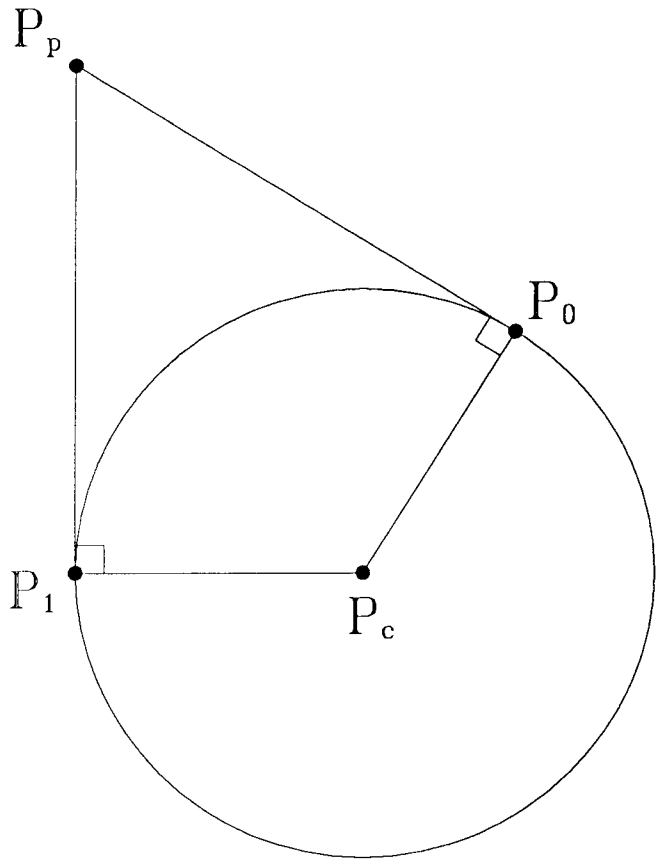

Figure 3.15: Tangent Line Intersection

If we compare the lines $\overline{\mathbf{P}_0\mathbf{P}_p}$ and $\overline{\mathbf{P}_1\mathbf{P}_p}$ we will find that

$$\left| \overline{\mathbf{P}_0\mathbf{P}_p} \right| = \left| \overline{\mathbf{P}_1\mathbf{P}_p} \right|$$

The points $\mathbf{P}_0$, $\mathbf{P}_p$, and $\mathbf{P}_1$ could be used as the control polygon for the arc of the circle from $\mathbf{P}_0$ to $\mathbf{P}_1$. Using our process, circular arcs require three-point control polygons with sides of equal length. Therefore, we will not necessarily use the midpoint of $\overline{\mathbf{P}_1\mathbf{P}_2}$ for the

new tangent point $\mathbf{P}_3^1$. Instead, $\mathbf{P}_3^1$ is chosen so that

$$\left| \overline{\mathbf{P}_1\mathbf{P}_3^1} \right| = \left| \overline{\mathbf{P}_0\mathbf{P}_1} \right|$$

and

$$\left| \overline{\mathbf{P}_3^1\mathbf{P}_2} \right| = \left| \overline{\mathbf{P}_2\mathbf{P}_3} \right|$$

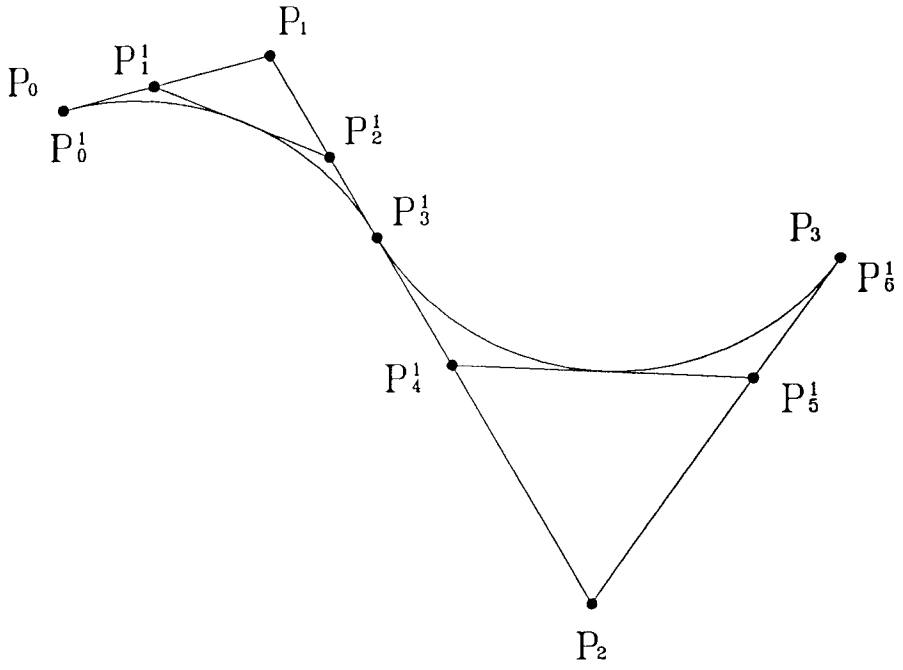

Figure 3.16: Rational Chaikin's to Produce Arcs of Circles

Once we have guaranteed that the edges of our separated control polygons are of equal length we may return to the midpoint method for choosing our new tangent points. With the insertion of $\mathbf{P}_3^1$ we separate our original control polygon into two parts. Part **a** is $\{\mathbf{P}_0^1, \mathbf{P}_2, \mathbf{P}_3^1\}$ and part **b** is $\{\mathbf{P}_3^1, \mathbf{P}_2, \mathbf{P}_6^1\}$ where $\mathbf{P}_0^1 = \mathbf{P}_0^0$ and $\mathbf{P}_6^1 = \mathbf{P}_3^0$. Points $\mathbf{P}_1^1$, $\mathbf{P}_2^1$, $\mathbf{P}_4^1$, and $\mathbf{P}_5^1$ are obtained using ratios. These ratios are based on the angles between the sides of the separated control polygons. The new tangent point $\mathbf{P}_3^1$ is

$$\mathbf{P}_3^1 = (1 - t_0)\,\mathbf{P}_1 + t_0\mathbf{P}_2$$

where

$$t_0 = \frac{\left|\overline{\mathbf{P}_0\mathbf{P}_1}\right|}{\left|\overline{\mathbf{P}_1\mathbf{P}_2}\right|}$$

The new non-tangent points are

$$\begin{aligned}\mathbf{P}_1^1 &= (1 - t_{0,a})\,\mathbf{P}_0 + t_{0,a}\mathbf{P}_1 \\ \mathbf{P}_2^1 &= (1 - t_{0,a})\,\mathbf{P}_1 + t_{0,a}\mathbf{P}_3^1\end{aligned}$$

where

$$t_{0,a} = \frac{\cos\theta_{0,a}}{1 + \cos\theta_{0,a}}$$

$$\theta_{0,a} = \frac{1}{2}\left[\pi - \cos^{-1}\left(\frac{\langle \mathbf{P}_3^1 - \mathbf{P}_1\rangle \cdot \langle \mathbf{P}_0 - \mathbf{P}_1\rangle}{\left|\overline{\mathbf{P}_3^1\mathbf{P}_1}\right|\left|\overline{\mathbf{P}_0\mathbf{P}_1}\right|}\right)\right]$$

and

$$\begin{aligned}\mathbf{P}_4^1 &= (1 - t_{0,b})\,\mathbf{P}_3^1 + t_{0,b}\mathbf{P}_2 \\ \mathbf{P}_5^1 &= (1 - t_{0,b})\,\mathbf{P}_3 + t_{0,b}\mathbf{P}_2\end{aligned}$$

where

$$t_{0,b} = \frac{\cos\theta_{0,b}}{1 + \cos\theta_{0,b}}$$

$$\theta_{0,b} = \frac{1}{2}\left[\pi - \cos^{-1}\left(\frac{\langle \mathbf{P}_3^1 - \mathbf{P}_2\rangle \cdot \langle \mathbf{P}_3 - \mathbf{P}_2\rangle}{\left|\overline{\mathbf{P}_3^1\mathbf{P}_2}\right|\left|\overline{\mathbf{P}_3\mathbf{P}_2}\right|}\right)\right]$$

Notice that we do not use $\theta_0 = \frac{\pi}{4}$ for our initial refinements. The initial value, θ_0, is $\frac{1}{2}$ the supplement of the interior angle between adjacent edges.

This initial angle (α) is called the *parent* and this value is used at each level as its *children* are refined. Using the original interior angle (α) between adjacent sides, the general form for θ is

$$\theta_k = \frac{\pi - \alpha}{2^{k+1}}$$

When we are refining a circular arc, we may measure the interior angle (ϕ) between adjacent edges at any level k of refinement and find

$$\theta_k = \frac{\pi - \alpha}{2^{k+1}} = \frac{\pi - \phi}{2}$$

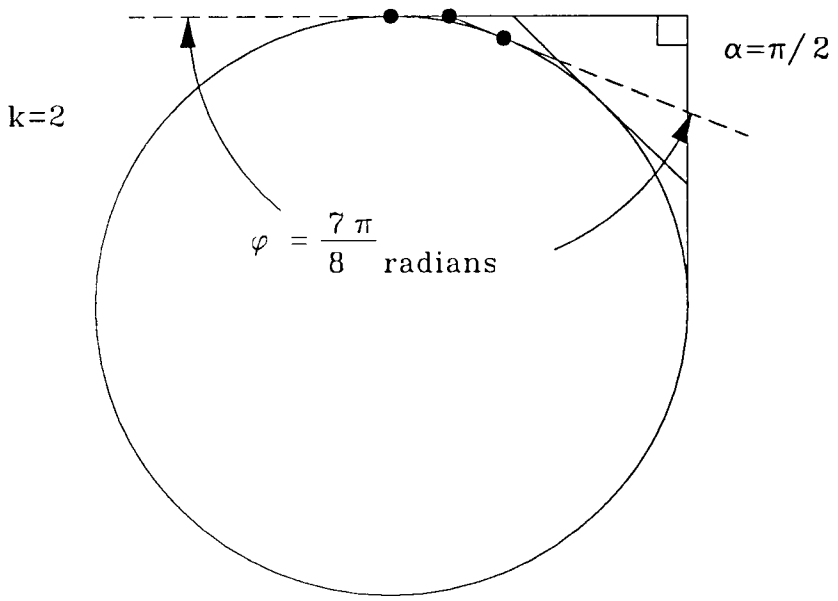

Figure 3.17: Measured Angle at Level $k = 2$

For example, in Figure 3.17 we have refined our quadrant twice ($k = 2$).

The interior angle (ϕ) is measured to be $\frac{7\pi}{8}$ and $\alpha = \frac{\pi}{2}$. θ_2 is calculated to be

$$\theta_2 = \frac{\pi - \frac{\pi}{2}}{2^3} = \frac{\pi}{16}$$

$\frac{1}{2}$ the supplement of ϕ is

$$\frac{\pi - \frac{7\pi}{8}}{2} = \frac{\pi}{16}$$

3.4 Ellipses

Consider an ellipse centered on the origin with its axes aligned with the x and y axes of the form

$$\frac{x^2}{C^2} + \frac{y^2}{D^2} = 1$$

We may scale this ellipse by D^2 resulting in an ellipse with a minor axis of one and the same ratio of major to minor axes.

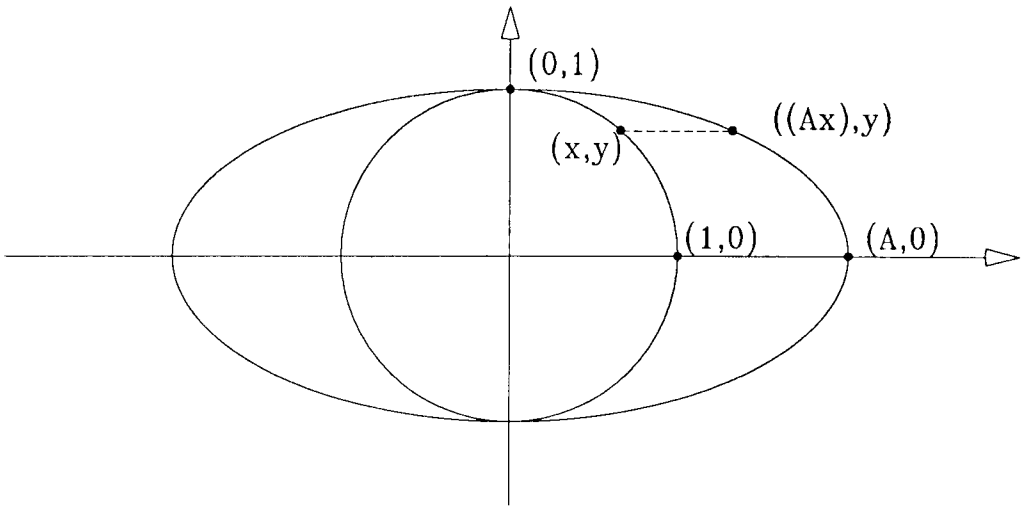

Figure 3.18: Sphere Scaled to an Ellipse

Letting

$$A^2 = \frac{C^2}{D^2}$$

we have an ellipse

$$\frac{x^2}{A^2} + y^2 = 1$$

Now compare this to the unit circle centered on the origin

$$x^2 + y^2 = 1$$

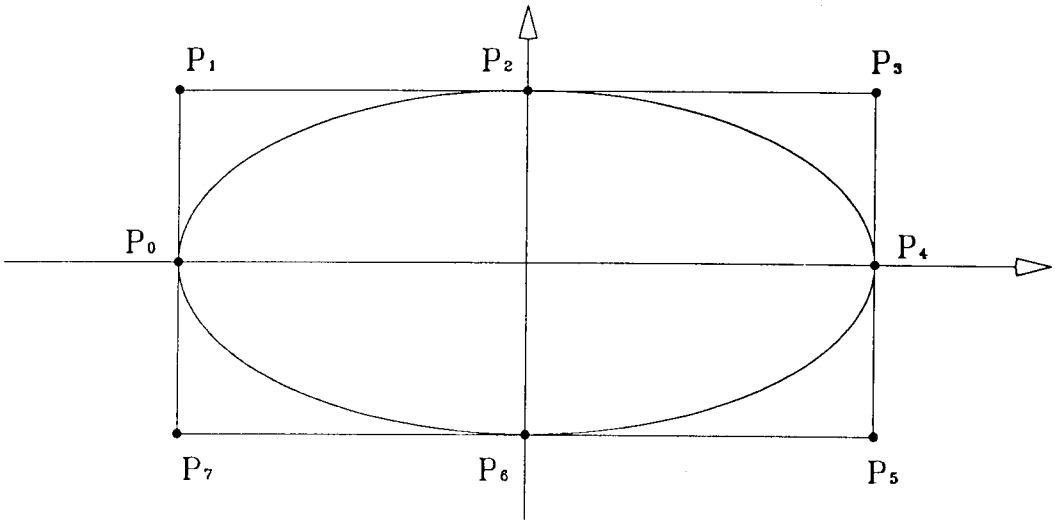

Figure 3.19: Control Polygon of an Ellipse

Figure 3.18 we may take any point $\mathbf{P}_c(x, y)$ on the unit circle and scale it to a corresponding point $\mathbf{P}_e(Ax, y)$ on the ellipse. [9, pages 201–210]

Similarly, we may take a square with vertices $(\pm 1, \pm 1)$ that can be used as the control polygon for the unit circle, stretch it into a rectangle with vertices $(\pm A, \pm 1)$, and use it as the control polygon of the ellipse (Figure 3.19)

$$\frac{x^2}{A^2} + y^2 = 1$$

Consider two non-opposite points, $\mathbf{P}_0^c$ and $\mathbf{P}_1^c$, on a circle in Figure 3.20. Lines tangent to the circle at these two points intersect at $\mathbf{P}^c$. We may generate the midpoint, $\mathbf{P}_{\frac{1}{2}}^c$, of the arc between them using the standard parametric ratio[3] where α is the interior angle between the lines $\overline{\mathbf{P}_0^c\mathbf{P}^c}$ and $\overline{\mathbf{P}_1^c\mathbf{P}^c}$. If we scale the x coordinates of these points by A we will obtain the corresponding points on the ellipse, $\mathbf{P}_0^e$, $\mathbf{P}_1^e$, and $\mathbf{P}_{\frac{1}{2}}^e$.

We may refine each quadrant individually. Starting with the upper right quadrant in Figure 3.21, we use the same method as in section 3.2.2, using the standard parametric ratio $\cos\frac{\pi-\alpha}{2^{(k+1)}}$. The parent angle (α) is the angle between a pair of original adjacent

[3]See Equation 3.1 on page 21

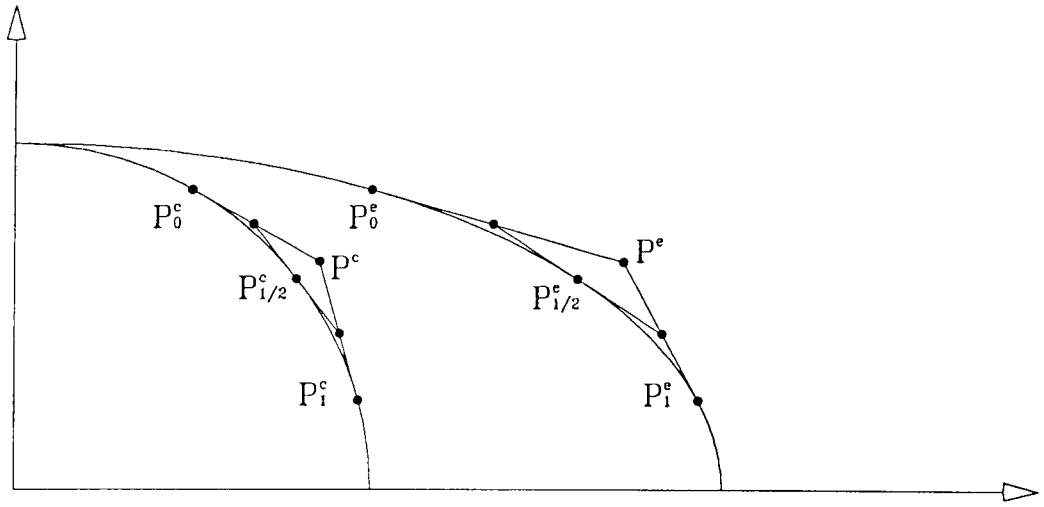

Figure 3.20: Scaling a circle to an Ellipse

edges. To refine elliptical curves, we will require that the parent angle (α) is $\frac{\pi}{2}$. As shown in Figure 3.17, when refining a circular arc, we may stop at any level k, measure the supplement of the interior angle between any two adjacent edges, and find it to be $\frac{\pi-\alpha}{2^k}$. This is not the case with the rectangle; the scaling transformation, while affine, is not angle preserving. However, if we use standard parametric ratio $\cos\frac{\pi-\alpha}{2^{(k+1)}}$ in our refinement and begin with all α angles of $\frac{\pi}{2}$, the resulting curve will be piecewise elliptical. Refining the rectangle to level k using this non-stationary ratio is equivalent to refining the square to level k and then applying the scaling transformation to the resulting figure.

For example, in Figure 3.22 we are given a control polygon, $\{\mathbf{P}_0, \mathbf{P}_1, \mathbf{P}_2, \mathbf{P}_3, \mathbf{P}_4\}$. We begin by inserting new tangent point $\mathbf{P}_3^1$ at the midpoint of $\overline{\mathbf{P}_1\mathbf{P}_2}$ and $\mathbf{P}_6^1$ at the midpoint of $\overline{\mathbf{P}_2\mathbf{P}_3}$. Now each section, $\{\mathbf{P}_0^1, \mathbf{P}_1, \mathbf{P}_3^1\}$, $\{\mathbf{P}_3^1, \mathbf{P}_2, \mathbf{P}_6^1\}$, and $\{\mathbf{P}_6^1, \mathbf{P}_3, \mathbf{P}_9^1\}$ is processed. Note that $\mathbf{P}_0^1 = \mathbf{P}_0^0$ and $\mathbf{P}_9^1 = \mathbf{P}_4$. In this example, the first arc is tangent to $\mathbf{P}_0^1$ and $\mathbf{P}_3^1$, the second is tangent to $\mathbf{P}_3^1$ and $\mathbf{P}_6^1$, and the third is tangent to $\mathbf{P}_6^1$ and $\mathbf{P}_9^1$. The arc from $\mathbf{P}_0$ to $\mathbf{P}_3^1$ is the arc of a circle since

$$\left|\overline{\mathbf{P}_0\mathbf{P}_1}\right| = \left|\overline{\mathbf{P}_3^1\mathbf{P}_2}\right|$$

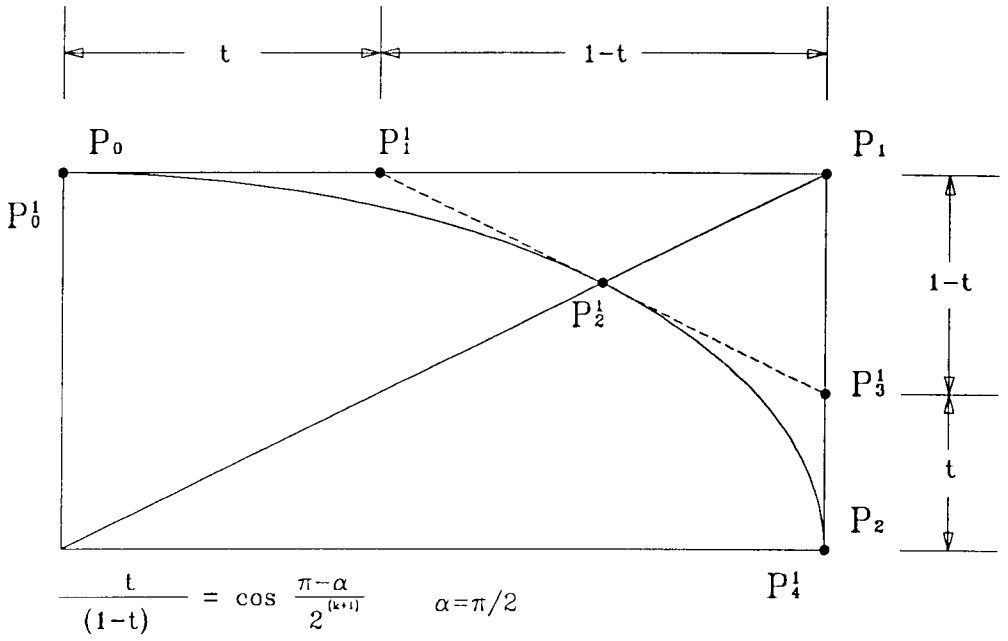

Figure 3.21: Quadrant of an Ellipse

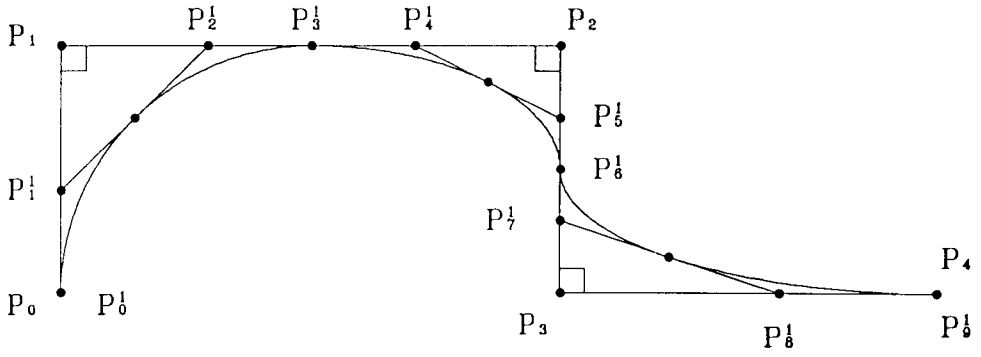

Figure 3.22: Piecewise Elliptical Curve

3.5 New Tangent Point Selection

When we generated arcs of circles in section 3.3, we chose a value for t such that the new tangent point, $\mathbf{P}_3^1$, was not guaranteed to be at the midpoint of $\overline{\mathbf{P_1P_2}}$ (see Figure 3.16). However, in section 3.4 we used midpoints for our new tangent points to generate ellipses (see Figure 3.22). In general, we are free to chose the level $k = 0$ new tangent points as we please. To obtain arcs of circles, the new tangent point was chosen so that each separated control polygon would have edges of equal length; this is a requirement of circular arcs. For rational curves we will always choose the midpoint of the new edge as our new tangent point.

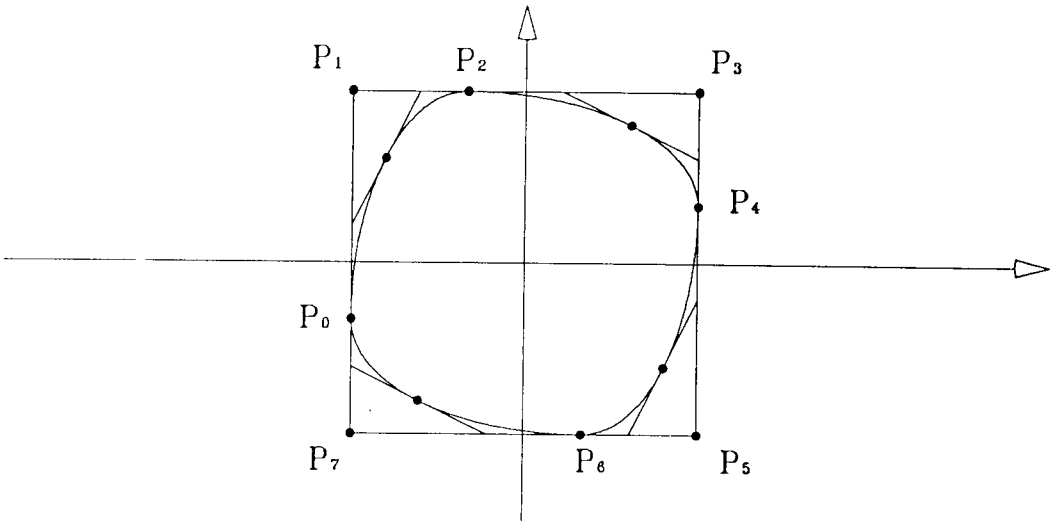

Figure 3.23: Closed Piecewise Elliptical Curve

In Figure 3.12 of section 3.2.2 we chose points $\mathbf{P}_0$, $\mathbf{P}_2$, $\mathbf{P}_4$, and $\mathbf{P}_6$ at the midpoints of the square's edges so that they would be on the inscribed circle. If we choose different new tangent points at level $k = 0$ and, then, for $k = 1, 2, 3, 4...$, use the midpoint method to define new tangent points and the standard parametric ratio, $\cos\frac{\pi-\alpha}{2^{k+1}}$, where $\alpha = \frac{\pi}{2}$, we would generate a closed curve made from elliptical arcs. In Figure 3.23 the tangent points,

$\mathbf{P}_0$, $\mathbf{P}_2$, $\mathbf{P}_4$, and $\mathbf{P}_6$ were chosen so that

$$\frac{\left|\overline{\mathbf{P}_i\mathbf{P}_{i+1}}\right|}{\left|\overline{\mathbf{P}_{i+1}\mathbf{P}_{i+2}}\right|} = \frac{1}{3}$$

for $i = 1, 3, 5, 7$ with all subscripts modulo 8.

With appropriately chosen new tangent points it is possible to begin with any polygon that has all of its sides tangent to the circle and refine it to produce the circle. To do this we use a different α for each section so that each is equal to the interior angle of that section.

3.6 Sheared Circles and Ellipses

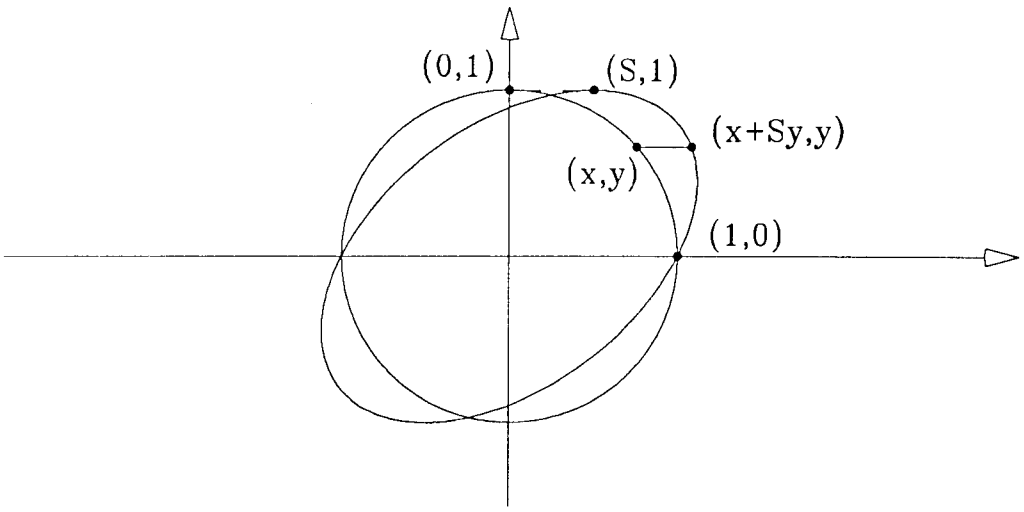

Figure 3.24: Sheared Circle

If we apply a shear transformation to the square $(\pm 1, \pm 1)$ along the x axis, we get the parallelogram $(1 + S, 1)$, $(1 - S, -1)$, $(-1 - S, -1)$, and $(-1 + S, 1)$, such that every point (x, y) on the square becomes a point $(x + Sy, y)$ on the parallelogram [9, pages 201–210]. Again, we may create a sheared circle by applying the shear transformation to each point on the circle (Figure 3.24)[4].

[4] We note that a sheared circle and a sheared ellipse are both ellipses

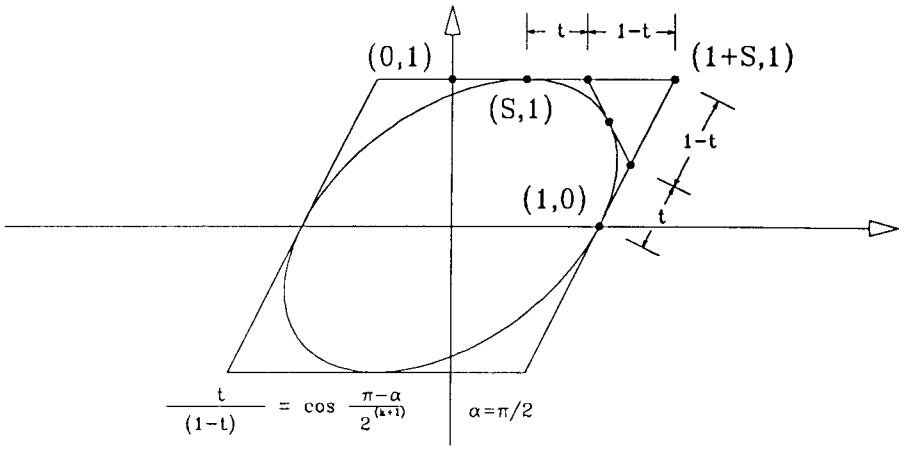

Figure 3.25: Sheared Square Control Polygon

We may obtain the same results by beginning with the parallelogram as our control polygon and refining it using the midpoint method from section 3.5 and the standard parametric ratio, $\cos \frac{\pi-\alpha}{2^{k+1}}$, with $\alpha = \frac{\pi}{2}$ (Figure 3.25).

When we apply both a scaling and shearing transformation to a square, we have another parallelogram (Figure 3.26). We may use this for our control polygon and obtain a sheared ellipse when the refinement method is applied.

If we consider an octant of this parallelogram, we find that it may be used as a model for a general two-dimensional control polygon. In the general case (Figure 3.27), using the midpoint method and the standard parametric ratio, this method produces curves that are piecewise elliptical arcs.

Given a control polygon, $\{\mathbf{P}_0, \mathbf{P}_1, \mathbf{P}_2, \mathbf{P}_3\}$, we insert $\mathbf{P}_3^1$ at the midpoint of $\overline{\mathbf{P}_1\mathbf{P}_2}$. As before, we begin by breaking this into two control polygons, $\{\mathbf{P}_0^1, \mathbf{P}_1, \mathbf{P}_3^1\}$ and $\{\mathbf{P}_3^1, \mathbf{P}_2, \mathbf{P}_6^1\}$, and proceed as above. Here we have two elliptical arcs. The first is tangent to $\mathbf{P}_0$ and $\mathbf{P}_3^1$, and the second is tangent to $\mathbf{P}_3^1$ and $\mathbf{P}_3$.

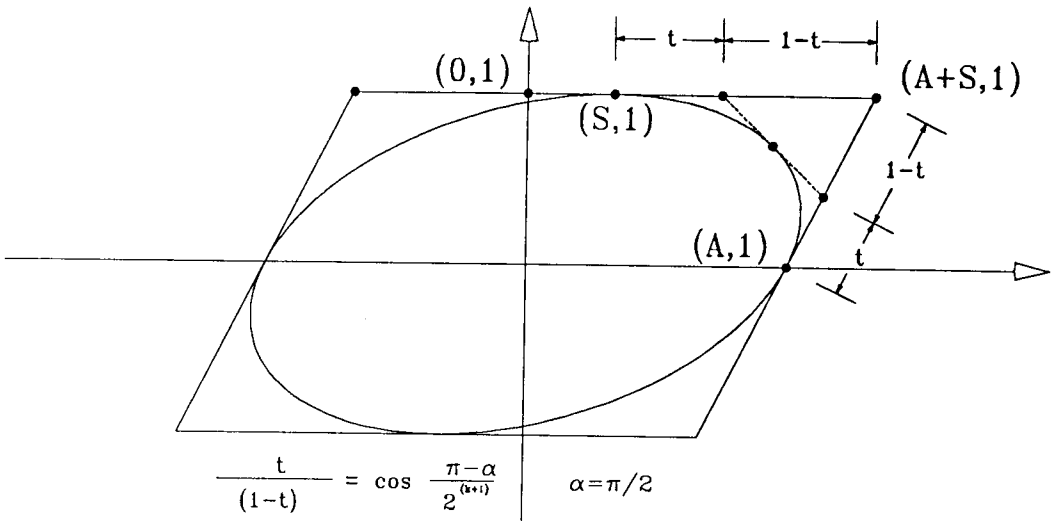

Figure 3.26: Parallelogram Control Polygon

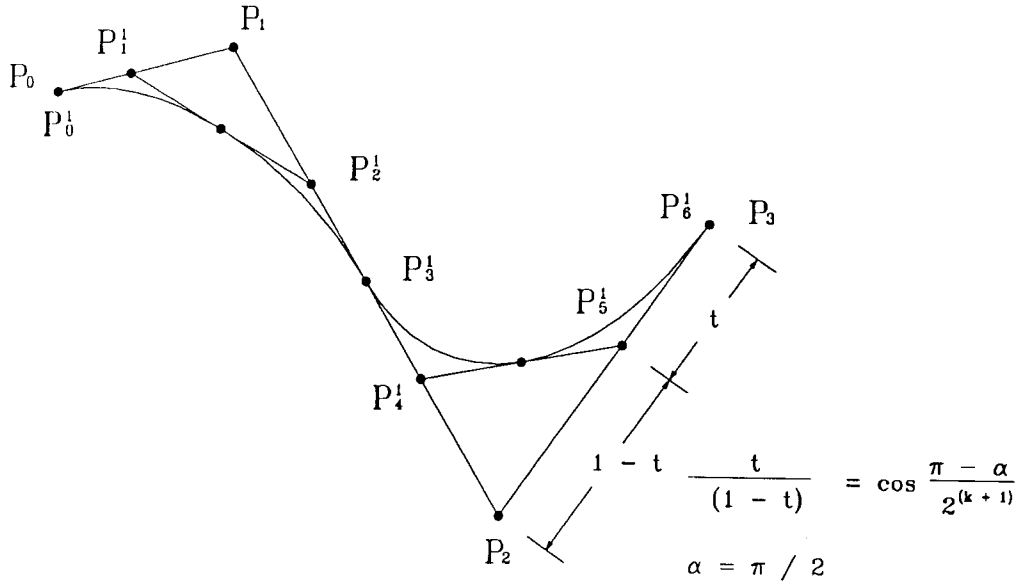

Figure 3.27: Piecewise Elliptical Curve

Chapter 4

Three Dimensions

We will extend the method presented to refine a control polygon into a circle so that we may refine control polyhedra into a sphere. To that end, we will lay groundwork for operations and relations in three dimensions.

4.1 Preliminaries

4.1.1 Planes and Lines

Projecting a Point onto a Plane

Given a plane defined by a point, $\mathbf{P}$, and a normal vector, $\vec{n}$ [1], consider a point, $\mathbf{Q}$, and a vector direction, $\vec{v}$, in $\mathbb{R}^3$. We calculate the projection of $\mathbf{Q}$ onto the plane in the direction of the vector $\vec{v}$, by calculating the intersection of the line

$$\mathbf{Q} - t\vec{v}$$

and the plane, as in Figure 4.1.

In this case, we have that the vector $\langle(\mathbf{Q} - t\vec{v}) - \mathbf{P}\rangle$ must lie in the plane, and so

$$\begin{aligned} 0 &= \langle(\mathbf{Q} + t\vec{v}) - \mathbf{P}\rangle \cdot \vec{n} \\ &= \langle\langle\mathbf{Q} - \mathbf{P}\rangle + t\vec{v}\rangle \cdot \vec{n} \\ &= (\langle\mathbf{Q} - \mathbf{P}\rangle \cdot \vec{n}) + (t\vec{v} \cdot \vec{n}) \end{aligned}$$

[1] We assume all normal vectors, $\vec{n}$, are unit vectors

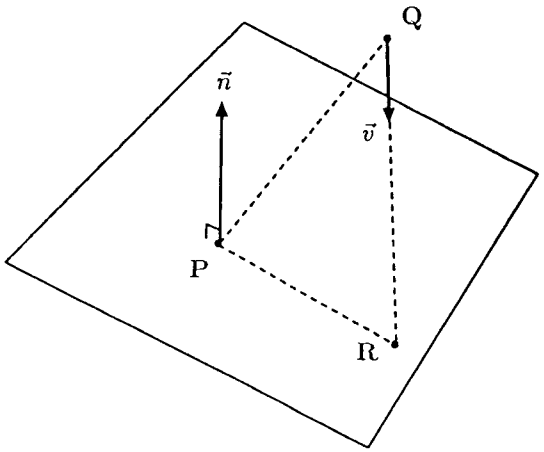

Figure 4.1: Projecting a Point onto a Plane

We have

$$t = \frac{\langle \mathbf{P} - \mathbf{Q} \rangle \cdot \vec{n}}{\vec{v} \cdot \vec{n}}$$

and the projected point of intersection $\mathbf{R}$ is equal to

$$\mathbf{R} = \mathbf{Q} + \frac{\langle \mathbf{P} - \mathbf{Q} \rangle \cdot \vec{n}}{\vec{v} \cdot \vec{n}} \vec{v}$$

Projecting a Vector onto a Plane

Given a plane defined by a point, $\mathbf{P}$, and a normal vector, $\vec{n}$, and a vector, $\vec{v}$, in $\mathbb{R}^3$ (Figure 4.2). We calculate the projection of $\vec{v}$ onto the plane by calculating the intersection of the line

$$(\mathbf{P} + \vec{v}) - t\vec{n}$$

and the plane.

This follows exactly the treatment of the above case, with $\mathbf{Q}$ replaced by $\mathbf{P} + \vec{v}$ and $\vec{v}$ replaced with $-\vec{n}$. We obtain

$$\begin{aligned} 0 &= [\mathbf{P} + \vec{v} + t(-\vec{n}) - \mathbf{P}] \cdot \vec{n} \\ &= [\vec{v} + t(-\vec{n})] \cdot \vec{n} \\ &= \vec{v} \cdot \vec{n} - t \end{aligned}$$

assuming that $\vec{n}$ is a unit vector. Therefore,

$$t = \vec{v} \cdot \vec{n}$$

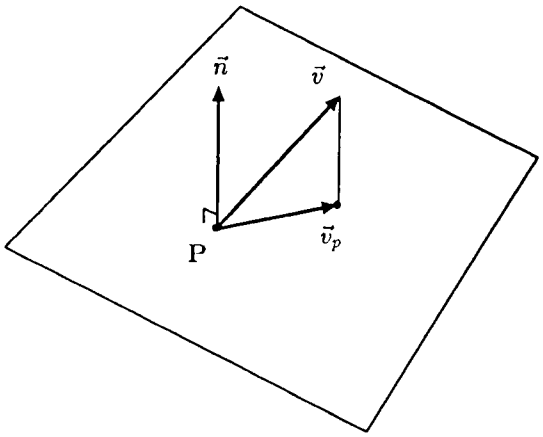

Figure 4.2: Projecting a Vector onto a Plane

and the vector projection $\vec{v}_p$ is equal to

$$\vec{v}_p = \vec{v} - [\vec{v} \cdot \vec{n}]\,\vec{n}$$

Closest Point on a Plane to a Point

Given a plane, $\mathcal{P}$, defined by the point-vector pair $(\mathbf{P}, \vec{n})$, we may find the closest point, $\mathbf{R}$, on this plane to a point, $\mathbf{Q}$, by projecting $\mathbf{Q}$ onto $\mathcal{P}$ along normal vector $\vec{n}$. Using the same method as above, we have:

$$\begin{aligned} \mathrm{R} &= \mathrm{Q} + \left[\frac{\langle \mathrm{P} - \mathrm{Q} \rangle \cdot \vec{n}}{\vec{n} \cdot \vec{n}}\right] \vec{n} \\ &= \mathrm{Q} + [\langle \mathrm{P} - \mathrm{Q} \rangle \cdot \vec{n}]\,\vec{n} \end{aligned}$$

The Closest Point on a Line to a Point

Given a line, $\overline{\mathrm{P_0P_1}}$, and a point, $\mathbf{P}$, we may find the closest point, $\mathbf{P}_p$, on $\overline{\mathrm{P_0P_1}}$ to $\mathbf{P}$.

$$\mathrm{P}_p = \mathrm{P}_0 + \left[\frac{\langle \mathrm{P}_1 - \mathrm{P}_0 \rangle \cdot \langle \mathrm{P} - \mathrm{P}_0 \rangle}{|\,\mathrm{P}_1 - \mathrm{P}_0\,|\,|\,\mathrm{P} - \mathrm{P}_0\,|}\right] \langle \mathrm{P}_1 - \mathrm{P}_0 \rangle$$

The Intersection of Two Planes

Two non-parallel planes intersect in a line (Figure 4.3). Consider two such planes defined by the point-and-vector pairs $(\mathbf{P}_1, \vec{n}_1)$ and $(\mathbf{P}_2, \vec{n}_2)$ respectively. We can uniquely specify

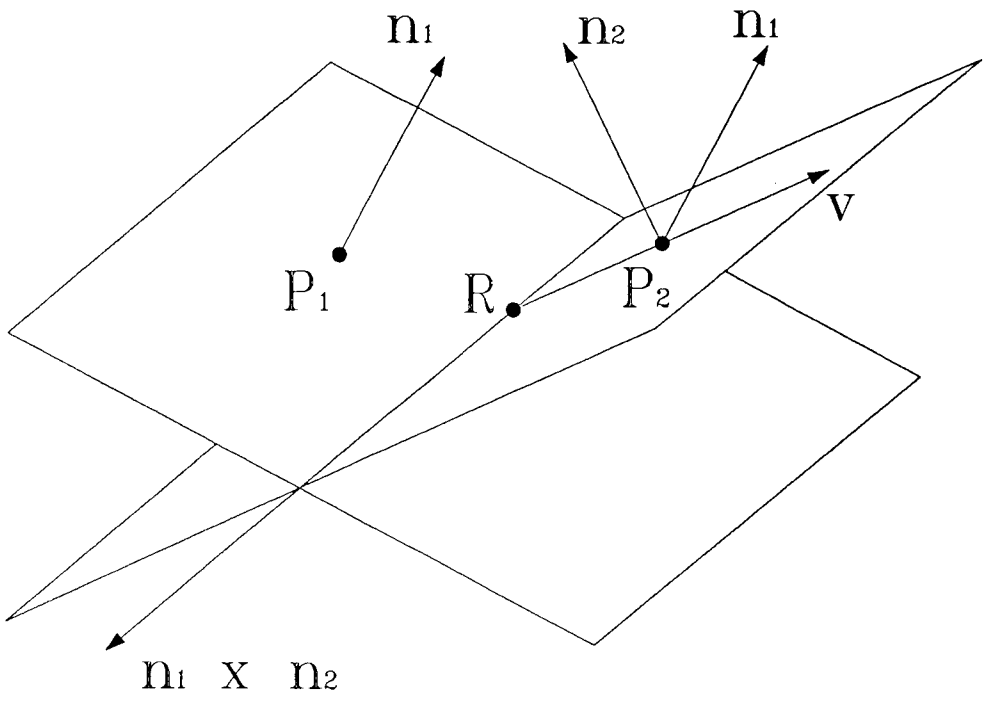

Figure 4.3: Intersection of Two Planes

the intersection line by exhibiting both its direction and a point on the line. These can be determined by the following process:

- Determine the direction vector for the line of intersection. This vector is clearly $\vec{n}_1 \times \vec{n}_2$.
- Let $\vec{v}$ be the projection of $\vec{n}_1$ onto the plane defined by $\mathbf{P}_2$ and $\vec{n}_2$.
- Let $\mathbf{R}$ be the projection of $\mathbf{P}_2$ onto the plane defined by $\mathbf{P}_1$ and $\vec{n}_1$ in the direction $\vec{v}$.

Then the line is specified by the pair $(\mathbf{R}, \vec{n}_1 \times \vec{n}_2)$.

The Intersection of Three Planes

The intersection of three planes is a point provided:

- No two of the three are parallel
- There does not exist a fourth plane to which all three are perpendicular

If we consider three planes, $(\mathbf{P}_1, \vec{n}_1)$, $(\mathbf{P}_2, \vec{n}_2)$, and $(\mathbf{P}_3, \vec{n}_3)$, then the calculation of the intersection point proceeds as follows:

- By the above procedure find the equation of a line that is the intersection of the planes $(\mathbf{P}_1, \vec{n}_1)$ and $(\mathbf{P}_2, \vec{n}_2)$. Let $\mathbf{Q}$ be a point on this line and $\vec{v}$ be the vector direction of the line.
- Project the point $\mathbf{Q}$ along the direction $\vec{v}$ onto the plane $(\mathbf{P}_3, \vec{n}_3)$. The resulting point is the point of intersection of the three planes.

4.1.2 Subscripts

Given a cube, we will present a method to obtain piecewise planar approximations of the inscribed sphere and, in the limit, the sphere itself. We will consider this cube and the objects obtained from it to be control polyhedra for the sphere. When considering a vertex, $\mathbf{P}_i^k$, of the control polyhedron, it will be helpful to be able to refer to the features in its vicinity. We will refer to the edges incident to the vertex as $\mathbf{e}_{i,j}^k$ for $j = 0, 1, ..., n-1$ where n is the valence of the vertex. [2] The vertex at the other end of edge $\mathbf{e}_{i,j}^k$ is $\mathbf{P}_{i,j}^k$. If we pick an edge and label it $\mathbf{e}_{i,0}^k$, then the next edge counter-clockwise around the vertex is $\mathbf{e}_{i,1}^k$, then $\mathbf{e}_{i,2}^k$, etc. Each pair of consecutive edges emanating from a vertex define a plane. Given two edges, $\mathbf{e}_{i,j}^k$ and $\mathbf{e}_{i,j+1}^k$, we will label the plane defined by them $\mathcal{P}_{i,j+2}^k$. It will be useful to consider a plane to be a point-vector pair. Given a plane, $\mathcal{P}_{i,j}^k$, it will have a point, $\mathbf{C}_{i,j}^k$, and a normal vector, $\vec{n}_{i,j}^k$. When an edge, $\mathbf{e}_{i,j}^k$, is replaced by a new Type E face, this face will lie in the plane $\mathcal{P}_{i,j}^{k+1}$. Using Doo's method, a Type V face that replaces $\mathbf{P}_i^k$ lies in the plane labeled $\mathcal{P}_{i,j}^{k+1}$ where j is the valence of $\mathbf{P}_i^k$.

4.1.3 Geometry of Spheres

It will be useful to consider relationships between spheres, circles, and various lines and points. We give the following definitions.

[2] The subscript j is always modulo n

Pencil of Planes

Consider a line, $\mathbf{L}$, in $\mathbb{R}^3$ along with the set of all planes in which $\mathbf{L}$ lies. We will call this set of planes the *pencil* of planes of the line $\mathbf{L}$.

Common Perpendicular

In $\mathbb{R}^3$, consider a line, $\mathbf{L}$, and two points, $\mathbf{P}_0$ and $\mathbf{P}_1$, such that neither point lies on $\mathbf{L}$. There are two points that lie on $\mathbf{L}$ that are the closest points on $\mathbf{L}$ to $\mathbf{P}_0$ and $\mathbf{P}_1$ respectively. When these closest points coincide we will consider this to be one point and call it the *common perpendicular* to $\mathbf{P}_0$ and $\mathbf{P}_1$ on $\mathbf{L}$.

Normal Vector of a Sphere

Consider a point, $\mathbf{C}$, on the surface of a sphere along with the normal vector to the sphere at $\mathbf{C}$, $\vec{n}$. Vector $\vec{n}$ is

$$\vec{n} = \frac{\langle \mathbf{C} - \mathbf{P}_c \rangle}{| \langle \mathbf{C} - \mathbf{P}_c \rangle |}$$

where $\mathbf{P}_c$ is the center of the sphere. If the sphere is a unit sphere centered on the origin, then we may say

$$\vec{n} = \langle \mathbf{C} \rangle$$

We note that $\vec{n}$ will lie in any plane that $\overline{\mathbf{CP}_c}$ does.

Great Circle

If we intersect a sphere with a plane, $\mathcal{P}$, that passes through the center of the sphere, $\mathbf{P}_c$, we obtain a *great circle*. This is a circle that lies in $\mathcal{P}$ and has the same radius and center as the sphere. Consequently, every point on the circle lies on the sphere. Consider a point, $\mathbf{C}$, on this great circle, and the normal vector to the sphere, $\vec{n}$, at this point. Since $\overline{\mathbf{CP}_c}$ lies in $\mathcal{P}$, $\vec{n}$ does also. Consequently, $\vec{n}$ is normal to the great circle at $\mathbf{C}$. Consider the diameter on which $\mathbf{C}$ lies. Every great circle formed by a plane from the pencil of planes for this diameter will pass through $\mathbf{C}$ and the point on the surface of the sphere opposite to $\mathbf{C}$. Conversely, every great circle passing through a point on the surface of the sphere lies in a plane from the pencil of planes of the diameter to that point.

Angular Measurements

Consider a circle along with three points on the circle, C_0, C_1, and C_2. By the definition of a radian, we may say that if the arc distance from C_0 to C_1, $\left|\widehat{C_0C_1}\right|$, is equal to the arc distance $\left|\widehat{C_1C_2}\right|$, then the angle between the radius to C_0 and the radius to C_1 is equal to the angle between the radius to C_1 and the radius to C_2. We will call the arc distance between two points on the circle the *distance* between them. Additionally, we may say

$$\left|\overline{C_0C_1}\right| = \left|\overline{C_1C_2}\right|$$

The line segment $\overline{C_0C_1}$ is called the *chord* from C_0 to C_1 and the distance $\left|\overline{C_0C_1}\right|$ is called the *chord distance* to differentiate it from arc distance.

Spherical Coordinate System

It will be useful to establish a coordinate system for a sphere similar to that used on the Earth. There will be two diametrically opposed points called *poles*. The diameter to these poles will be called the *axis* and the great circle perpendicular to the axis will be called the *equator*. We may fully define a coordinate system by specifying a point on the surface of the sphere to be a pole, or by specifying a great circle to be the equator. Circles formed by the intersection of the sphere with planes parallel to the plane of the equator will be called *latitude lines*. Excluding the equator, latitude lines are not great circles. We may measure a latitude line's distance from the equator or from one of the poles. Consider a point, C, on the surface of the sphere from which segments of two great circles, $\widehat{e_0}$ and $\widehat{e_1}$, emanate. If we set C as the pole we may determine the points, C_0 and C_1, at which $\widehat{e_0}$ and $\widehat{e_1}$ will intersect the equator. We will call the arc distance between C_0 and C_1 the *hour angle* between $\widehat{e_0}$ and $\widehat{e_1}$ and designate it $\angle_h(C)$. This is the same angle we would find between the normal vectors of the planes in which $\widehat{e_0}$ and $\widehat{e_1}$ lie.

Spherical Triangles

We may define a *spherical triangle* by three points, C_0, C_1, and C_2, on the surface of a sphere, such that

1. Vectors $\langle C_i - P_c \rangle$, $i = 0, 1, 2$ are linearly independent. This implies that no pair is diametrically opposed and they do not coincide.

2. $0 < \angle_h(\mathbf{C}_i) < \pi$

A spherical triangle has edges, $\widehat{\mathbf{C}_0\mathbf{C}_1}$, $\widehat{\mathbf{C}_1\mathbf{C}_2}$, and $\widehat{\mathbf{C}_2\mathbf{C}_0}$, that are arcs of great circles. We will let $\mathbf{c}_i = \left|\mathbf{C}_{i+1}\widehat{\mathbf{C}}_{i+2}\right|$, that is, $\mathbf{c}_i$ is the length of the side opposite $\mathbf{C}_i$. Since the lengths of these edges are angles, spherical triangles have six angular components: three arc angles and three hour angles. For any of these spherical triangles we may say the following

$$\pi < \angle_h(\mathbf{C}_0) + \angle_h(\mathbf{C}_1) + \angle_h(\mathbf{C}_2) \tag{4.1}$$

$$\cos\angle_h(\mathbf{C}_i) = \frac{\cos(\mathbf{c}_i) - [\cos(\mathbf{c}_{i+1})\cos(\mathbf{c}_{i+2})]}{\sin(\mathbf{c}_{i+1})\sin(\mathbf{c}_{i+2})} \tag{4.2}$$

We will be interested in spherical triangles where $\angle_h(\mathbf{C}_i) \leq \frac{\pi}{2}$. To prove this true, we can show that $\cos\angle_h(\mathbf{C}_i) \geq 0$. Consider equation 4.2. First we will look at the denominator, $\sin(\mathbf{c}_{i+1})\sin(\mathbf{c}_{i+2})$. From requirement 2 we may say $0 < \mathbf{c}_i \leq \pi$. Therefore, we may say $0 < \sin(\mathbf{c}_i) \leq 1$ and conclude that the denominator is positive. Considering the numerator, we may conclude

$$\cos(\mathbf{c}_i) \geq \cos(\mathbf{c}_{i+1})\cos(\mathbf{c}_{i+2}) \Leftrightarrow \cos\angle_h(\mathbf{C}_i) \geq 0 \tag{4.3}$$

Geodesic Arcs

Consider two differing points on the surface of a sphere, $\mathbf{C}_0$ and $\mathbf{C}_1$. The shortest arc between these points is called the *geodesic*. Suppose that $\mathbf{C}_0$ and $\mathbf{C}_1$ are diametrically opposed. Then there are infinitely many arcs of the same length between them. We may find one of these geodesics, $\widehat{\mathbf{C}_0\mathbf{C}_1}$, by choosing a plane from the pencil of planes of the diameter from $\mathbf{C}_0$ to $\mathbf{C}_1$. Intersect this plane with the sphere and choose one of it halves to be the geodesic. Otherwise, define a plane, $\mathcal{P}_c$, using points $\mathbf{C}_0$, $\mathbf{C}_1$, and the center of the sphere. Then intersect $\mathcal{P}_c$ with the sphere. The resulting great circle passes through $\mathbf{C}_0$ and $\mathbf{C}_1$ and is divided into two parts by them. The smaller of these two parts is the geodesic from $\mathbf{C}_0$ to $\mathbf{C}_1$. As noted in the definition **Great Circles**, the vectors normal to the sphere at points $\mathbf{C}_0$ and $\mathbf{C}_1$ lie in $\mathcal{P}_c$ and are normal to this great circle.

Projecting a Point onto a Sphere

We may define a line, $\overline{\mathbf{P}_c\mathbf{R}}$, where $\mathbf{P}_c$ is the center of a sphere and $\mathbf{R}$ is some different point. If we intersect $\overline{\mathbf{P}_c\mathbf{R}}$ with the sphere we will obtain a point of intersection $\hat{\mathbf{R}}$. We will say

that $\hat{\mathbf{R}}$ is the *projection* of $\mathbf{R}$ onto the sphere. We note that every point on $\overline{\mathbf{P}_c\mathbf{R}}$ projects to $\hat{\mathbf{R}}$.

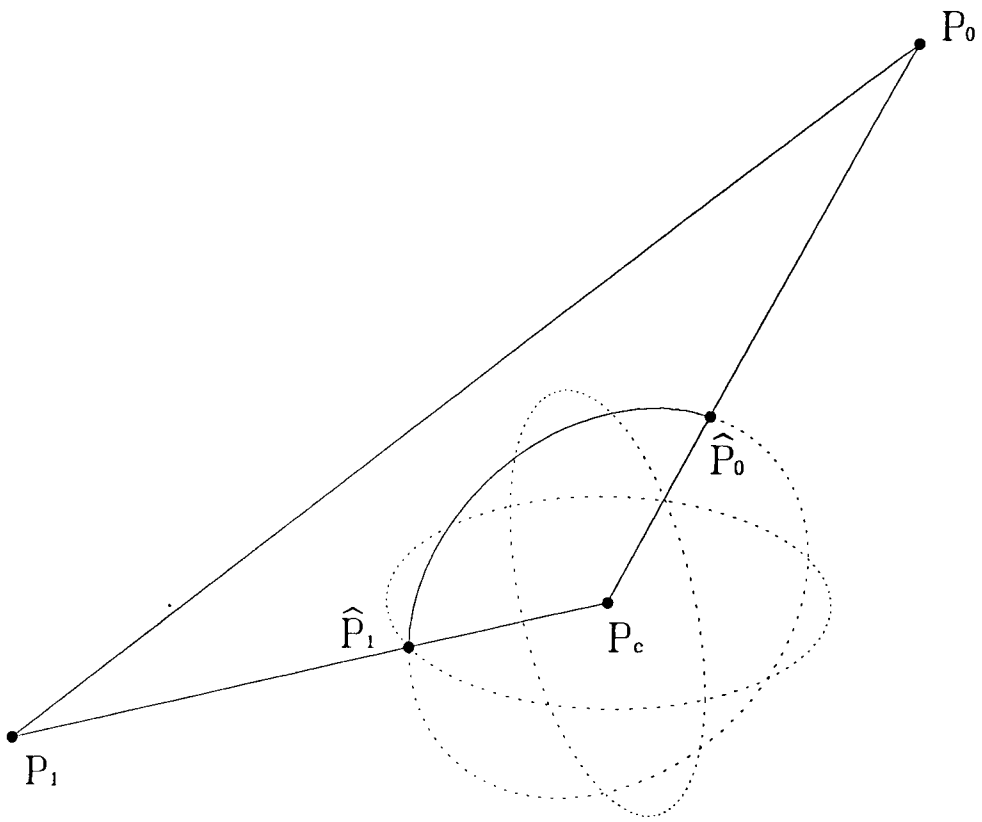

Figure 4.4: Line Projected onto Sphere

Projecting a Line onto a Sphere

We may define a line, $\mathbf{L}$, and a sphere such that $\mathbf{L}$ does not pass through the center of the sphere, $\mathbf{P}_c$. Using $\mathbf{L}$ and $\mathbf{P}_c$, we may define a plane, $\mathcal{P}_c$. If we intersect $\mathcal{P}_c$ with the sphere, we will obtain a great circle, $\hat{\mathbf{L}}$. We will say that $\hat{\mathbf{L}}$ is the *projection* of $\mathbf{L}$ onto the sphere. We note that any line in the plane $\mathcal{P}_c$ will project to $\hat{\mathbf{L}}$. Consider a segment of $\mathbf{L}$, $\mathbf{e}$, with end points $\mathbf{P}_0$ and $\mathbf{P}_1$, neither at infinity (Figure 4.4). If we project points $\mathbf{P}_0$ and $\mathbf{P}_1$ onto

the sphere, we will obtain projected points $\hat{\mathbf{P}}_0$ and $\hat{\mathbf{P}}_1$. The two projected points will lie on $\hat{\mathbf{L}}$ and divide it into two arcs. We will call the minor arc the *projection* of **e** onto the sphere and label it $\hat{\mathbf{e}}$. From the definition **Projecting a Point onto a Sphere** we note that a line from any point on the line $\overline{\mathbf{P}_0\mathbf{P}_c}$ to any point on the line $\overline{\mathbf{P}_1\mathbf{P}_c}$ will project to $\hat{\mathbf{e}}$. Projected line $\hat{\mathbf{e}}$ is the geodesic from $\hat{\mathbf{P}}_0$ to $\hat{\mathbf{P}}_1$ on the surface of the sphere. Since the geodesic lies in the plane $\mathcal{P}_c$ and is an arc of $\hat{\mathbf{L}}$, its length is the arc distance from $\hat{\mathbf{P}}_0$ to $\hat{\mathbf{P}}_1$ measured along $\hat{\mathbf{L}}$.

4.2 Doo's Algorithm cannot be Extended to Create Spheres

We were successful in our attempt to modify Chaikin's algorithm so that it could generate rational curves. However, we will show that it is impossible to directly extend Doo's algorithm so that it will produce a sphere when applied to a cube. Consider a cube with side length 2 and vertices $(\pm 1, \pm 1, \pm 1)$. Each of the cube's faces lies in a plane tangent to the inscribed unit sphere centered on the origin. As the cube is refined, we would like all new faces to continue to be tangent to the unit sphere. First we will need to choose a ratio so that the resulting Type **E** faces are tangent to the unit sphere. Because of the symmetry of the cube, a level $k = 1$ Type **E** face is parallel to the edge it replaces and has an alpha angle of $\frac{3\pi}{4}$ to the faces adjacent to this edge. With an appropriate ratio, the new Type **E** faces will be tangent to the unit sphere at their centroids. Given this, we may define the planes in which the new Type **E** faces lie.

For instance, consider vertices (Figure 4.7)

$$\begin{aligned} \mathbf{P}_0 &= (1,1,1) \\ \mathbf{P}_{0,0} &= (-1,1,1) \\ \mathbf{P}_{0,1} &= (1,-1,1) \\ \mathbf{P}_{0,2} &= (1,1,-1) \end{aligned}$$

Point $\mathbf{P}_0$ has three adjacent faces with centroids

$$\begin{aligned} \mathbf{C}_{0,0} &= (1,0,0) \\ \mathbf{C}_{0,1} &= (0,1,0) \\ \mathbf{C}_{0,2} &= (0,0,1) \end{aligned}$$

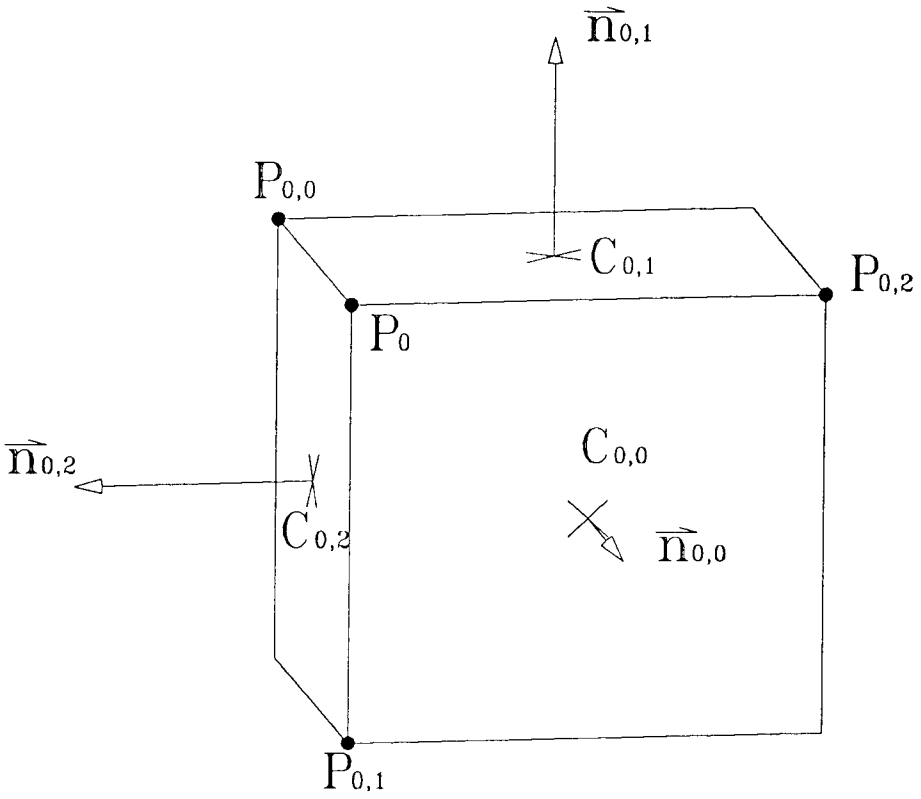

Figure 4.5: Vertex $\mathbf{P}_0$ of the Cube

these faces have normal vectors

$$\begin{aligned} \vec{n}_{0,0} &= \langle 1, 0, 0 \rangle \\ \vec{n}_{0,1} &= \langle 0, 1, 0 \rangle \\ \vec{n}_{0,2} &= \langle 0, 0, 1 \rangle \end{aligned}$$

and they lie in planes tangent to the unit sphere

$$\begin{aligned} \mathcal{P}_{0,0} &= (\mathbf{C}_{0,0}, \vec{n}_{0,0}) \\ \mathcal{P}_{0,1} &= (\mathbf{C}_{0,1}, \vec{n}_{0,1}) \\ \mathcal{P}_{0,2} &= (\mathbf{C}_{0,2}, \vec{n}_{0,2}) \end{aligned}$$

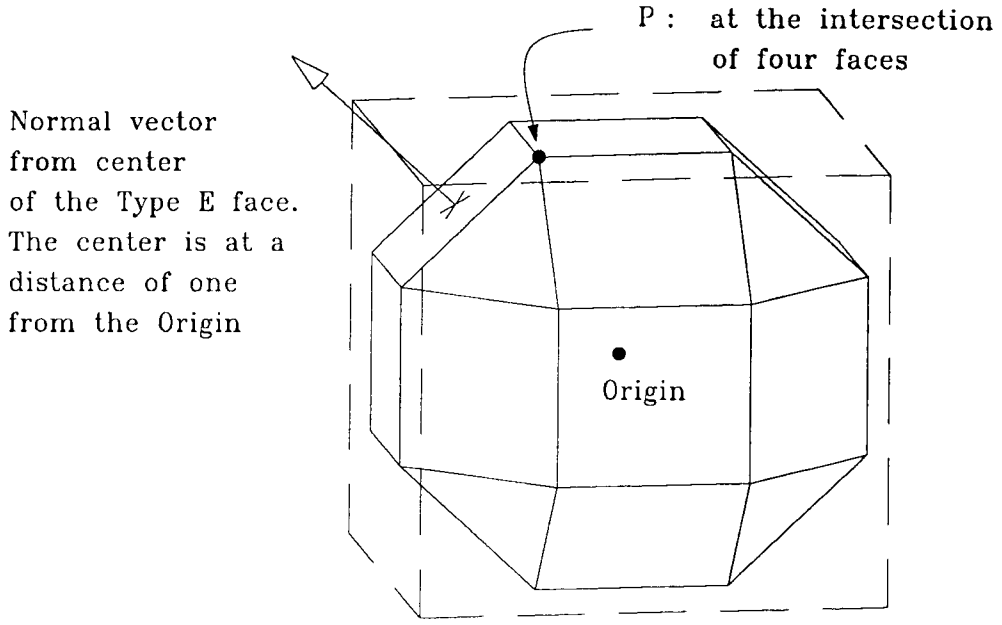

Figure 4.6: Type E Face Tangent to the Unit Sphere

Each edge will be replaced by a Type E face that lies in a plane that is tangent to the unit sphere such that the centroid of these new faces will touch the sphere (Figure 4.6). For example, edge $\overline{\mathbf{P}_0\mathbf{P}_{0,0}}$ will be replaced by a face tangent to the unit sphere at its centroid

$$\mathbf{C}^1_{0,0} = \left(0, \frac{\sqrt{2}}{2}, \frac{\sqrt{2}}{2}\right)$$

and it will lie in a plane with normal vector

$$\vec{n}^1_{0,0} = \left\langle 0, \frac{\sqrt{2}}{2}, \frac{\sqrt{2}}{2} \right\rangle$$

This gives the plane

$$\mathcal{P}^1_{0,0} = \left(\mathbf{C}^1_{0,0}, \vec{n}^1_{0,0}\right)$$

Similarly the other two edges adjacent to $\mathbf{P}_0$, $\overline{\mathbf{P}_0\mathbf{P}_{0,1}}$ and $\overline{\mathbf{P}_0\mathbf{P}_{0,2}}$ are replaced by faces that lie in planes

$$\mathcal{P}^1_{0,1} = \left(\mathbf{C}^1_{0,1}, \vec{n}^1_{0,1}\right)$$

$$\mathcal{P}^1_{0,2} = \left(\mathbf{C}^1_{0,2}, \vec{n}^1_{0,2}\right)$$

where

$$\mathbf{C}^1_{0,1} = \left(\frac{\sqrt{2}}{2}, 0, \frac{\sqrt{2}}{2}\right)$$
$$\mathbf{C}^1_{0,2} = \left(\frac{\sqrt{2}}{2}, \frac{\sqrt{2}}{2}, 0\right)$$

are the centroids of the faces and

$$\vec{n}^1_{0,1} = \left\langle \frac{\sqrt{2}}{2}, 0, \frac{\sqrt{2}}{2} \right\rangle$$
$$\vec{n}^1_{0,2} = \left\langle \frac{\sqrt{2}}{2}, \frac{\sqrt{2}}{2}, 0 \right\rangle$$

are the normal vectors of the planes.

Using Doo's method, each valence-three vertex of the cube is replaced by three new points. These new points lie in the planes of the faces adjacent to the vertex and are a combination of the vertex and the centroid of the face using an appropriate weight t_0. For $\mathbf{P}_0$ these three new face points are

$$\mathbf{P}^1_{0,0} = (1 - t_0)\,\mathbf{P}_0 + t_0\mathbf{C}_{0,0}$$
$$\mathbf{P}^1_{0,1} = (1 - t_0)\,\mathbf{P}_0 + t_0\mathbf{C}_{0,1}$$
$$\mathbf{P}^1_{0,2} = (1 - t_0)\,\mathbf{P}_0 + t_0\mathbf{C}_{0,2}$$

Additionally, these new points lie at the intersection of four faces: one original face, two of the new Type E faces, and a new Type V face. Using the method presented in section 4.1.1, we may calculate the point of intersection using any three of these planes (Figure 4.7). For instance, $\mathbf{P}^1_{0,0}$ is at the intersection of planes $\mathcal{P}_{0,0}$, $\mathcal{P}^1_{0,1}$, and $\mathcal{P}^1_{0,2}$. Using this to calculate $\mathbf{P}^1_{0,0}$, we may discover the appropriate weight to use. First, we will calculate the line of intersection, $\mathbf{L}^1_{0,1}(\mathbf{Q}, \vec{v})$, between $\mathcal{P}_{0,0}$ and $\mathcal{P}^1_{0,1}$. $\mathbf{L}^1_{0,1}$ is defined by a point, $\mathbf{Q}$, that lies on the line and a direction vector, $\vec{v}$. The direction vector, $\vec{v}$, is simply the cross product of the normal vectors of $\mathcal{P}_{0,0}$ and $\mathcal{P}^1_{0,1}$

$$\begin{aligned}\vec{v} &= \vec{n}_{0,0} \times \vec{n}^1_{0,1} \\ &= \langle 1, 0, 0 \rangle \times \left\langle \frac{\sqrt{2}}{2}, 0, \frac{\sqrt{2}}{2} \right\rangle \\ &= \left\langle 0, \frac{\sqrt{2}}{2}, 0 \right\rangle\end{aligned}$$

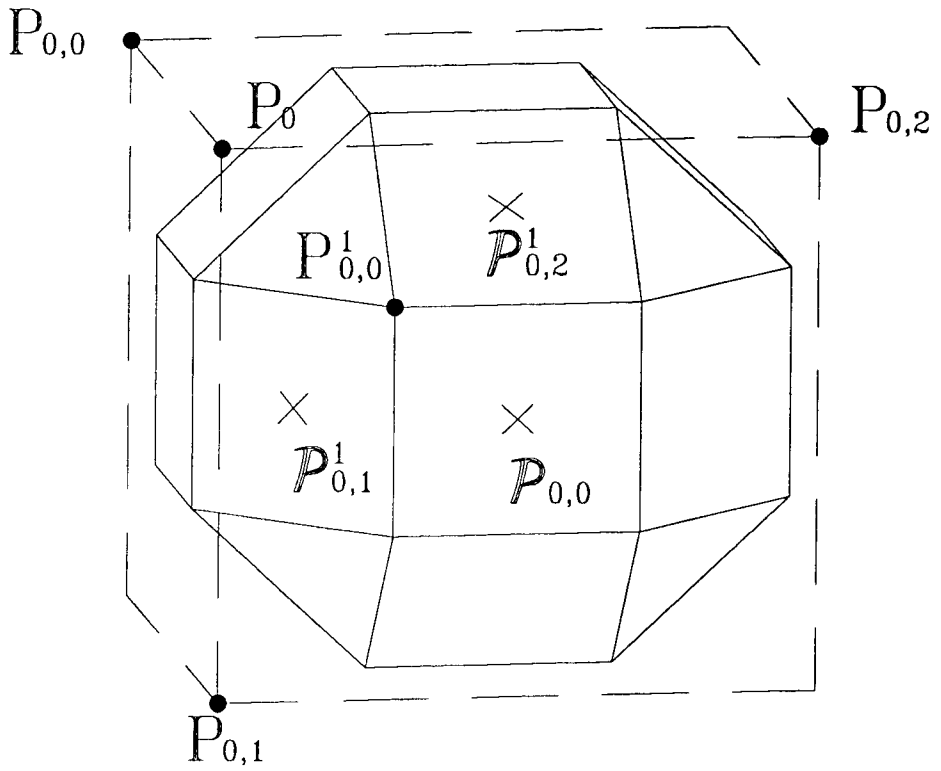

Figure 4.7: Cube after First Refinement Using Rational Doo's

A point, $\mathbf{Q}$, on this line may be defined by projecting a point on $\mathcal{P}_{0,0}$, $\mathbf{C}_{0,0}$, onto $\mathcal{P}^1_{0,1}$ using any vector that lies in $\mathcal{P}_{0,0}$. We may find a vector, $\vec{v_p}$, that lies in $\mathcal{P}_{0,0}$ by projecting $\vec{n}^1_{0,1}$ onto $\mathcal{P}_{0,0}$

$$\begin{aligned}
\vec{v_p} &= \vec{n}^1_{0,1} - \left(\vec{n}^1_{0,1} \cdot \vec{n}_{0,0}\right) \vec{n}_{0,0} \\
&= \left\langle \frac{\sqrt{2}}{2}, 0, \frac{\sqrt{2}}{2} \right\rangle - \left(\left\langle \frac{\sqrt{2}}{2}, 0, \frac{\sqrt{2}}{2} \right\rangle \cdot \langle 1,0,0 \rangle \right) \langle 1,0,0 \rangle \\
&= \left\langle \frac{\sqrt{2}}{2}, 0, \frac{\sqrt{2}}{2} \right\rangle - \left(\frac{\sqrt{2}}{2} \right) \langle 1,0,0 \rangle
\end{aligned}$$

$$
\begin{aligned}
&= \left\langle \frac{\sqrt{2}}{2}, 0, \frac{\sqrt{2}}{2} \right\rangle - \left\langle \frac{\sqrt{2}}{2}, 0, 0 \right\rangle \\
&= \left\langle 0, 0, \frac{\sqrt{2}}{2} \right\rangle
\end{aligned}
$$

Then we will project $\mathbf{C}_{0,0}$ onto $\mathcal{P}^1_{0,1}$ along $\vec{v_p}$

$$
\begin{aligned}
\mathbf{Q} &= \mathbf{C}_{0,0} + \frac{\left\langle \mathbf{C}^1_{0,1} - \mathbf{C}_{0,0} \right\rangle \cdot \vec{n}^1_{0,1}}{\vec{v_p} \cdot \vec{n}^1_{0,1}} \vec{v_p} \\
&= (1,0,0) + \frac{\left\langle \left(\frac{\sqrt{2}}{2}, 0, \frac{\sqrt{2}}{2}\right) - (1,0,0) \right\rangle \cdot \left\langle \frac{\sqrt{2}}{2}, 0, \frac{\sqrt{2}}{2} \right\rangle}{\left\langle 0, 0, \frac{\sqrt{2}}{2} \right\rangle \cdot \left\langle \frac{\sqrt{2}}{2}, 0, \frac{\sqrt{2}}{2} \right\rangle} \left\langle 0, 0, \frac{\sqrt{2}}{2} \right\rangle \\
&= (1,0,0) + \frac{1 - \frac{\sqrt{2}}{2}}{\frac{1}{2}} \left\langle 0, 0, \frac{\sqrt{2}}{2} \right\rangle \\
&= (1,0,0) + \left\langle 0, 0, \sqrt{2} - 1 \right\rangle \\
&= \left(1, 0, \sqrt{2} - 1\right)
\end{aligned}
$$

which gives

$$
\mathbf{L}^1_{0,1} = \left(\left(1, 0, \sqrt{2} - 1\right), \left\langle 0, \frac{\sqrt{2}}{2}, 0 \right\rangle \right)
$$

Now, we may find the point, $\mathbf{P}^1_{0,0}$, that is the intersection of planes $\mathcal{P}_{0,0}$, $\mathcal{P}^1_{0,1}$, and $\mathcal{P}^1_{0,2}$ by projecting point $\mathbf{Q}$ onto $\mathcal{P}^1_{0,2}$ along $\vec{v}$

$$
\begin{aligned}
\mathbf{P}^1_{0,0} &= \mathbf{Q} + \frac{\left\langle \mathbf{C}^1_{0,2} - \mathbf{Q} \right\rangle \cdot \vec{n}^1_{0,2}}{\vec{v} \cdot \vec{n}^1_{0,2}} \vec{v} \\
&= \left(1, 0, \sqrt{2} - 1\right) + \\
&\quad \frac{\left\langle \left(\frac{\sqrt{2}}{2}, \frac{\sqrt{2}}{2}, 0\right) - \left(1, 0, \sqrt{2} - 1\right) \right\rangle \cdot \left\langle \frac{\sqrt{2}}{2}, \frac{\sqrt{2}}{2}, 0 \right\rangle}{\left\langle 0, \frac{\sqrt{2}}{2}, 0 \right\rangle \cdot \left\langle \frac{\sqrt{2}}{2}, \frac{\sqrt{2}}{2}, 0 \right\rangle} \left\langle 0, \frac{\sqrt{2}}{2}, 0 \right\rangle \\
&= \left(1, 0, \sqrt{2} - 1\right) + \frac{1 - \frac{\sqrt{2}}{2}}{\frac{1}{2}} \left\langle 0, \frac{\sqrt{2}}{2}, 0 \right\rangle \\
&= \left(1, 0, \sqrt{2} - 1\right) + \left\langle 0, \sqrt{2} - 1, 0 \right\rangle \\
&= \left(1, \sqrt{2} - 1, \sqrt{2} - 1\right)
\end{aligned}
$$

We may now solve for the weight, t_0, used to obtain this point

$$
\mathbf{P}^1_{0,0} = (1 - t_0)\,\mathbf{P}_0 + t_0 \mathbf{C}_{0,0}
$$

$$
\begin{aligned}
\left(1, \sqrt{2}-1, \sqrt{2}-1\right) &= (1-t_0)(1,1,1) + t_0(1,0,0) \\
\left(1, \sqrt{2}-1, \sqrt{2}-1\right) &= (1,1,1) - t_0(1,1,1) + t_0(1,0,0) \\
\left(1, \sqrt{2}-1, \sqrt{2}-1\right) &= (1,1,1) + t_0[(1,0,0) - (1,1,1)] \\
\left(0, \sqrt{2}-2, \sqrt{2}-2\right) &= t_0(0,-1,-1) \\
\left(0, 2-\sqrt{2}, 2-\sqrt{2}\right) &= t_0(0,1,1) \\
t_0 &= 2-\sqrt{2}
\end{aligned}
$$

Using this value for t_0 we solve for $\mathbf{P}^1_{0,1}$ and $\mathbf{P}^1_{0,2}$ getting

$$
\begin{aligned}
\mathbf{P}^1_{0,1} &= \left(\sqrt{2}-1, 1, \sqrt{2}-1\right) \\
\mathbf{P}^1_{0,2} &= \left(\sqrt{2}-1, \sqrt{2}-1, 1\right)
\end{aligned}
$$

These are the vertices of the new Type V face that replaces vertex $\mathbf{P}_0$. Calculating this face's centroid we get

$$
\begin{aligned}
\mathbf{C}^1_{0,3} &= \frac{\left(\mathbf{P}^1_{0,0} + \mathbf{P}^1_{0,1} + \mathbf{P}^1_{0,2}\right)}{3} \\
\mathbf{C}^1_{0,3} &= \frac{\left(\frac{\sqrt{2}}{2} + \sqrt{2} - 1, \frac{\sqrt{2}}{2} + \sqrt{2} - 1, \frac{\sqrt{2}}{2} + \sqrt{2} - 1\right)}{3}
\end{aligned}
$$

However, the point does not lie on the unit sphere; it is ≈ 1.0556 from the origin (Figure 4.8). Using the method described in section 4.1.1, we can show that this is the closest point to the origin on the plane in which this face lies. Of course, if a different weight were chosen so that this Type V face were on the unit sphere, the adjacent Type E faces would be inside of the unit sphere. It appears, then, that there is no weighting function that can be used to obtain a sphere from a cube using Doo's method.

4.3 Generating a Sphere from a Cube

4.3.1 General Idea

In two dimensions we started with a square where each of its edges was tangent to the inscribed circle. The corner vertices were cut off and replaced with edge lines that were also tangent to the circle. In three dimensions we start with a cube where each of its face planes is tangent to the inscribed sphere.

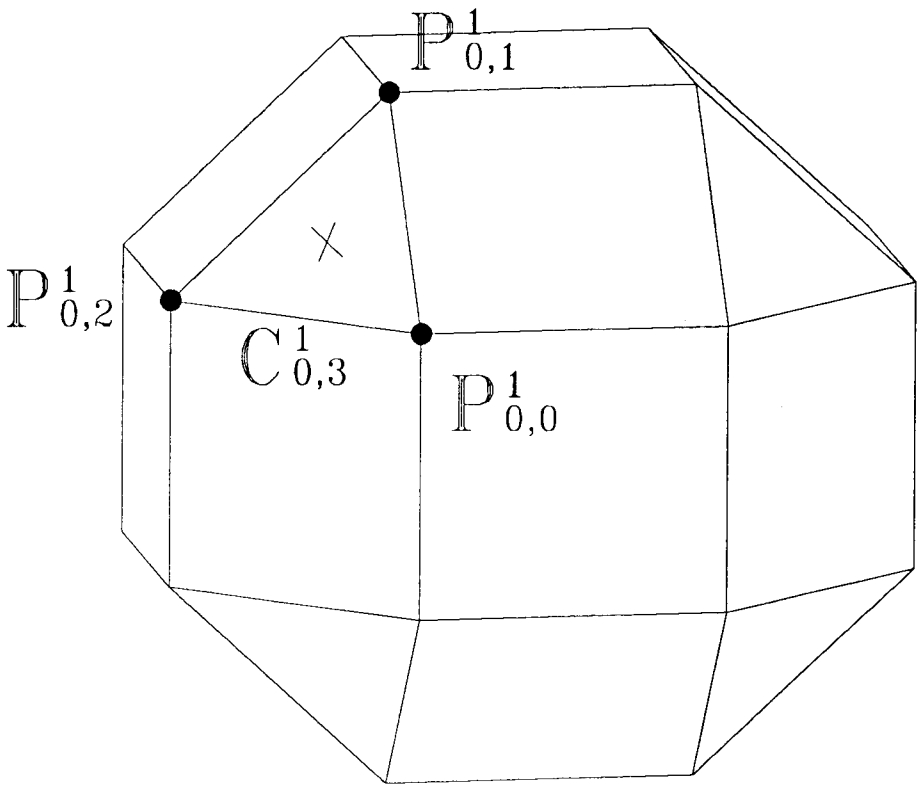

Figure 4.8: Type V Face not on Sphere

We cut off each edge line and replace it with a new face plane that is tangent to the sphere and will refer to this as *edge-beveling*. In this way, we iteratively produce polyhedra that have a structure similar to the cube, that is, each face lies in a plane that is tangent to the sphere, and each edge and vertex lies at the intersection of adjacent tangent planes. Beginning with the six-faced cube (Figure 4.9), after one iteration the number of faces grows to eighteen.

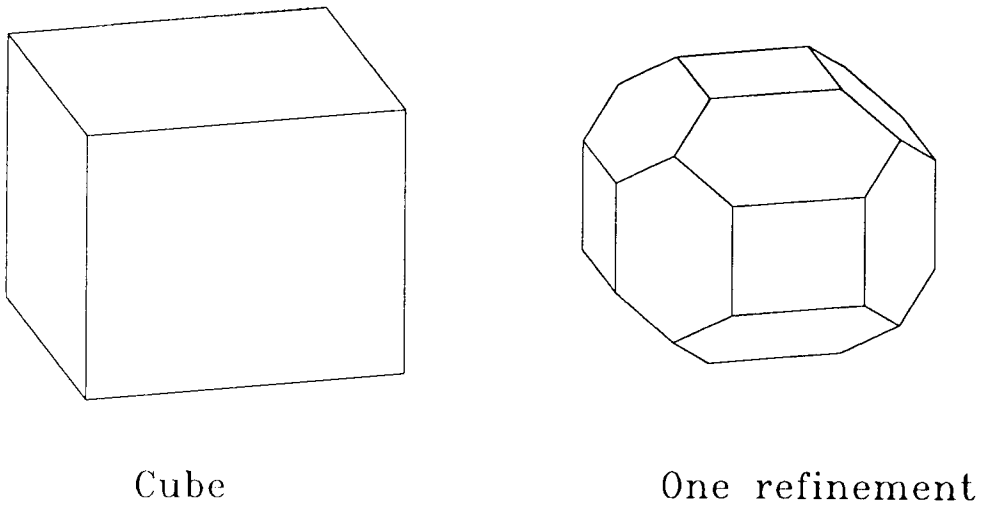

Figure 4.9: Results of First Refinement Step

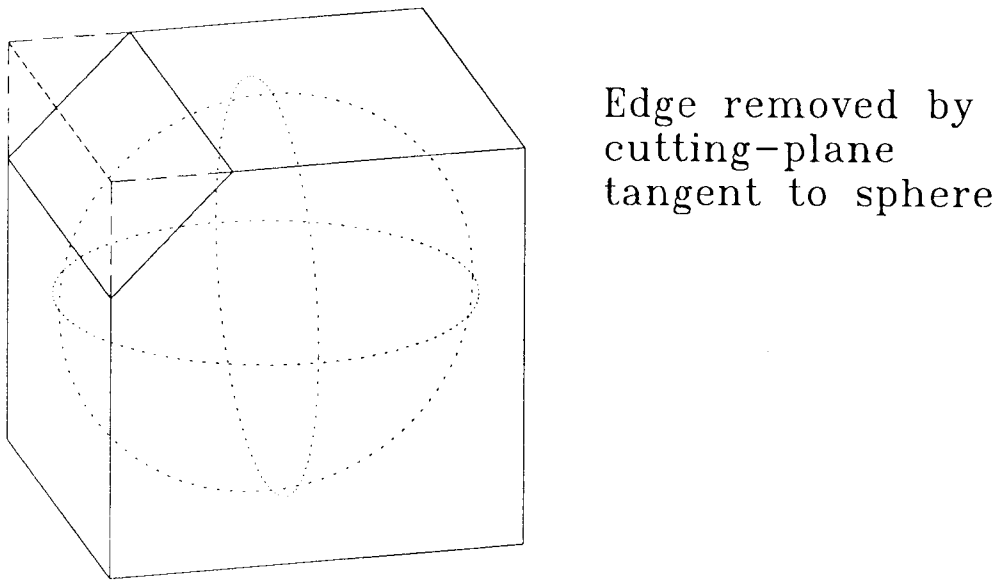

Figure 4.10: Cube's Edge Removed by Cutting Plane

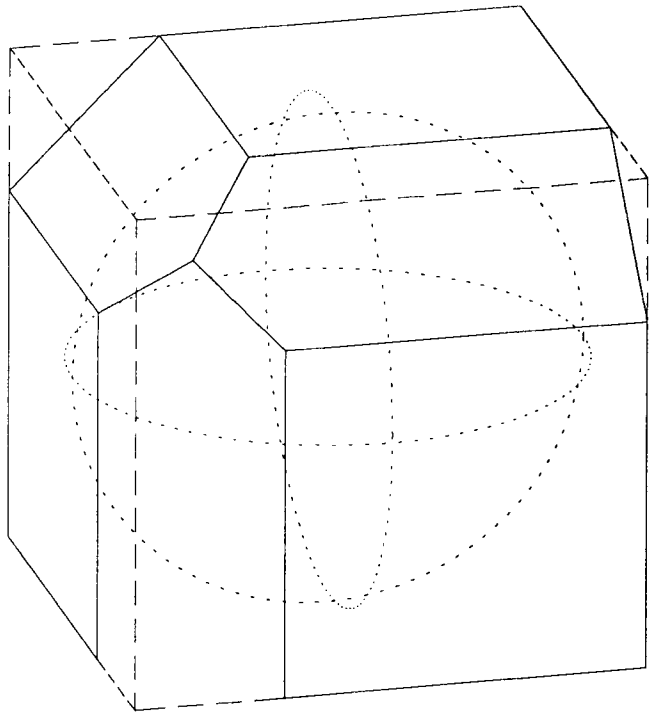

Figure 4.11: Intersection of Three New Type **E** Faces

We restrict the following discussion to the cube with vertices $(\pm 1, \pm 1, \pm 1)$ and its inscribed unit sphere. Consider two adjacent faces of the cube, $\mathcal{P}_0$ and $\mathcal{P}_1$. These faces are tangent to the sphere at points $\mathbf{C}_0$ and $\mathbf{C}_1$, respectively. The geodesic connecting these points is an arc of the great circle at the intersection of the sphere and the plane defined by $\mathbf{C}_0$, $\mathbf{C}_1$, and the origin. To cut off the edge between these faces, we construct a plane, $\mathcal{P}$, parallel to this edge and tangent to the sphere at the midpoint of this geodesic (Figure 4.10). Using $\mathcal{P}$ as a cutting plane, we remove the edge, replacing it with a face that lies in $\mathcal{P}$. After we have defined a cutting plane for each edge of the cube, all planes are clipped against adjacent planes. The new faces have edges that lie in the lines of intersection between adjacent planes. (Figure 4.11).

Since our construction is symmetric, we need only consider an octant of the cube. We will describe its refinement in the following. The faces of the figures are tangent to the sphere at the dots.

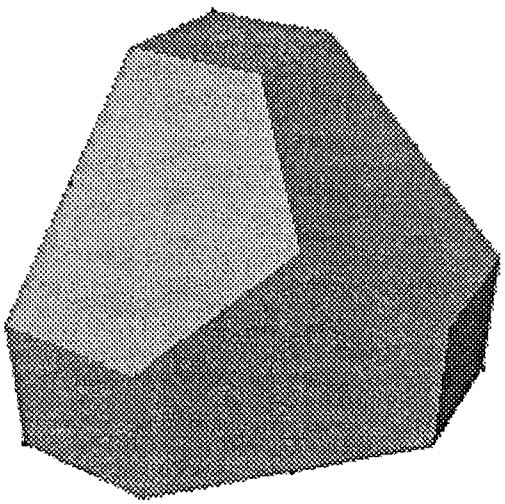

Figure 4.12: Level $k = 1$ Faces

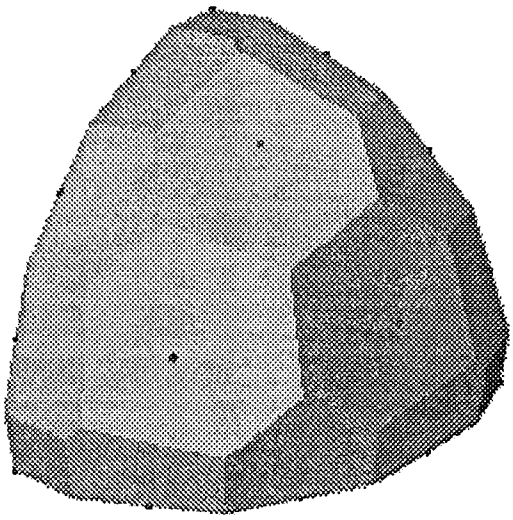

Figure 4.13: Level $k = 2$ Faces

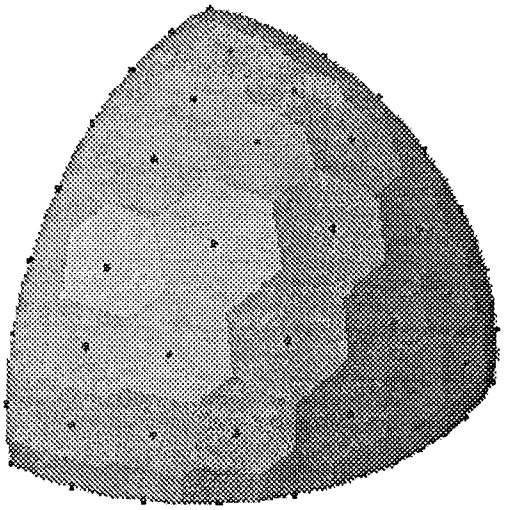

Figure 4.14: Level $k = 3$ Faces

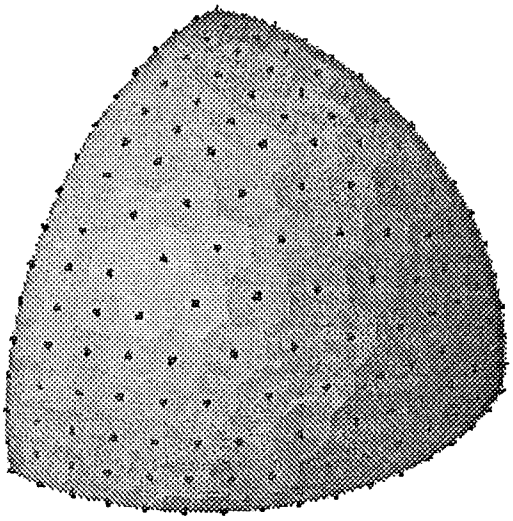

Figure 4.15: Level $k = 4$ Faces

4.3.2 A Tessellation of the Sphere

As introduced in section 4.3.1, we will present an algorithm that will iteratively produce polyhedra that are piecewise planar approximations of an inscribed sphere. We will define a set of tessellations of the surface of the sphere and show that there is a correspondence between each of these polyhedra and one of these tessellations, such that, from one we may find the other.

Given one of these polyhedra, a vertex of the tessellation will be a projection of a vertex of this polyhedron and an edge of the tessellation will be the projection of an edge of this polyhedron, thus, each tile of the tessellation will correspond to a face of the polyhedron. Consequently, the valence of a polyhedron's vertex is the same as the valence of the corresponding tessellation vertex. Each tile will contain the point at which the corresponding face is tangent to the sphere; we will call this point the *data point.* Since we begin with the cube, our tessellations will never have fewer than six data points. We will show that an edge of a tile will be an arc of a great circle such that every point on the arc is equidistant from the data points in the tiles adjacent to the edge. We will call these arcs *arcs of equal influence.* Since this arc is equidistant from adjacent data points, it intersects the geodesic between these data points at the geodesic's midpoint, and we will show that the hour angles at this intersection are $\frac{\pi}{2}$. The vertices of the tessellation will fall at the intersection of arcs of equal influence and be called *points of equal influence.* All points on the surface of the sphere within a tile will be closer to the data point of that tile than to any other data point. Thus, we will call the region within a tile the *region of influence* of that tile's data point. To summarize, our set of tessellations have the following properties

1. Each projected edge and projected vertex is equidistant from the data points adjacent to it.

2. Any point on the surface of the sphere that lies within one of the tiles is closer to the data point of that tile than it is to any of the other data points.

3. The intersection of a geodesic between adjacent data points with the tessellation edge separating these data points falls at the midpoint of the geodesic and intersects at hour angles of $\frac{\pi}{2}$.

Given the Polyhedron, find the Tessellation

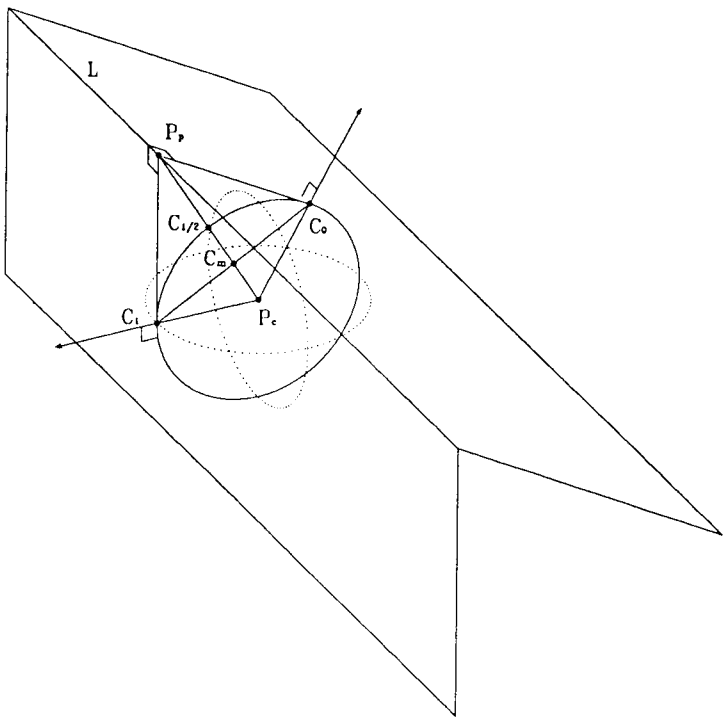

Figure 4.16: Intersection of Two Tangent Planes

Although we will only deal with tessellations that contain six or more data points, we will describe them beginning with fewer data points. First, we will show that the line of intersection between two planes tangent to a sphere is equidistant from the tangent points of these planes. Consider two differing and non-diametrically-opposed points, $\mathbf{C_0}$ and $\mathbf{C_1}$, on the surface of a sphere and the planes tangent at these points, $\mathcal{P}_0$ and $\mathcal{P}_1$ (Figure 4.16). As described in **The Intersection of Two Planes** of section 4.1.1, these planes will intersect at a line that we will label **L**. Now add the plane, $\mathcal{P}_c$, defined by points $\mathbf{C_0}$, $\mathbf{C_1}$, and the center of the sphere, $\mathbf{P_c}$. These three planes, $\mathcal{P}_0$, $\mathcal{P}_1$, and $\mathcal{P}_c$, will intersect at a

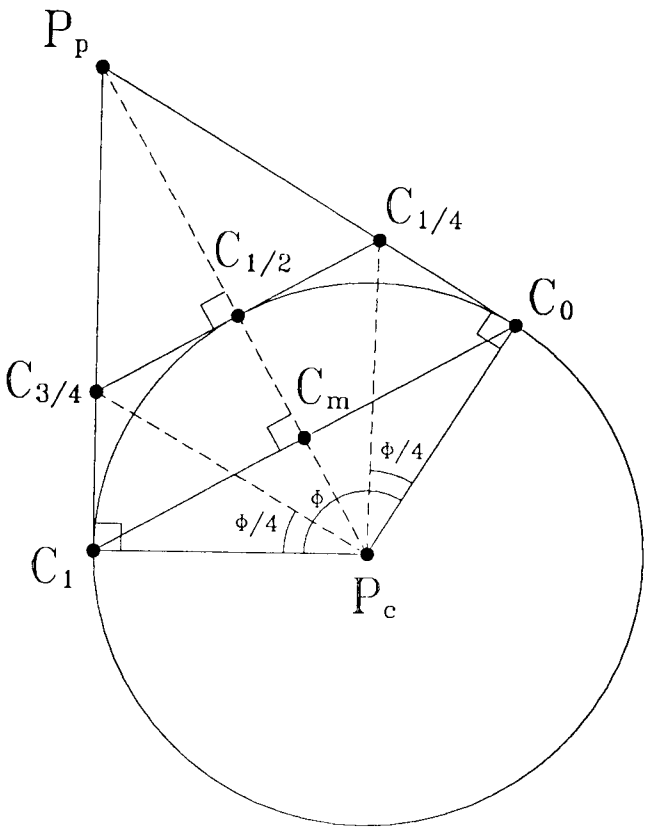

Figure 4.17: Cross-section of the Sphere

point that we will label $\mathbf{P}_p$. If we intersect $\mathcal{P}_c$ with each of the following: $\mathcal{P}_0$, $\mathcal{P}_1$, and the sphere, we will have the $I\!R^2$ figure 4.17. Using some basic trigonometry, we see that point $\mathbf{P}_p$, on the line of intersection, $\mathbf{L}$, is equidistant from points $\mathbf{C}_0$ and $\mathbf{C}_1$. Referring again to **The Intersection of Two Planes** in section 4.1.1, we know that the direction of $\mathbf{L}$ is determined by the cross product of the normals at $\mathbf{C}_0$ and $\mathbf{C}_1$. As noted in the definition **Great Circles** from section 4.1.3 these normals lie in the plane $\mathcal{P}_c$. Therefore, $\mathbf{L}$ is perpendicular to $\mathcal{P}_c$ and point $\mathbf{P}_p$ is the common perpendicular on $\mathbf{L}$ to $\mathbf{C}_0$ and $\mathbf{C}_1$. Now, consider some other point on $\mathbf{L}$, $\mathbf{P}_s$. We may construct two triangles designated by their vertices, $\{\mathbf{P}_s, \mathbf{P}_p, \mathbf{C}_0\}$ and $\{\mathbf{P}_s, \mathbf{P}_p, \mathbf{C}_1\}$. We know that these are right triangles since

$\mathbf{L}$ is perpendicular to both $\overline{\mathbf{C_0P}_p}$ and $\overline{\mathbf{C_1P}_p}$. Therefore, since

$$\left|\overline{\mathbf{C_0P}_p}\right| = \left|\overline{\mathbf{C_1P}_p}\right|$$

we may say

$$\left|\overline{\mathbf{C_0P}_s}\right| = \left|\overline{\mathbf{C_1P}_s}\right|$$

So, every point on $\mathbf{L}$ is equidistant from $\mathbf{C_0}$ and $\mathbf{C_1}$.

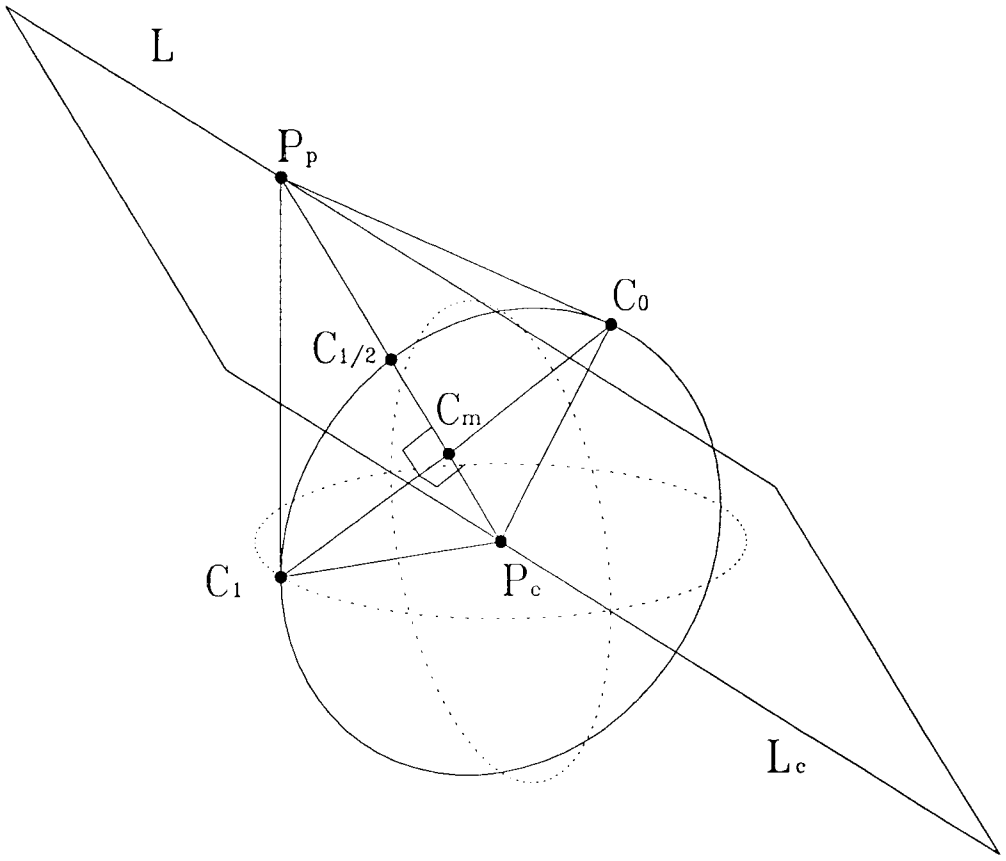

Figure 4.18: Plane of Equidistance

Now we will define a plane, $\mathcal{P}_l$, that we will show is equidistant from data points $\mathbf{C_0}$ and $\mathbf{C_1}$. The plane $\mathcal{P}_l$ is defined by the line of intersection, $\mathbf{L}$, and the center of the sphere, $\mathbf{P}_c$ (Figure 4.18). Since $\mathbf{L}$ is perpendicular to $\mathcal{P}_c$, $\mathcal{P}_l$ is also. The line of intersection

between $\mathcal{P}_c$ and $\mathcal{P}_l$ is $\overline{\mathbf{P}_c\mathbf{P}_p}$. Let $\angle(\mathbf{C}_0, \mathbf{P}_c, \mathbf{C}_1)$ be the angle between the radii $\overline{\mathbf{P}_c\mathbf{C}_0}$ and $\overline{\mathbf{P}_c\mathbf{C}_1}$. If we consider the line $\overline{\mathbf{P}_c\mathbf{P}_p}$ in Figure 4.17, we see that it bisects $\angle(\mathbf{C}_0, \mathbf{P}_c, \mathbf{C}_1)$. Consequently, the intersection of $\overline{\mathbf{P}_c\mathbf{P}_p}$ with $\overline{\mathbf{C}_0\mathbf{C}_1}$, $\mathbf{C}_m$, is the midpoint of $\overline{\mathbf{C}_0\mathbf{C}_1}$, and $\overline{\mathbf{P}_c\mathbf{P}_p}$ is perpendicular to $\overline{\mathbf{C}_0\mathbf{C}_1}$. Therefore, $\mathbf{P}_p$ is the closest point on $\mathbf{L}$ to $\mathbf{C}_m$, and $\overline{\mathbf{C}_m\mathbf{P}_p}$ is perpendicular to $\mathbf{L}$.

Since $\mathbf{C}_m$ is the common perpendicular to $\mathbf{C}_0$ and $\mathbf{C}_1$ on $\overline{\mathbf{P}_c\mathbf{P}_p}$, it is the common perpendicular to these on the plane $\mathcal{P}_l$. Now consider some other point on $\mathcal{P}_l$, $\mathbf{P}_r$. Again we may form two right triangles, $\{\mathbf{P}_r, \mathbf{C}_m, \mathbf{C}_0\}$ and $\{\mathbf{P}_r, \mathbf{C}_m, \mathbf{C}_1\}$, and show that any point on the plane $\mathcal{P}_l$ is equidistant from points $\mathbf{C}_0$ and $\mathbf{C}_1$. Thus $\mathcal{P}_l$ separates $\mathbb{R}^3$ into two parts, one in which every point is closer to $\mathbf{C}_0$ than to $\mathbf{C}_1$ and one in which every point is closer to $\mathbf{C}_1$ than to $\mathbf{C}_0$.

In the plane of equidistance, $\mathcal{P}_l$, we may find the great circle that is equidistant from data points $\mathbf{C}_0$ and $\mathbf{C}_1$. First, we project $\mathbf{L}$ onto the sphere and obtain $\hat{\mathbf{L}}$. Since $\hat{\mathbf{L}}$ lies in the plane $\mathcal{P}_l$, every point on $\hat{\mathbf{L}}$ is equidistant from points $\mathbf{C}_0$ and $\mathbf{C}_1$. Consequently, any point on the sphere between $\hat{\mathbf{L}}$ and $\mathbf{C}_0$ is closer to $\mathbf{C}_0$ than to $\mathbf{C}_1$. Thus, $\hat{\mathbf{L}}$ separates the sphere into two tiles, one containing $\mathbf{C}_0$ and all points on the sphere closer to it than to $\mathbf{C}_1$ and one containing $\mathbf{C}_1$ and all points closer to it than to $\mathbf{C}_0$. Consider the geodesic from $\mathbf{C}_0$ to $\mathbf{C}_1$, $\widehat{\mathbf{C}_0\mathbf{C}_1}$. Since the midpoint of $\widehat{\mathbf{C}_0\mathbf{C}_1}$, $\mathbf{C}_{1/2}$, is equidistant from $\mathbf{C}_0$ and $\mathbf{C}_1$, it must lie in the plane of equidistance, $\mathcal{P}_l$. Since $\mathbf{C}_{1/2}$ is on the surface of the sphere, it must lie on $\hat{\mathbf{L}}$. Therefore, $\mathbf{C}_{1/2}$ lies at the intersection of $\hat{\mathbf{L}}$ and $\widehat{\mathbf{C}_0\mathbf{C}_1}$. Suppose we establish a coordinate system where $\mathbf{C}_{1/2}$ is a pole and pass a latitude line, $\mathbf{l}$, through $\mathbf{C}_0$ and $\mathbf{C}_1$. Consider the intersection points of $\hat{\mathbf{L}}$ and $\mathbf{l}$ that we will label $\mathbf{C}_a$ and $\mathbf{C}_b$. Since every point on $\hat{\mathbf{L}}$ is equidistant from points $\mathbf{C}_0$ and $\mathbf{C}_1$, we may say

$$\begin{aligned} \left|\widehat{\mathbf{C}_0\mathbf{C}_a}\right| &= \left|\widehat{\mathbf{C}_1\mathbf{C}_a}\right| \\ \left|\widehat{\mathbf{C}_0\mathbf{C}_b}\right| &= \left|\widehat{\mathbf{C}_1\mathbf{C}_b}\right| \end{aligned}$$

Additionally, since very point on $\mathbf{l}$ is equidistant from $\mathbf{C}_{1/2}$ we may say

$$\left|\widehat{\mathbf{C}_{1/2}\mathbf{C}_0}\right| = \left|\widehat{\mathbf{C}_{1/2}\mathbf{C}_1}\right| = \left|\widehat{\mathbf{C}_{1/2}\mathbf{C}_a}\right| = \left|\widehat{\mathbf{C}_{1/2}\mathbf{C}_b}\right|$$

Therefore, we may say

$$\left|\widehat{\mathbf{C}_0\mathbf{C}_a}\right| = \left|\widehat{\mathbf{C}_1\mathbf{C}_a}\right| = \left|\widehat{\mathbf{C}_0\mathbf{C}_b}\right| = \left|\widehat{\mathbf{C}_1\mathbf{C}_b}\right|$$

and conclude that the hour angles at the intersection of $\hat{\mathbf{L}}$ and $\widehat{\mathbf{C_0C_1}}$ are $\frac{\pi}{2}$. Therefore, we have a trivial tessellation that meets the three requirements above, although clearly we cannot find an equivalent polyhedron that will enclose the sphere.

To produce a more complex tessellation, let us consider three points, $\mathbf{C}_{i,0}$, $\mathbf{C}_{i,1}$, and $\mathbf{C}_{i,2}$, on the surface of a sphere that satisfy the requirements for spherical triangles as defined in section 4.1.3. Planes tangent at these points are $\mathcal{P}_{i,0}$, $\mathcal{P}_{i,1}$, and $\mathcal{P}_{i,2}$. We will label the lines of intersection between these planes

$$\mathbf{L}_{i,j} = \mathcal{P}_{i,j+1} \cap \mathcal{P}_{i,j+2}$$

These three planes will intersect at the point $\mathbf{P}_i$. Since every point on the line of intersection, $\mathbf{L}_{i,j}$, is equidistant from points $\mathbf{C}_{i,j+1}$ and $\mathbf{C}_{i,j+2}$, we may say that $\mathbf{P}_i$ is equidistant from points $\mathbf{C}_{i,0}$, $\mathbf{C}_{i,1}$, and $\mathbf{C}_{i,2}$. We may project the lines of intersection onto the sphere and obtain great circles $\widehat{\mathbf{L}_{i,0}}$, $\widehat{\mathbf{L}_{i,1}}$, and $\widehat{\mathbf{L}_{i,2}}$. Consider the projection of $\mathbf{P}_i$, $\hat{\mathbf{P}}_i$. Since $\mathbf{P}_i$ lies on $\mathbf{L}_{i,j}$, it will project onto $\widehat{\mathbf{L}_{i,j}}$. So we may say that $\hat{\mathbf{P}}_i$ lies at an intersection of $\widehat{\mathbf{L}_{i,0}}$, $\widehat{\mathbf{L}_{i,1}}$, and $\widehat{\mathbf{L}_{i,2}}$. Since these great circles intersect at $\hat{\mathbf{P}}_i$ they belong to the pencil of planes of the diameter through $\hat{\mathbf{P}}_i$, $\overline{\mathbf{P}_i\mathbf{P}_c}$. Recall that projected line $\widehat{\mathbf{L}_{i,j}}$ is equidistant from points $\mathbf{C}_{i,j+1}$ and $\mathbf{C}_{i,j+2}$. However, $\widehat{\mathbf{L}_{i,j}}$ is equidistant from $\mathbf{C}_{i,j}$, $\mathbf{C}_{i,j+1}$, and $\mathbf{C}_{i,j+2}$ only at projected point $\hat{\mathbf{P}}_i$ and the point diametrically opposed to $\hat{\mathbf{P}}_i$. Any other point on $\widehat{\mathbf{L}_{i,j}}$ is either closer to or farther from $\mathbf{C}_{i,j}$ than it is to $\mathbf{C}_{i,j+1}$ or $\mathbf{C}_{i,j+2}$. We will define a segment of $\widehat{\mathbf{L}_{i,j}}$, $\widehat{\mathbf{e}_{i,j}}$, such that any point on $\widehat{\mathbf{e}_{i,j}}$ is not closer to $\mathbf{C}_{i,j}$ than it is to either $\mathbf{C}_{i,j+1}$ or $\mathbf{C}_{i,j+2}$. Segments $\widehat{\mathbf{e}_{i,0}}$, $\widehat{\mathbf{e}_{i,1}}$, and $\widehat{\mathbf{e}_{i,2}}$ separate the sphere into three tiles such that any point within the tile containing data point $\mathbf{C}_{i,j}$ is closer to it than it is to either of the other two data points. The valence-three vertices of this tessellation, $\hat{\mathbf{P}}_i$ and the point diametrically opposed to it, are equidistant from data points $\mathbf{C}_{i,0}$, $\mathbf{C}_{i,1}$, and $\mathbf{C}_{i,2}$. Again, we have a tessellation that meets the three requirements above, but still we cannot find an equivalent polyhedron. Without considering the minimum number of data points needed to produce an enclosing polyhedron, we note that the six that coincide with the faces of a cube are sufficient.

Given the Tessellation find the Polyhedron

Suppose we have an edge, $\hat{\mathbf{e}}$, from a tessellation that corresponds to an enclosing polyhedron. Additionally, we have the end points of $\hat{\mathbf{e}}$, $\hat{\mathbf{P}}_0$ and $\hat{\mathbf{P}}_1$, along with the adjacent data points, $\mathbf{C}_0$ and $\mathbf{C}_1$, and the center of the sphere, $\mathbf{P}_c$. As noted in the definition **Projecting a Line**

onto a Sphere in section 4.1.3, a line from any point on $\overline{\hat{\mathbf{P}}_0\mathbf{P}_c}$ to any point on $\overline{\hat{\mathbf{P}}_1\mathbf{P}_c}$ will project to $\hat{\mathbf{e}}$. However, given tangent points $\mathbf{C}_0$ and $\mathbf{C}_1$, we may recover the unique points, $\mathbf{P}_0$ and $\mathbf{P}_1$, and the line segment, $\mathbf{e}$, that lie at the intersection of the planes tangent to the sphere at $\mathbf{C}_0$ and $\mathbf{C}_1$. First define a plane, $\mathcal{P}_0$

$$\begin{aligned} \mathcal{P}_0 &= (\mathbf{C}_0, \vec{n}_0) \\ \vec{n} &= \frac{\langle \mathbf{C}_0 \rangle}{|\langle \mathbf{C}_0 \rangle|} \end{aligned}$$

Next, define two vectors,

$$\begin{aligned} \vec{v}_0 &= \left\langle \hat{\mathbf{P}}_0 - \mathbf{P}_c \right\rangle \\ \vec{v}_1 &= \left\langle \hat{\mathbf{P}}_1 - \mathbf{P}_c \right\rangle \end{aligned}$$

Point $\mathbf{P}_0$ is the projection of $\hat{\mathbf{P}}_0$ onto $\mathcal{P}_0$ along $\vec{v}_0$, $\mathbf{P}_1$ is the projection of $\hat{\mathbf{P}}_1$ onto $\mathcal{P}_0$ along $\vec{v}_1$ and $\mathbf{e}$ is the line segment between $\mathbf{P}_0$, and $\mathbf{P}_1$.

Latitude Lines and Spherical Triangles

It will be useful to consider two relationships between a valence-three tessellation vertex, $\hat{\mathbf{P}}_i$, and its adjacent data points, $\hat{\mathbf{C}}_{i,0}$, $\hat{\mathbf{C}}_{i,1}$, and $\hat{\mathbf{C}}_{i,2}$.

1. Latitude Line of a Tessellation Vertex
   As we have shown

   $$\left|\mathbf{P}_i\widehat{\mathbf{C}_{i,0}}\right| = \left|\mathbf{P}_i\widehat{\mathbf{C}_{i,1}}\right| = \left|\mathbf{P}_i\widehat{\mathbf{C}_{i,2}}\right|$$

   Establishing a coordinate system with $\hat{\mathbf{P}}_i$ as a pole, the intersection of the sphere with the plane defined by $\mathbf{C}_{i,0}$, $\mathbf{C}_{i,1}$, and $\mathbf{C}_{i,2}$ is a latitude line, $\mathbf{l}_i$. We will call $\mathbf{l}_i$ the *latitude line* of $\hat{\mathbf{P}}_i$. Every point on $\mathbf{l}_i$ is equidistant from $\hat{\mathbf{P}}_i$. We will say that a point on the surface of the sphere that lies in the region between $\hat{\mathbf{P}}_i$ and $\mathbf{l}_i$ is *inside* of $\mathbf{l}_i$, while points in the other region of the sphere are *outside* of $\mathbf{l}_i$ (Figure 4.19). Consider the axis to $\hat{\mathbf{P}}_i$. The point diametrically opposed to $\hat{\mathbf{P}}_i$ is also equidistant from every point on $\mathbf{l}_i$. We note that this axis is normal to the plane in which $\mathbf{l}_i$ lies and intersects the circle defined by $\mathbf{l}_i$ at its center.

   Suppose we had only points $\mathbf{C}_{i,0}$, $\mathbf{C}_{i,1}$, and $\mathbf{C}_{i,2}$. We could find $\hat{\mathbf{P}}_i$ and the point diametrically opposed to it as follows. First, intersect the plane defined by $\mathbf{C}_{i,0}$, $\mathbf{C}_{i,1}$,

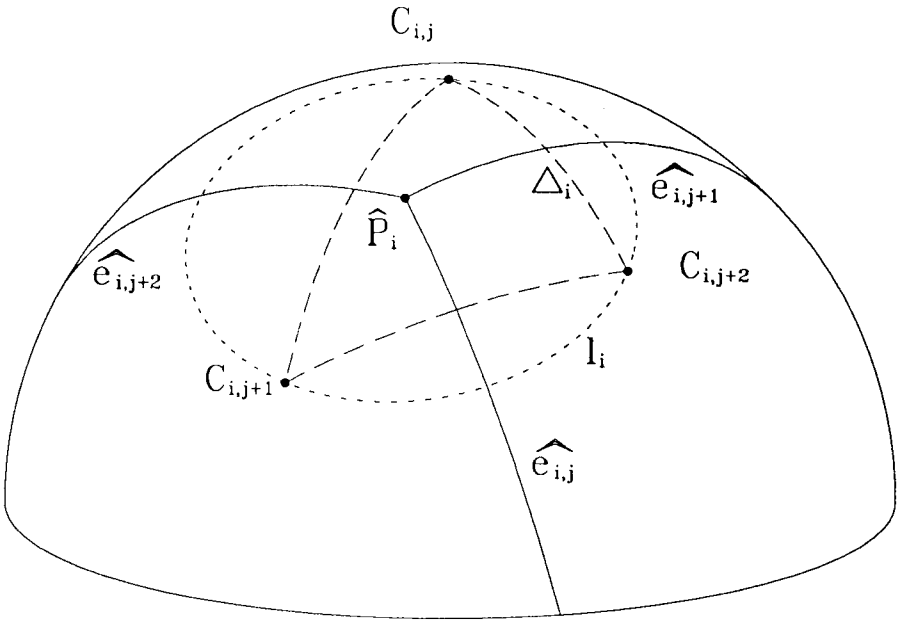

Figure 4.19: Projected Point with Projected Lines

and $\mathbf{C}_{i,2}$ with the sphere to obtain $\mathbf{l}_i$. Next, find the line that is normal to this plane and passes through the center of $\mathbf{l}_i$. Now, intersect this line with the sphere and obtain $\hat{\mathbf{P}}_i$ and the point diametrically opposed to it.

2. Spherical Triangle of a Tessellation Vertex

   We will call the spherical triangle formed by $\mathbf{C}_{i,0}$, $\mathbf{C}_{i,1}$, and $\mathbf{C}_{i,2}$ the *triangle* of the tessellation vertex $\hat{\mathbf{P}}_i$ and label it $\triangle_i$. Given a tessellation vertex, $\hat{\mathbf{P}}_i$, and its triangle, $\triangle_i$, we may classify them by the location of $\hat{\mathbf{P}}_i$. If $\hat{\mathbf{P}}_i$ lies strictly within $\triangle_i$, we will call both this tessellation vertex and its triangle Type **I** for inside. If $\hat{\mathbf{P}}_i$ lies outside of $\triangle_i$ or falls on an edge of $\triangle_i$, we will call these Type **O** for outside.

Latitude Line of a Tessellation Vertex

Considering the latitude line, $\mathbf{l}_i$, of a valence-three tessellation vertex, $\hat{\mathbf{P}}_i$, we will show the following

1. There is no data point within $\mathbf{l}_i$.
2. There are exactly three data points on $\mathbf{l}_i$.
3. No data point outside of $\mathbf{l}_i$ affects $\hat{\mathbf{P}}_i$.

We will consider the tessellation of the sphere in the vicinity of $\hat{\mathbf{P}}_i$ and how this tessellation would be affected if we were to insert another data point, $\mathbf{C}$, on the surface of the sphere differing from $\mathbf{C}_{i,0}$, $\mathbf{C}_{i,1}$, and $\mathbf{C}_{i,2}$.

If $\mathbf{C}$ were to be inside of $\mathbf{l}_i$, then $\hat{\mathbf{P}}_i$ would be closer to $\mathbf{C}$ than to $\mathbf{C}_{i,0}$, $\mathbf{C}_{i,1}$, or $\mathbf{C}_{i,2}$ and strictly within $\mathbf{C}$'s region of influence. As we have shown, there could not be a tessellation vertex at $\hat{\mathbf{P}}_i$ because it must be equidistant from the adjacent data points, at a point of equal influence.

Suppose $\mathbf{C}$ were to lie on $\mathbf{l}_i$ between $\mathbf{C}_{i,j}$ and $\mathbf{C}_{i,j+1}$. Clearly, $\mathbf{C}$ would be closer to the arc of equal influence between $\mathbf{C}_{i,j}$ and $\mathbf{C}_{i,j+1}$ than they, and this arc could no longer be part of the tessellation. This arc of equal influence would be replaced by two new ones, one between $\mathbf{C}$ and $\mathbf{C}_{i,j}$ and one between $\mathbf{C}$ and $\mathbf{C}_{i,j+1}$. We will show that these two new arcs pass through $\hat{\mathbf{P}}_i$, therefore increasing its valence by one.

Suppose $\mathbf{C}$ and $\mathbf{C}_{i,j}$ are opposite from one another on $\mathbf{l}_i$. Then the geodesic $\widehat{\mathbf{C}\mathbf{C}_{i,j}}$ would pass through $\hat{\mathbf{P}}_i$. Since $\mathbf{C}$ and $\mathbf{C}_{i,j}$ are on $\mathbf{l}_i$, $\hat{\mathbf{P}}_i$ would be at the midpoint of $\widehat{\mathbf{C}\mathbf{C}_{i,j}}$. Therefore, the arc of equal influence between $\mathbf{C}$ and $\mathbf{C}_{i,j}$ would pass through $\hat{\mathbf{P}}_i$. In the case where $\widehat{\mathbf{C}\mathbf{C}_{i,j}}$ does not pass through $\hat{\mathbf{P}}_i$, we will consider the spherical triangle $\{\hat{\mathbf{P}}_i, \mathbf{C}, \mathbf{C}_{i,j}\}$. Since $\mathbf{C}$ and $\mathbf{C}_{i,j}$ lie on $\mathbf{l}_i$, we may say that this triangle is isosceles since for sides $\widehat{\hat{\mathbf{P}}_i\mathbf{C}}$ and $\widehat{\hat{\mathbf{P}}_i\mathbf{C}_{i,j}}$

$$\left|\widehat{\hat{\mathbf{P}}_i\mathbf{C}}\right| = \left|\widehat{\hat{\mathbf{P}}_i\mathbf{C}_{i,j}}\right|$$

As shown, the arc of equal influence between these points intersects $\widehat{\mathbf{C}\mathbf{C}_{i,j}}$ at an hour angle of $\frac{\pi}{2}$. Therefore, this arc of equal influence passes through $\hat{\mathbf{P}}_i$ (Figure 4.20).

Likewise, the arc of equal influence between $\mathbf{C}$ and $\mathbf{C}_{i,j+1}$ must pass through $\hat{\mathbf{P}}_i$ also. Therefore, there are now two arcs of equal influence passing through $\hat{\mathbf{P}}_i$ that have replaced

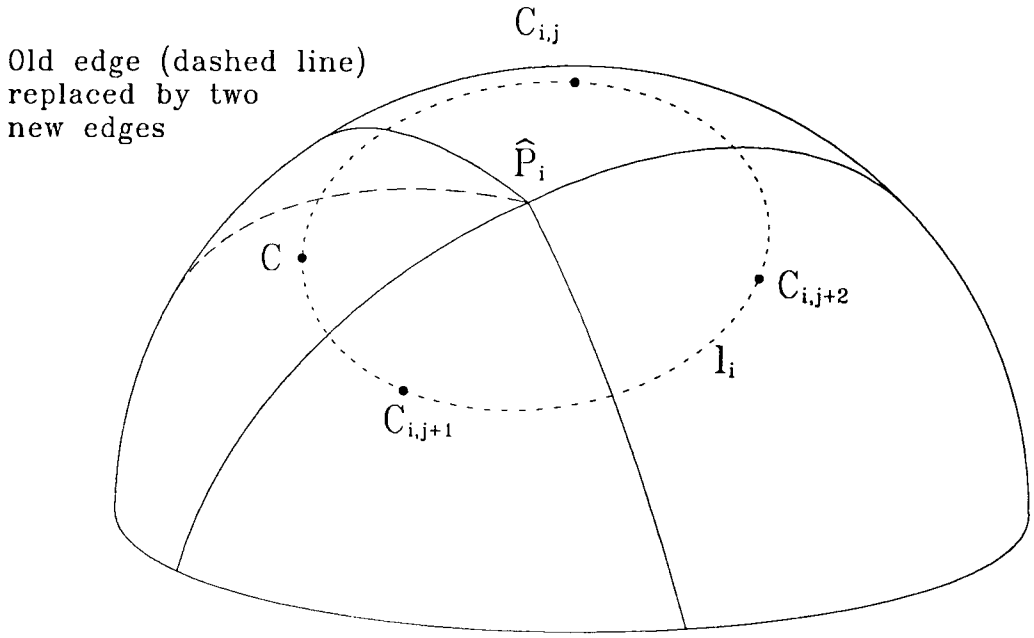

Figure 4.20: Data Point C on Latitude Line l_i

one of the originals, increasing the valence by one. We may conclude, then, that if C were to lie on l_i, $\hat{P}_i$ can no longer be valence three.

Finally, suppose C were outside of l_i. Then, C would be too far from $\hat{P}_i$ to have an influence on it since a vertex of the tessellation is equidistant from adjacent data points.

Spherical Triangle of a Tessellation Vertex

Now, consider the spherical triangle of a valence-three tessellation vertex, $\hat{P}_i$. We will show that if all hour angles of $\triangle_i$ are less than or equal to $\frac{\pi}{2}$, we may conclude that $\hat{P}_i$ and $\triangle_i$ are Type I.

For tessellation vertex $\hat{P}_i$ we will require that points $C_{i,0}$, $C_{i,1}$, and $C_{i,2}$ lie within the same hemisphere as $\hat{P}_i$. As shown, the tessellation edges emanating from $\hat{P}_i$ intersect geodesic sides of $\triangle_i$ at the midpoints of these sides. However, in general, we cannot ensure that $\hat{P}_i$ is Type I, that is, it lies within $\triangle_i$ (Figure 4.21).

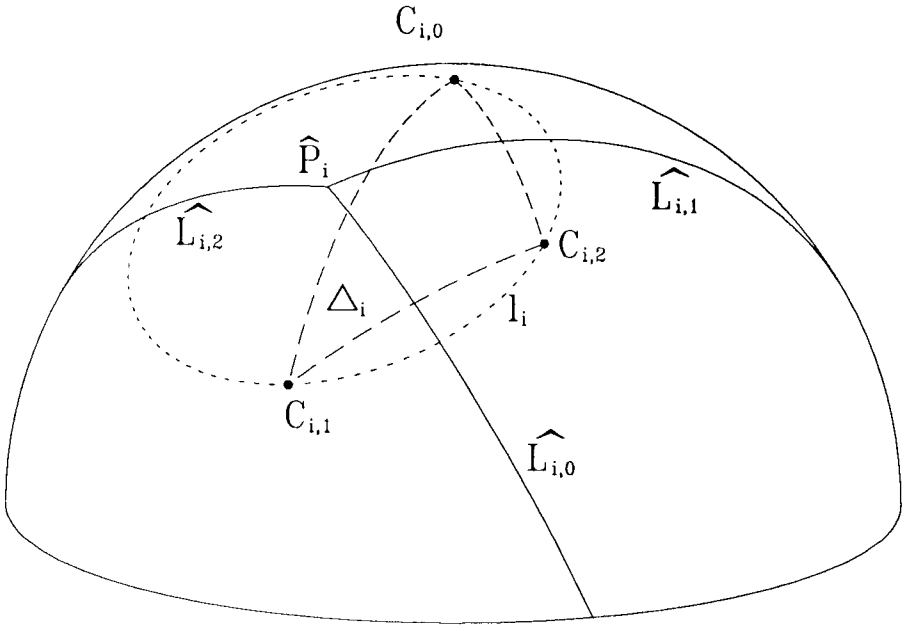

Figure 4.21: Vertex not within the Spherical Triangle

To guarantee that $\hat{\mathbf{P}}_i$ will be Type **I**, we must set certain restrictions on the shape of $\triangle_i$.

As shown in Figure 4.22, consider an edge of $\triangle_i$, geodesic $\mathbf{C}_{i,j}\widehat{\mathbf{C}_{i,j+2}}$, that is a segment of a projected line, $\hat{\mathbf{L}}$. The tessellation edge equidistant between $\mathbf{C}_{i,j}$ and $\mathbf{C}_{i,j+2}$ is a segment of projected line $\mathbf{L}_{\widehat{i,j+1}}$, and the intersection of $\mathbf{L}_{\widehat{i,j+1}}$ with $\mathbf{C}_{i,j}\widehat{\mathbf{C}_{i,j+2}}$ is the midpoint of $\mathbf{C}_{i,j}\widehat{\mathbf{C}_{i,j+2}}$, $\mathbf{C}^1_{i,j+1}$. We know that $\hat{\mathbf{P}}_i$ must lie on $\mathbf{L}_{\widehat{i,j+1}}$ and that

$$\left|\mathbf{P}_i\widehat{\mathbf{C}_{i,j}}\right| = \left|\mathbf{P}_i\widehat{\mathbf{C}_{i,j+1}}\right| = \left|\mathbf{P}_i\widehat{\mathbf{C}_{i,j+2}}\right|$$

To meet this requirement and ensure that $\hat{\mathbf{P}}_i$ lies within $\triangle_i$, we must restrict the region in which $\mathbf{C}_{i,j+1}$ may lie. We may say that $\mathbf{C}_{i,j+1}$ does not lie on $\hat{\mathbf{L}}$. If it were to lie on $\hat{\mathbf{L}}$, the point equidistant from $\mathbf{C}_{i,j}$, $\mathbf{C}_{i,j+1}$, and $\mathbf{C}_{i,j+2}$ would be one of the poles defined by making $\hat{\mathbf{L}}$ the equator, and we have defined these points to be within the same hemisphere as $\hat{\mathbf{P}}_i$. To further define the permissible region, we will establish a coordinate system with $\mathbf{C}^1_{i,j+1}$

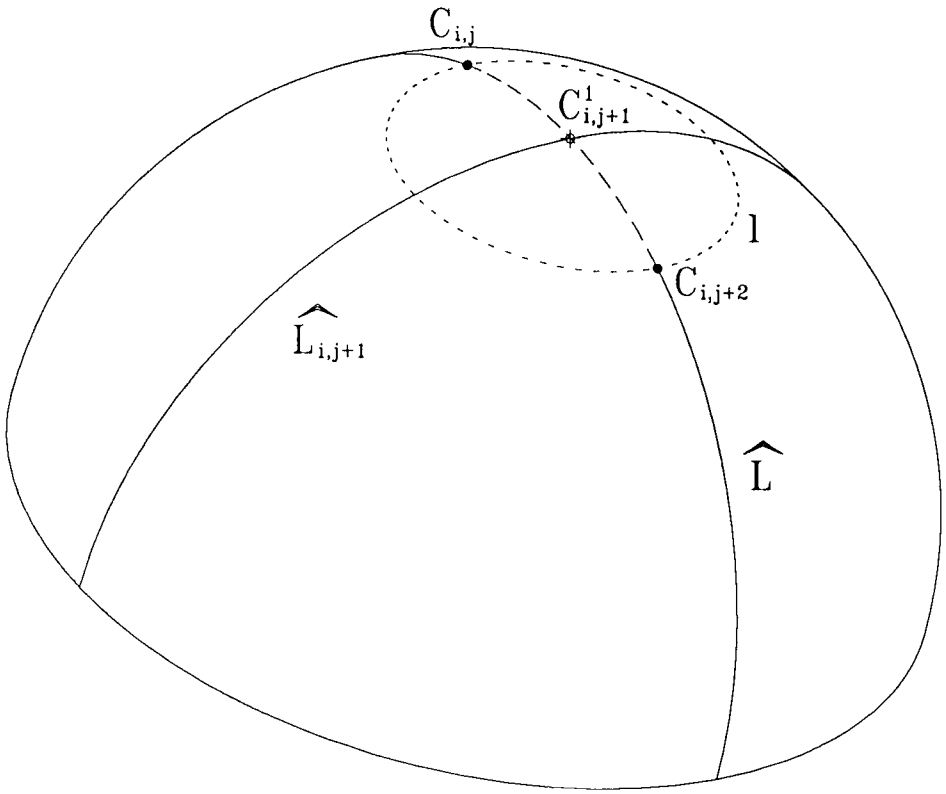

Figure 4.22: One Edge of the Spherical Triangle

as a pole and create a latitude line, l, through $\mathbf{C}_{i,j}$ and $\mathbf{C}_{i,j+2}$. Consider the position of $\mathbf{C}_{i,j+1}$. If it were to lie on l then $\mathbf{C}^1_{i,j+1}$ would be equidistant from $\mathbf{C}_{i,j}$, $\mathbf{C}_{i,j+1}$, and $\mathbf{C}_{i,j+2}$, so $\hat{\mathbf{P}}_i$ would coincide with $\mathbf{C}^1_{i,j+1}$. We note that when $\hat{\mathbf{P}}_i$ and $\mathbf{C}^1_{i,j+1}$ coincide, l and $\mathbf{l}_i$ also coincide. Now suppose $\mathbf{C}_{i,j+1}$ were to lie within l. It would have to lie on an arc from $\mathbf{C}^1_{i,j+1}$ to some point, C, that lies on l. As we have noted, if $\mathbf{C}_{i,j+1}$ lies on l, then l and $\mathbf{l}_i$ coincide. However, as the position of $\mathbf{C}_{i,j+1}$ is moved toward $\mathbf{C}^1_{i,j+1}$ along $\widehat{\mathbf{C}\mathbf{C}^1_{i,j+1}}$, l and $\mathbf{l}_i$ will no longer coincide. Latitude line $\mathbf{l}_i$ will tilt so that less of it lies on the same side of $\widehat{\mathbf{L}}$ as $\mathbf{C}_{i,j+1}$ and more of it lies on the side of $\widehat{\mathbf{L}}$ opposite $\mathbf{C}_{i,j+1}$. As noted in **Latitude Lines and Spherical Triangles**, the diameter line through $\hat{\mathbf{P}}_i$ is normal to the plane of $\mathbf{l}_i$ and passes through its center. Therefore. we may conclude that as $\mathbf{C}_{i,j+1}$ is moved toward

$\mathbf{C}^1_{i,j+1}$ from $\mathbf{C}$, $\hat{\mathbf{P}}_i$ is moved away from $\mathbf{C}^1_{i,j+1}$ into the area on the opposite side of $\hat{\mathbf{L}}$ from $\mathbf{C}_{i,j+1}$, outside of $\triangle_i$. In either case, $\triangle_i$ would be Type **O**.

Therefore, $\mathbf{C}_{i,j+1}$ must lie outside of l for $\triangle_i$ to be Type **I**. Thus, if we have a valence three projected vertex such that each adjacent data point, $\mathbf{C}_{i,j}$, $j = 0, 1, 2$, meets this requirement, then we may conclude that $\triangle_i$ is Type **I**.

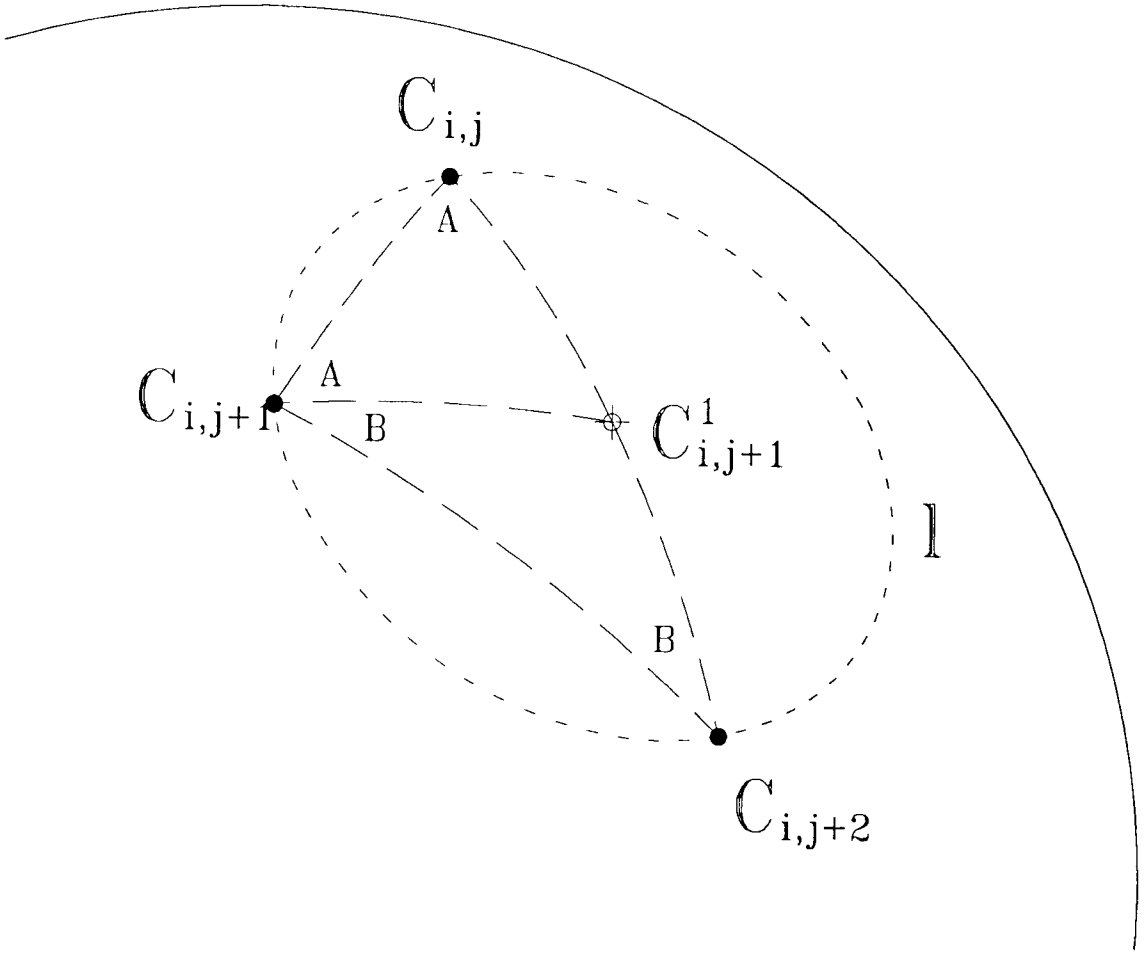

Figure 4.23: $\mathbf{C}_{i,j+1}$ on l

We will be interested in a subset of all Type **I** triangles, those that have hour angles that are not greater than $\frac{\pi}{2}$, which we will call *acute triangles*. To show that acute triangles are Type **I**, we will establish a coordinate system with the midpoint of the geodesic $\mathbf{C}_{i,j}\widehat{\mathbf{C}_{i,j+2}}$, $\mathbf{C}^1_{i,j+1}$, as a pole and create a latitude line, l, through $\mathbf{C}_{i,j}$ and $\mathbf{C}_{i,j+2}$ (Figure 4.22). We

must show that $\mathbf{C}_{i,j+1}$ does not lie on or within $\mathbf{l}$ to show that $\triangle_i$ is Type **I**. Suppose $\mathbf{C}_{i,j+1}$ were to lie on $\mathbf{l}$ (Figure 4.23). Then we may say

$$\left|\mathbf{C}_{i,j}\widehat{\mathbf{C}^{\mathbf{l}}_{i,j+1}}\right| = \left|\mathbf{C}_{i,j+1}\widehat{\mathbf{C}^{\mathbf{l}}_{i,j+1}}\right| = \left|\mathbf{C}_{i,j+2}\widehat{\mathbf{C}^{\mathbf{l}}_{i,j+1}}\right|$$

This makes triangles $\left\{\mathbf{C}_{i,j}, \mathbf{C}^{\mathbf{l}}_{i,j+1}, \mathbf{C}_{i,j+1}\right\}$ and $\left\{\mathbf{C}_{i,j+2}, \mathbf{C}^{\mathbf{l}}_{i,j+1}, \mathbf{C}_{i,j+1}\right\}$ isosceles triangles. Therefore, for these isosceles triangles, we may say hour angles

$$\begin{aligned} \mathbf{A} &= \mathbf{A} \\ \mathbf{B} &= \mathbf{B} \end{aligned}$$

Additionally, since $\triangle_i$ is a spherical triangle, we may say

$$\mathbf{A} + \mathbf{B} + \mathbf{A} + \mathbf{B} > \pi$$

Clearly, $\mathbf{A} + \mathbf{B}$ must be greater than $\frac{\pi}{2}$ if $\mathbf{C}_{i,j+1}$ is to lie on $\mathbf{l}$. Suppose $\mathbf{C}_{i,j+1}$ were to lie within $\mathbf{l}$. It must lie on an arc from $\mathbf{C}^{\mathbf{l}}_{i,j+1}$ to a point, $\mathbf{C}$, that lies on $\mathbf{l}$. If $\mathbf{C}_{i,j+1}$ coincides with $\mathbf{C}$, we have seen that its hour angle is greater than π. As the position of $\mathbf{C}_{i,j+1}$ is moved along this arc toward $\mathbf{C}^{\mathbf{l}}_{i,j+1}$, the hour angles at $\mathbf{C}_{i,j}$ and $\mathbf{C}_{i,j+2}$ decrease. These hour angles approach zero as $\mathbf{C}_{i,j+1}$ approaches $\mathbf{C}^{\mathbf{l}}_{i,j+1}$. Since the sum of the three hour angles must be greater than π, the hour angle at $\mathbf{C}_{i,j+1}$ must increase. Therefore, given a valence three projected vertex and its associated triangle, it is sufficient to show that all hour angles are less than or equal to $\frac{\pi}{2}$ to show they are Type **I**. We will define a subset of the tessellations described above that we will call *acute* tessellations. For each vertex of an acute tessellation we may say

1. The vertex is valence three.
2. The triangle of the vertex has hour angles less than or equal to $\frac{\pi}{2}$, that is, it is an acute triangle.
3. Therefore, the vertex and its triangle are Type **I**.

Acute Tessellations

When we have an acute tessellation we can show that data points other than the three adjacent to a tessellation vertex do not affect this vertex. Referring to Figure 4.24, consider

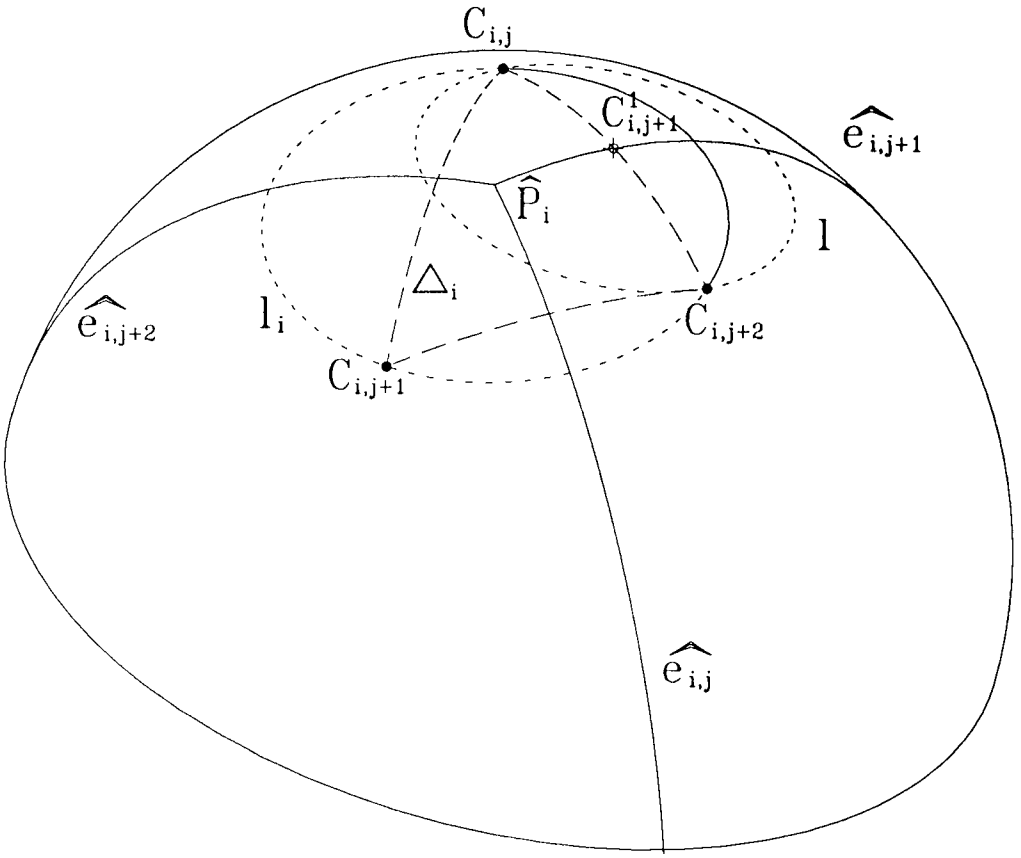

Figure 4.24: $\mathbf{l}_i$ and $\mathbf{l}$

how the position of $\hat{\mathbf{P}}_i$ and $\mathbf{l}_i$ depends on the position of $\mathbf{C}_{i,j+1}$. Let us assume that $\mathbf{C}_{i,j+1}$ lies to the left of $\mathbf{C}_{i,j}\widehat{\mathbf{C}_{i,j+2}}$. Keeping $\mathbf{C}_{i,j+1}$ within the bounds established for a Type **I** projected vertex, we may place $\mathbf{C}_{i,j+1}$ any place on $\mathbf{l}_i$ (dotted portion) without affecting the position of $\hat{\mathbf{P}}_i$. Suppose we were to move $\mathbf{C}_{i,j+1}$ farther to the left of $\mathbf{C}^1_{i,j+1}$ than the current $\mathbf{l}_i$. Then $\hat{\mathbf{P}}_i$ would move to the left, away from $\mathbf{C}^1_{i,j+1}$ along $\widehat{\mathbf{L}_{i,j+1}}$. Latitude $\mathbf{l}_i$ would also move, so that the solid portion would protrude less into the area to the right of $\mathbf{C}_{i,j}\widehat{\mathbf{C}_{i,j+2}}$. Conversely, if we move $\mathbf{C}_{i,j+1}$ closer to $\mathbf{C}^1_{i,j+1}$, $\hat{\mathbf{P}}_i$ would also move closer to $\mathbf{C}^1_{i,j+1}$, and $\mathbf{l}_i$ would shift so that the solid portion would protrude more deeply into the area to the right of $\mathbf{C}_{i,j}\widehat{\mathbf{C}_{i,j+2}}$. Continuing to move $\mathbf{C}_{i,j+1}$ toward $\mathbf{C}^1_{i,j+1}$, it would eventually approach $\mathbf{l}$ but cannot reach it if this is to remain Type **I**. As $\mathbf{C}_{i,j+1}$ came closer and closer to $\mathbf{l}$, $\mathbf{l}_i$ would

come closer and closer to coinciding with $\mathbf{l}$. However, since $\mathbf{C}_{i,j+1}$ can never reach $\mathbf{l}$, the portion of $\mathbf{l}_i$ to the right of $\mathbf{C}_{i,j}\widehat{\mathbf{C}_{i,j+2}}$ would always fall within $\mathbf{l}$.

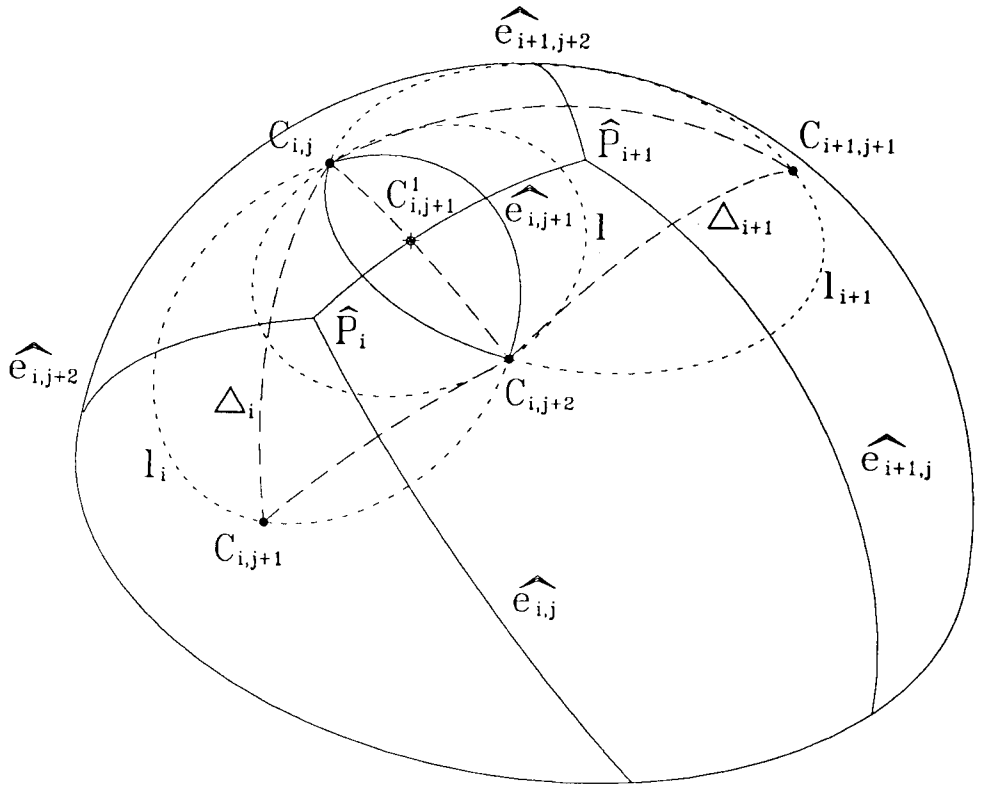

Figure 4.25: Neighboring Spherical Triangle

Now, consider the neighboring tessellation vertex to $\hat{\mathbf{P}}_i$ along the tessellation's projected edge $\widehat{\mathbf{e}_{i,j+1}}$, $\hat{\mathbf{P}}_{i+1}$ (Figure 4.25). We may assume $\hat{\mathbf{P}}_{i+1}$ is valence three since this is an acute tessellation. Data points adjacent to $\hat{\mathbf{P}}_{i+1}$ are the shared points $\mathbf{C}_{i,j}$ and $\mathbf{C}_{i,j+2}$ and the non-shared point $\mathbf{C}_{i+1,j+1}$. We know that if $\mathbf{C}_{i+1,j+1}$ is to affect $\hat{\mathbf{P}}_i$, then $\mathbf{C}_{i+1,j+1}$ must fall on or within $\mathbf{l}_i$. However, if $\triangle_{i+1}$ is Type I, then $\mathbf{C}_{i+1,j+1}$ must lie outside of $\mathbf{l}$. So, we may conclude that if we have an acute tessellation and consider two neighboring tessellation vertices, the position of the non-shared data point adjacent to one vertex does not affect the other vertex. From this we may conclude that there is an edge of length greater than

zero between the tessellation's projected vertices, and the valence of one of these projected vertices is unaffected by the position of the non-shared data point of the other.

As shown above, we may find the unique line segment, $\mathbf{e}_{i,j+1}$, with endpoints $\mathbf{P}_i$ and $\mathbf{P}_{i+1}$ that corresponds to the tessellation edge $\widehat{\mathbf{e}_{i,j+1}}$. We may then conclude that $\mathbf{e}_{i,j+1}$ has length greater than zero.

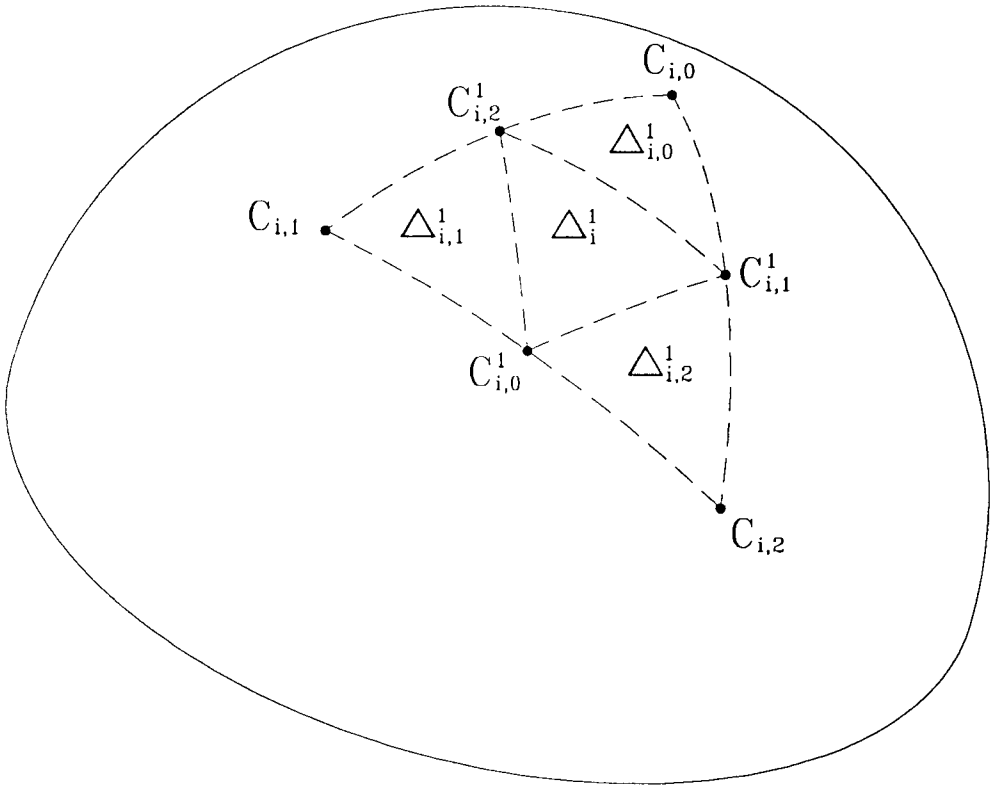

Figure 4.26: New Data Points

4.3.3 The Mathematics of Edge-Beveling

As stated in section 4.3.1, new polyhedra are produced by edge-beveling. Consider a vertex, $\mathbf{P}_i^k$, of a level k polyhedron that we will assume is valence three. It has three faces adjacent to it that lie in planes, $\mathcal{P}_{i,0}^k$, $\mathcal{P}_{i,1}^k$, and $\mathcal{P}_{i,2}^k$. Plane $\mathcal{P}_{i,j}^k$ is tangent to the sphere at point $\mathbf{C}_{i,j}^k$. Edges emanating from $\mathbf{P}_i^k$ lie in the lines of intersection between adjacent planes. Edge $\mathbf{e}_{i,j}^k$

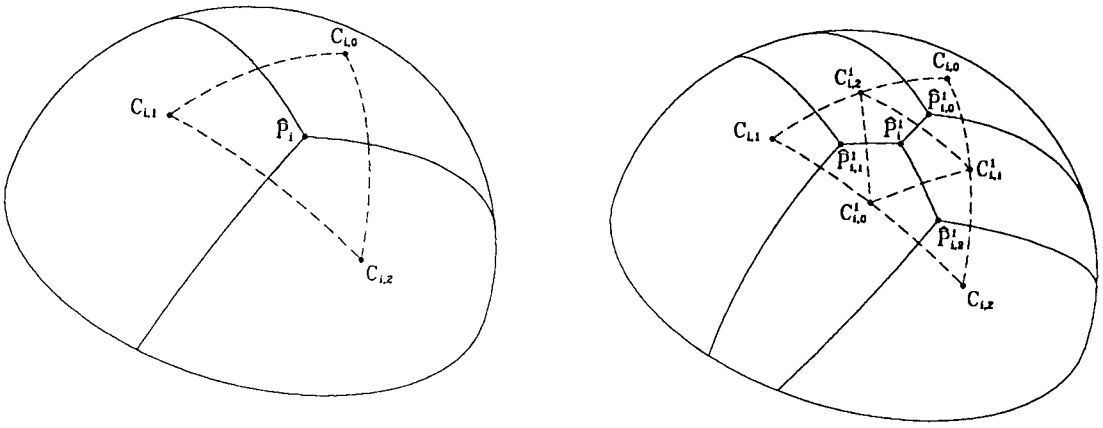

Figure 4.27: New Tessellation

will lie in line $\mathbf{L}^k_{i,j}$ where

$$\mathbf{L}^k_{i,j} = \mathcal{P}^k_{i,j+1} \cap \mathcal{P}^k_{i,j+2}$$

Edges $\mathbf{e}^k_{i,j}$, $j = 0, 1, 2$, will be replaced by faces that lie in planes $\mathcal{P}^{k+1}_{i,j}$. These new level $k+1$ planes are tangent to the inscribed sphere at the midpoint of the geodesics from $\mathbf{C}^k_{i,j}$ to $\mathbf{C}^k_{i,j+1}$, $\mathbf{C}^k_{i,j}\widehat{\mathbf{C}^k_{i,j+1}}$, $j = 0, 1, 2$. [3]

Triangle Subdivision

Now, consider the corresponding tessellation to this polyhedron. When we edge-bevel the polyhedron by inserting new tangent points at the midpoints of $\mathbf{C}^k_{i,j}\widehat{\mathbf{C}^k_{i,j+1}}$, $j = 0, 1, 2$, the corresponding tessellation will also have three new data points that coincide with these tangent points. These new data points will lie at the midpoints of the sides of triangle $\triangle^k_i$. When referring to the tessellation, we will call the process of inserting new data points at the midpoints of existing triangle sides *triangle subdivision.* We will break existing triangles, $\triangle^k_i$, into four smaller triangles, $\triangle^{k+1}_i$, $\triangle^{k+1}_{i,0}$, $\triangle^{k+1}_{i,1}$, and $\triangle^{k+1}_{i,2}$, (see Figure 4.26) and produce new tessellations of the sphere with projected vertices, $\hat{\mathbf{P}}^{k+1}_i$, $\hat{\mathbf{P}}^{k+1}_{i,0}$, $\hat{\mathbf{P}}^{k+1}_{i,1}$, and $\hat{\mathbf{P}}^{k+1}_{i,2}$, that replace $\hat{\mathbf{P}}^k_i$ (see Figure 4.27). If we begin with the cube, apply the edge-beveling algorithm k times, and then find the corresponding tessellation, we generate the same tessellation we would if we began with the tessellation that corresponds to the cube and applied triangle

[3] j modulo three

subdivision k times. We will refer to the triangles $\triangle_{i,j}^{k+1}$ as the *children* of $\triangle_i^k$. Likewise, projected vertices of the tessellation, $\hat{\mathbf{P}}_{i,j}^{k+1}$, are the children of $\hat{\mathbf{P}}_i^k$. Given a level k acute tessellation, we would like to be able to state that the level $k+1$ tessellation is acute also.

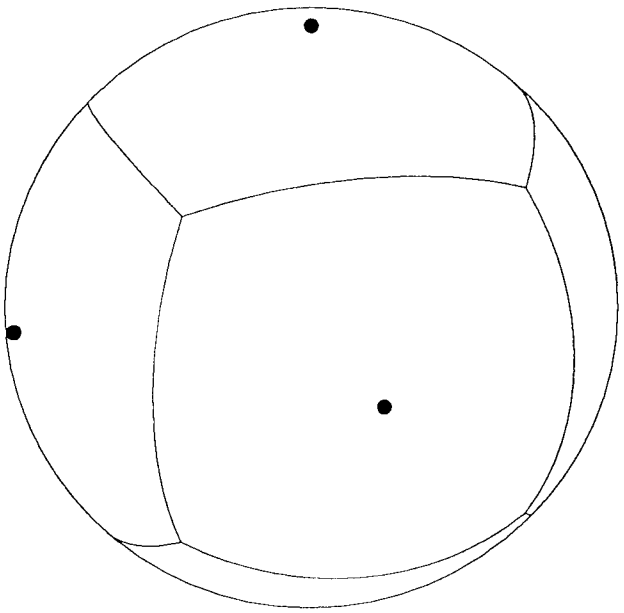

Figure 4.28: Projection of the Cube onto the Sphere

We begin with the cube whose faces are tangent to the inscribed sphere at their centroids (Figure 4.28). Therefore, triangles of the tessellation that corresponds to the cube are octants of the sphere. Clearly, as polyhedra are produced by edge-beveling, we will never have corresponding tessellations with triangles larger than an octant. An octant triangle is acute so we may say that it is Type I, and the tessellation that corresponds to the cube is an acute tessellation. We will show that when the octants are repeatedly subdivided,

the resulting tessellations are also acute tessellations. From this we may conclude that the corresponding polyhedra are valence three. To this end we will show that, the child triangles obtained by applying triangle subdivision to an octant are acute.

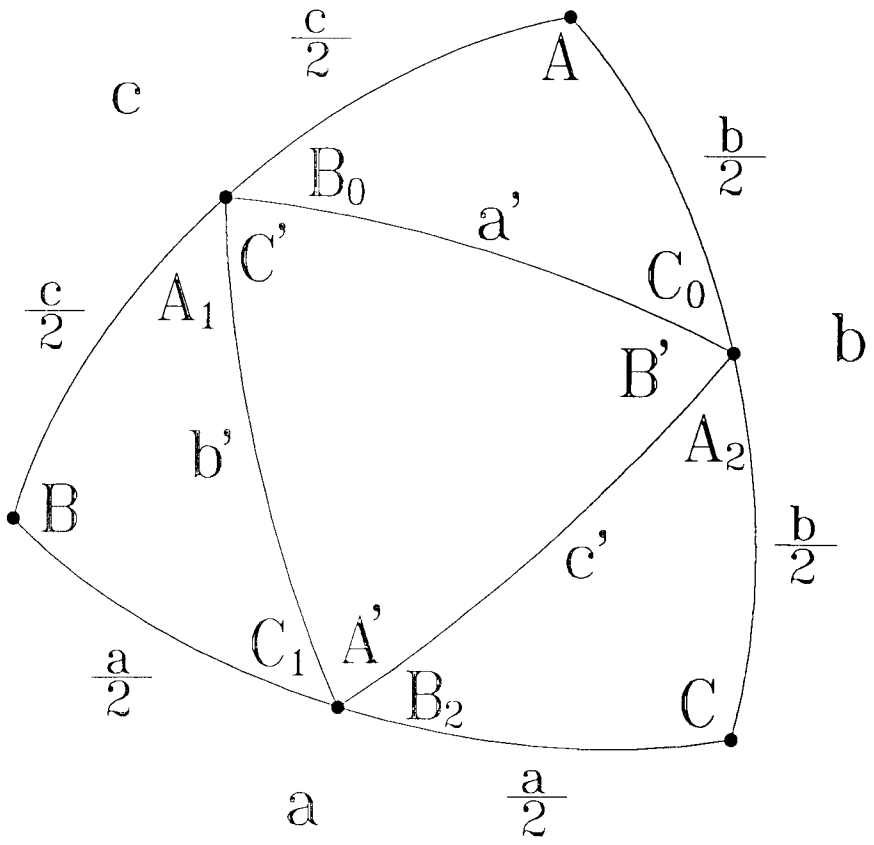

Figure 4.29: Simplified Labeling

First, we will introduce a simplified labeling for an octant of the sphere (Figure 4.29). Here, upper case letters represent hour angles and lower case represent arc angles. Beginning with the octant, we may say

$$\frac{\pi}{2} = A = B = C = a = b = c$$
$$\frac{\pi}{4} = \frac{a}{2} = \frac{b}{2} = \frac{c}{2}$$

Rearranging equation 4.2 we may solve for $\mathbf{a}'$

$$\begin{aligned} \cos \mathbf{a}' &= \cos \frac{\mathbf{b}}{2} \cos \frac{\mathbf{c}}{2} + \sin \frac{\mathbf{b}}{2} \sin \frac{\mathbf{c}}{2} \cos \mathbf{A} \\ &= \frac{1}{2} \end{aligned}$$

Similarly

$$\frac{1}{2} = \cos \mathbf{b}' = \cos \mathbf{c}'$$

Solving for $\cos \mathbf{A}'$ we get

$$\cos \mathbf{A}' = \frac{\cos \mathbf{a}' - \cos \mathbf{b}' \cos \mathbf{c}'}{\sin \mathbf{b}' \sin \mathbf{c}'} = \frac{1}{3}$$

So we may say

$$\approx 1.230959 = \mathbf{A}' = \mathbf{B}' = \mathbf{C}'$$

We find $\cos \mathbf{B}_0$ to be

$$\cos \mathbf{B}_0 = \frac{\cos \frac{\mathbf{b}}{2} - \cos \frac{\mathbf{c}}{2} \cos \mathbf{a}'}{\sin \frac{\mathbf{c}}{2} \sin \mathbf{a}'} = \frac{\sqrt{3}}{3}$$

Which leads to

$$\approx .955317 = \mathbf{B}_0 = \mathbf{C}_0 = \mathbf{A}_1 = \mathbf{C}_1 = \mathbf{B}_2 = \mathbf{A}_2$$

After one subdivision, all hour angles are less than or equal to $\frac{\pi}{2}$; the triangles are acute. Therefore, we may conclude that the corresponding polyhedron is valence three and each of the original vertices has been replaced by four new ones. That is, we started with the eight vertices of the cube and now have twenty-four.

Now consider a triangle, $\triangle_i^k$, chosen from among those obtained by applying triangle subdivision to the octant and then to the resulting children for a total of k subdivisions. Labeling $\triangle_i^k$ as above we may say

$$\begin{aligned} \frac{\pi}{2} &\geq \mathbf{a}, \mathbf{b}, \mathbf{c} > 0 \\ 0 &\leq \cos \mathbf{a}, \cos \mathbf{b}, \cos \mathbf{c} < 1 \\ \frac{\pi}{2} &> \frac{\mathbf{a}}{2}, \frac{\mathbf{b}}{2}, \frac{\mathbf{c}}{2} > 0 \\ 0 &< \cos \frac{\mathbf{a}}{2}, \cos \frac{\mathbf{b}}{2}, \cos \frac{\mathbf{c}}{2} < 1 \end{aligned}$$

We will assume that $\triangle_i^k$ is an acute triangle, that is,

$$\begin{aligned} \frac{\pi}{2} &\geq \mathbf{A}, \mathbf{B}, \mathbf{C} > 0 \\ 0 &\leq \cos \mathbf{A}, \cos \mathbf{B}, \cos \mathbf{C} < 1 \end{aligned} \tag{4.4}$$

and will show that the children of $\triangle_i^k$ are acute by showing that the cosines of their hour angles are non-negative. Using inequality 4.3 and the assumed inequality 4.4, we may say the following

$$\cos \mathbf{a} \geq \cos \mathbf{b} \cos \mathbf{c} \tag{4.5}$$

$$\cos \mathbf{b} \geq \cos \mathbf{a} \cos \mathbf{c} \tag{4.6}$$

$$\begin{aligned} \cos \mathbf{c} &\geq \cos \mathbf{a} \cos \mathbf{b} \\ \cos \mathbf{a}' &\geq \cos \frac{\mathbf{b}}{2} \cos \frac{\mathbf{c}}{2} \\ \cos \mathbf{b}' &\geq \cos \frac{\mathbf{a}}{2} \cos \frac{\mathbf{c}}{2} \\ \cos \mathbf{c}' &\geq \cos \frac{\mathbf{a}}{2} \cos \frac{\mathbf{b}}{2} \end{aligned}$$

For $\cos \mathbf{A}$ we may say the following

$$\begin{aligned} \cos \mathbf{A} &= \frac{\cos \mathbf{a} - \cos \mathbf{b} \cos \mathbf{c}}{\sin \mathbf{b} \sin \mathbf{c}} \\ \cos \mathbf{A} &= \frac{\cos \mathbf{a}' - \cos \frac{\mathbf{b}}{2} \cos \frac{\mathbf{c}}{2}}{\sin \frac{\mathbf{b}}{2} \sin \frac{\mathbf{c}}{2}} \end{aligned}$$

So we may say

$$\begin{aligned} \frac{\cos \mathbf{a}' - \cos \frac{\mathbf{b}}{2} \cos \frac{\mathbf{c}}{2}}{\sin \frac{\mathbf{b}}{2} \sin \frac{\mathbf{c}}{2}} &= \frac{\cos \mathbf{a} - \cos \mathbf{b} \cos \mathbf{c}}{\sin \mathbf{b} \sin \mathbf{c}} \\ \frac{\cos \mathbf{a}' - \cos \frac{\mathbf{b}}{2} \cos \frac{\mathbf{c}}{2}}{\sin \frac{\mathbf{b}}{2} \sin \frac{\mathbf{c}}{2}} &= \frac{\left(2 \cos^2 \frac{\mathbf{a}}{2} - 1\right) - \left(2 \cos^2 \frac{\mathbf{b}}{2} - 1\right) \left(2 \cos^2 \frac{\mathbf{c}}{2} - 1\right)}{\left(2 \cos \frac{\mathbf{b}}{2} \sin \frac{\mathbf{b}}{2}\right) \left(2 \cos \frac{\mathbf{c}}{2} \sin \frac{\mathbf{c}}{2}\right)} \\ \frac{\cos \mathbf{a}' - \cos \frac{\mathbf{b}}{2} \cos \frac{\mathbf{c}}{2}}{\sin \frac{\mathbf{b}}{2} \sin \frac{\mathbf{c}}{2}} &= \frac{\left(2 \cos^2 \frac{\mathbf{a}}{2} - 1\right) - \left(4 \cos^2 \frac{\mathbf{b}}{2} \cos^2 \frac{\mathbf{c}}{2} - 2 \cos^2 \frac{\mathbf{b}}{2} - 2 \cos^2 \frac{\mathbf{c}}{2} + 1\right)}{4 \cos \frac{\mathbf{b}}{2} \sin \frac{\mathbf{b}}{2} \cos \frac{\mathbf{c}}{2} \sin \frac{\mathbf{c}}{2}} \\ \cos \mathbf{a}' - \cos \frac{\mathbf{b}}{2} \cos \frac{\mathbf{c}}{2} &= \frac{\left(2 \cos^2 \frac{\mathbf{a}}{2} - 1\right) - \left(4 \cos^2 \frac{\mathbf{b}}{2} \cos^2 \frac{\mathbf{c}}{2} - 2 \cos^2 \frac{\mathbf{b}}{2} - 2 \cos^2 \frac{\mathbf{c}}{2} + 1\right)}{4 \cos \frac{\mathbf{b}}{2} \cos \frac{\mathbf{c}}{2}} \\ \cos \mathbf{a}' - \cos \frac{\mathbf{b}}{2} \cos \frac{\mathbf{c}}{2} &= \frac{2 \cos^2 \frac{\mathbf{a}}{2} + 2 \cos^2 \frac{\mathbf{b}}{2} + 2 \cos^2 \frac{\mathbf{c}}{2} - 2}{4 \cos \frac{\mathbf{b}}{2} \cos \frac{\mathbf{c}}{2}} - \frac{4 \cos^2 \frac{\mathbf{b}}{2} \cos^2 \frac{\mathbf{c}}{2}}{4 \cos \frac{\mathbf{b}}{2} \cos \frac{\mathbf{c}}{2}} \end{aligned}$$

$$\cos \mathbf{a}' - \cos \frac{\mathbf{b}}{2} \cos \frac{\mathbf{c}}{2} = \frac{\cos^2 \frac{\mathbf{a}}{2} + \cos^2 \frac{\mathbf{b}}{2} + \cos^2 \frac{\mathbf{c}}{2} - 1}{2 \cos \frac{\mathbf{b}}{2} \cos \frac{\mathbf{c}}{2}} - \cos \frac{\mathbf{b}}{2} \cos \frac{\mathbf{c}}{2}$$

$$\cos \mathbf{a}' = \frac{\cos^2 \frac{\mathbf{a}}{2} + \cos^2 \frac{\mathbf{b}}{2} + \cos^2 \frac{\mathbf{c}}{2} - 1}{2 \cos \frac{\mathbf{b}}{2} \cos \frac{\mathbf{c}}{2}}$$

Similarly we have

$$\cos \mathbf{b}' = \frac{\cos^2 \frac{\mathbf{a}}{2} + \cos^2 \frac{\mathbf{b}}{2} + \cos^2 \frac{\mathbf{c}}{2} - 1}{2 \cos \frac{\mathbf{a}}{2} \cos \frac{\mathbf{c}}{2}}$$

$$\cos \mathbf{c}' = \frac{\cos^2 \frac{\mathbf{a}}{2} + \cos^2 \frac{\mathbf{b}}{2} + \cos^2 \frac{\mathbf{c}}{2} - 1}{2 \cos \frac{\mathbf{a}}{2} \cos \frac{\mathbf{b}}{2}}$$

Now we will consider $\cos \mathrm{B}_0$

$$\cos \mathrm{B}_0 = \frac{\cos \frac{\mathbf{b}}{2} - \cos \frac{\mathbf{c}}{2} \cos \mathbf{a}'}{\sin \frac{\mathbf{c}}{2} \sin \mathbf{a}'}$$

As noted in inequality 4.3, we can show that $\mathrm{B}_0 \leq \frac{\pi}{2}$ by showing

$$\begin{aligned}
\cos \frac{\mathbf{b}}{2} &\geq \cos \frac{\mathbf{c}}{2} \cos \mathbf{a}' \\
\cos \frac{\mathbf{b}}{2} &\geq \cos \frac{\mathbf{c}}{2} \left(\frac{\cos^2 \frac{\mathbf{a}}{2} + \cos^2 \frac{\mathbf{b}}{2} + \cos^2 \frac{\mathbf{c}}{2} - 1}{2 \cos \frac{\mathbf{b}}{2} \cos \frac{\mathbf{c}}{2}} \right) \\
\cos \frac{\mathbf{b}}{2} &\geq \frac{\cos^2 \frac{\mathbf{a}}{2} + \cos^2 \frac{\mathbf{b}}{2} + \cos^2 \frac{\mathbf{c}}{2} - 1}{2 \cos \frac{\mathbf{b}}{2}} \\
2 \cos^2 \frac{\mathbf{b}}{2} &\geq \cos^2 \frac{\mathbf{a}}{2} + \cos^2 \frac{\mathbf{b}}{2} + \cos^2 \frac{\mathbf{c}}{2} - 1 \\
\cos^2 \frac{\mathbf{b}}{2} &\geq \cos^2 \frac{\mathbf{a}}{2} + \cos^2 \frac{\mathbf{c}}{2} - 1 \\
\frac{1 + \cos \mathbf{b}}{2} &\geq \frac{1 + \cos \mathbf{a}}{2} + \frac{1 + \cos \mathbf{c}}{2} - 1 \\
1 + \cos \mathbf{b} &\geq 1 + \cos \mathbf{a} + 1 + \cos \mathbf{c} - 2 \\
1 + \cos \mathbf{b} &\geq \cos \mathbf{a} + \cos \mathbf{c}
\end{aligned}$$

From inequality 4.6 we may say $1 + \cos \mathbf{b} \geq 1 + \cos \mathbf{a} \cos \mathbf{c}$.
So, if we can show $1 + \cos \mathbf{a} \cos \mathbf{c} \geq \cos \mathbf{a} + \cos \mathbf{c}$,
we may conclude $1 + \cos \mathbf{b} \geq \cos \mathbf{a} + \cos \mathbf{c}$.

$$\begin{aligned}
1 + \cos \mathbf{a} \cos \mathbf{c} &\geq \cos \mathbf{a} + \cos \mathbf{c} \\
1 &\geq \cos \mathbf{a} + \cos \mathbf{c} - \cos \mathbf{a} \cos \mathbf{c} \\
1 &\geq \cos \mathbf{a} + \cos \mathbf{c} (1 - \cos \mathbf{a})
\end{aligned}$$

Since we have shown $0 \leq \cos \mathbf{a} < 1$ and $0 \leq \cos \mathbf{c} < 1$, we may say

$$1 \geq \cos \mathbf{a} + \cos \mathbf{c} \, (1 - \cos \mathbf{a})$$

Therefore, we may conclude

$$\begin{aligned} \cos \frac{\mathbf{b}}{2} &\geq \cos \frac{\mathbf{c}}{2} \cos \mathbf{a}' \\ \cos \mathrm{B}_0 &\geq 0 \\ \mathrm{B}_0 &\leq \tfrac{\pi}{2} \end{aligned}$$

Similarly, we may say

$$\frac{\pi}{2} \geq \mathrm{B}_0, \mathrm{C}_0, \mathrm{A}_1, \mathrm{C}_1, \mathrm{A}_2, \mathrm{B}_2$$

Turning to $\cos \mathbf{A}'$, we may say

$$\cos \mathrm{A}' = \frac{\cos \mathbf{a}' - \cos \mathbf{b}' \cos \mathbf{c}'}{\sin \mathbf{b}' \sin \mathbf{c}'}$$

Therefore,

$$\cos \mathbf{a}' \geq \cos \mathbf{b}' \cos \mathbf{c}' \Leftrightarrow \cos \mathbf{A}' \geq 0$$

$$\begin{aligned} \frac{\cos^2 \frac{\mathbf{a}}{2} + \cos^2 \frac{\mathbf{b}}{2} + \cos^2 \frac{\mathbf{c}}{2} - 1}{2 \cos \frac{\mathbf{b}}{2} \cos \frac{\mathbf{c}}{2}} &\geq \left(\frac{\cos^2 \frac{\mathbf{a}}{2} + \cos^2 \frac{\mathbf{b}}{2} + \cos^2 \frac{\mathbf{c}}{2} - 1}{2 \cos \frac{\mathbf{a}}{2} \cos \frac{\mathbf{c}}{2}} \right) \\ &\quad \left(\frac{\cos^2 \frac{\mathbf{a}}{2} + \cos^2 \frac{\mathbf{b}}{2} + \cos^2 \frac{\mathbf{c}}{2} - 1}{2 \cos \frac{\mathbf{a}}{2} \cos \frac{\mathbf{b}}{2}} \right) \\ \frac{\cos^2 \frac{\mathbf{a}}{2} + \cos^2 \frac{\mathbf{b}}{2} + \cos^2 \frac{\mathbf{c}}{2} - 1}{2 \cos \frac{\mathbf{b}}{2} \cos \frac{\mathbf{c}}{2}} &\geq \frac{\left(\cos^2 \frac{\mathbf{a}}{2} + \cos^2 \frac{\mathbf{b}}{2} + \cos^2 \frac{\mathbf{c}}{2} - 1 \right)^2}{4 \cos^2 \frac{\mathbf{a}}{2} \cos \frac{\mathbf{b}}{2} \cos \frac{\mathbf{c}}{2}} \\ \cos^2 \frac{\mathbf{a}}{2} + \cos^2 \frac{\mathbf{b}}{2} + \cos^2 \frac{\mathbf{c}}{2} - 1 &\geq \frac{\left(\cos^2 \frac{\mathbf{a}}{2} + \cos^2 \frac{\mathbf{b}}{2} + \cos^2 \frac{\mathbf{c}}{2} - 1 \right)^2}{2 \cos^2 \frac{\mathbf{a}}{2}} \\ 1 &\geq \frac{\cos^2 \frac{\mathbf{a}}{2} + \cos^2 \frac{\mathbf{b}}{2} + \cos^2 \frac{\mathbf{c}}{2} - 1}{2 \cos^2 \frac{\mathbf{a}}{2}} \\ 2 \cos^2 \frac{\mathbf{a}}{2} &\geq \cos^2 \frac{\mathbf{a}}{2} + \cos^2 \frac{\mathbf{b}}{2} + \cos^2 \frac{\mathbf{c}}{2} - 1 \\ \cos^2 \frac{\mathbf{a}}{2} &\geq \cos^2 \frac{\mathbf{b}}{2} + \cos^2 \frac{\mathbf{c}}{2} - 1 \\ \frac{1 + \cos \mathbf{a}}{2} &\geq \frac{1 + \cos \mathbf{b}}{2} + \frac{1 + \cos \mathbf{c}}{2} - 1 \\ 1 + \cos \mathbf{a} &\geq 1 + \cos \mathbf{b} + 1 + \cos \mathbf{c} - 2 \\ 1 + \cos \mathbf{a} &\geq \cos \mathbf{b} + \cos \mathbf{c} \end{aligned}$$

From inequality 4.5 we may say $1 + \cos \mathbf{a} \geq 1 + \cos \mathbf{b} \cos \mathbf{c}$.
So, if we can show $1 + \cos \mathbf{b} \cos \mathbf{c} \geq \cos \mathbf{b} + \cos \mathbf{c}$,
we may conclude $1 + \cos \mathbf{a} \geq \cos \mathbf{b} + \cos \mathbf{c}$.

$$\begin{aligned} 1 + \cos \mathbf{b} \cos \mathbf{c} &\geq \cos \mathbf{b} + \cos \mathbf{c} \\ 1 &\geq \cos \mathbf{b} + \cos \mathbf{c} - \cos \mathbf{b} \cos \mathbf{c} \\ 1 &\geq \cos \mathbf{b} + \cos \mathbf{c} (1 - \cos \mathbf{b}) \end{aligned}$$

Since we have shown $0 \leq \cos \mathbf{b} < 1$ and $0 \leq \cos \mathbf{c} < 1$, we may say

$$1 \geq \cos \mathbf{b} + \cos \mathbf{c} (1 - \cos \mathbf{b})$$

Therefore, we may conclude

$$\begin{aligned} \cos \mathbf{a}' &\geq \cos \mathbf{b}' \cos \mathbf{c}' \\ \cos \mathbf{A}' &\geq 0 \\ \mathbf{A}' &\leq \tfrac{\pi}{2} \end{aligned}$$

Similarly, we may say

$$\frac{\pi}{2} \geq \mathrm{B}', \mathrm{C}'$$

Therefore, we may conclude that any triangle obtained from repeatedly applying triangle subdivision to the octant and its children will be acute. Suppose we have a tessellation of the surface of the sphere that has been generated by applying triangle subdivision to the octants of the sphere and repeatedly to the resulting child triangles. Since each of these triangles is acute we may say that it is Type I and conclude that the tessellation is an acute tessellation. Additionally, we may conclude that the polyhedron that corresponds to this tessellation is valence three.

4.3.4 The Edge-Beveling Algorithm

Using labeling similar to that used in Doo's algorithm, we describe edge-beveling as follows. We have Type **F** faces and differently defined Type **E** faces. Eliminating the Type **V** face, we replace it with a new vertex called the **Y**-point, along with the three face points from Doo's algorithm. The **Y**-point is at the intersection of the Type **E** faces that replace the edges adjacent to a vertex.

We use a different definition for the *centers* of our faces. A center is chosen so that it is the point at which the face is tangent to the inscribed sphere. For an original face we use the centroid of that face for our center, that is, for each of the cube's faces the center is

$$\mathbf{C}_i^0 = \frac{1}{4}\sum_{i=1}^{4}\mathbf{P}_i^0$$

As the object is refined, centers are calculated for new Type **E** faces, but Type **F** faces retain their center points; they are not recalculated at each new level. As we have described, the center of each new Type **E** face is the midpoint of the geodesic between the centers of the Type **F** faces adjacent to it.

Given a level k vertex, $\mathbf{P}_i^k$, and the center points, $\mathbf{C}_{i,j}^k$ and $\mathbf{C}_{i,j+1}^k$, of two of the adjacent Type **F** faces, we may calculate the midpoint of this geodesic. Assuming a sphere centered on the origin, we will calculate the normal vectors at center points $\mathbf{C}_{i,j}^k$ and $\mathbf{C}_{i,j+1}^k$. Since these points are tangent to the sphere, the normal vectors are

$$\begin{aligned}\vec{n}_{i,j}^k &= \frac{\left\langle \mathbf{C}_{i,j}^k \right\rangle}{\left| \left\langle \mathbf{C}_{i,j}^k \right\rangle \right|} \\ \vec{n}_{i,j+1}^k &= \frac{\left\langle \mathbf{C}_{i,j+1}^k \right\rangle}{\left| \left\langle \mathbf{C}_{i,j+1}^k \right\rangle \right|}\end{aligned}$$

We note that $\left| \left\langle \mathbf{C}_{i,j}^k \right\rangle \right|$ is the radius of the sphere.
Let $\mathbf{P}_{p(i,j)}^k$ be the point on $\overline{\mathbf{P}_i^k\mathbf{P}_{i+2}^k}$ that is the common perpendicular to $\mathbf{C}_{i,j}^k$ and $\mathbf{C}_{i,j+1}^l$. As shown above, this is also the closest point on $\overline{\mathbf{P}_i^k\mathbf{P}_{i+2}^k}$ to $\frac{1}{2}\left(\mathbf{C}_{i,j}^k + \mathbf{C}_{i,j+1}^k\right)$. Then the new center point, $\mathbf{C}_{i,j+2}^{k+1}$, is

$$\mathbf{C}_{i,j+2}^{k+1} = (1-t_k)\,\mathbf{P}_{p(i,j)}^k + t_k\left[\frac{1}{2}\left(\mathbf{C}_{i,j}^k + \mathbf{C}_{i,j+1}^k\right)\right]$$

where

$$t_k = \frac{1}{1+\cos(\theta_k)}$$
$$\theta_k = \frac{\pi - \cos^{-1}\left(\vec{n}^k_{i,j} \cdot \vec{n}^k_{i,j+1}\right)}{2}$$

A new Type **E** face lies in the plane that is tangent to the inscribed sphere at $\mathbf{C}^{k+1}_{i+2}$. Therefore, the normal vector, $\vec{n}$, of this plane is

$$\vec{n} = \frac{\left\langle \mathbf{C}^{k+1}_{i+2} \right\rangle}{\left| \left\langle \mathbf{C}^{k+1}_{i+2} \right\rangle \right|}$$

With this point and vector we have defined the plane in which this face lies. Each vertex is replaced by a **Y**-point and three new face points. Since all vertices remain valence three, each vertex will have three new Type **E** faces that replace the edges incident to it. When we have defined the planes in which these three new Type **E** faces lie, we may calculate this vertex's **Y**-point along with the three face points that replace the vertex.

Following the development in section 4.2, we will consider a cube with side length 2 and vertices $(\pm 1, \pm 1, \pm 1)$ (Figure 4.30). Each of the cube's faces lies in a plane that is tangent to the inscribed unit sphere centered on the origin. As the cube is refined, all new faces continue to be tangent to the unit sphere (see Figure 4.5).

Again, consider vertices

$$\mathbf{P}_0 = (1,1,1)$$
$$\mathbf{P}_{0,0} = (-1,1,1)$$
$$\mathbf{P}_{0,1} = (1,-1,1)$$
$$\mathbf{P}_{0,2} = (1,1,-1)$$

along with the adjacent tangent planes

$$\mathcal{P}_{0,0} = (\mathbf{C}_{0,0}, \vec{n}_{0,0})$$
$$\mathcal{P}_{0,1} = (\mathbf{C}_{0,1}, \vec{n}_{0,1})$$
$$\mathcal{P}_{0,2} = (\mathbf{C}_{0,2}, \vec{n}_{0,2})$$

where the points at which the planes are tangent to the sphere are

$$\begin{aligned} \mathbf{C}_{0,0} &= (1,0,0) \\ \mathbf{C}_{0,1} &= (0,1,0) \\ \mathbf{C}_{0,2} &= (0,0,1) \end{aligned}$$

with normal vectors

$$\begin{aligned} \vec{n}_{0,0} &= \langle 1,0,0 \rangle \\ \vec{n}_{0,1} &= \langle 0,1,0 \rangle \\ \vec{n}_{0,2} &= \langle 0,0,1 \rangle \end{aligned}$$

The three edges adjacent to $\mathbf{P}_0$ are replaced with new Type **E** faces that lie in planes

$$\begin{aligned} \mathcal{P}^1_{0,0} &= \left(\mathbf{C}^1_{0,0}, \vec{n}^1_{0,0}\right) \\ \mathcal{P}^1_{0,1} &= \left(\mathbf{C}^1_{0,1}, \vec{n}^1_{0,1}\right) \\ \mathcal{P}^1_{0,2} &= \left(\mathbf{C}^1_{0,2}, \vec{n}^1_{0,2}\right) \end{aligned}$$

where

$$\begin{aligned} \mathbf{C}^1_{0,0} &= \left(0, \frac{\sqrt{2}}{2}, \frac{\sqrt{2}}{2}\right) \\ \mathbf{C}^1_{0,1} &= \left(\frac{\sqrt{2}}{2}, 0, \frac{\sqrt{2}}{2}\right) \\ \mathbf{C}^1_{0,2} &= \left(\frac{\sqrt{2}}{2}, \frac{\sqrt{2}}{2}, 0\right) \end{aligned}$$

are the centers of the faces and

$$\begin{aligned} \vec{n}^1_{0,0} &= \left\langle 0, \frac{\sqrt{2}}{2}, \frac{\sqrt{2}}{2} \right\rangle \\ \vec{n}^1_{0,1} &= \left\langle \frac{\sqrt{2}}{2}, 0, \frac{\sqrt{2}}{2} \right\rangle \\ \vec{n}^1_{0,2} &= \left\langle \frac{\sqrt{2}}{2}, \frac{\sqrt{2}}{2}, 0 \right\rangle \end{aligned}$$

are the normal vectors of the planes. We can calculate the **Y**-point and three face points by intersecting these planes.

$$\mathbf{Y}^1_0 = \mathcal{P}^1_{0,0} \cap \mathcal{P}^1_{0,1} \cap \mathcal{P}^1_{0,2}$$

$$
\begin{aligned}
&= \left(\frac{\sqrt{2}}{2}, \frac{\sqrt{2}}{2}, \frac{\sqrt{2}}{2}\right) \\
\mathbf{P}^1_{0,0} &= \mathcal{P}_{0,0} \cap \mathcal{P}^1_{0,1} \cap \mathcal{P}^1_{0,2} \\
&= \left(1, \sqrt{2}-1, \sqrt{2}-1\right) \\
\mathbf{P}^1_{0,1} &= \mathcal{P}_{0,1} \cap \mathcal{P}^1_{0,0} \cap \mathcal{P}^1_{0,2} \\
&= \left(\sqrt{2}-1, 1, \sqrt{2}-1\right) \\
\mathbf{P}^1_{0,2} &= \mathcal{P}_{0,1} \cap \mathcal{P}^1_{0,0} \cap \mathcal{P}^1_{0,1} \\
&= \left(\sqrt{2}-1, \sqrt{2}-1, 1\right)
\end{aligned}
$$

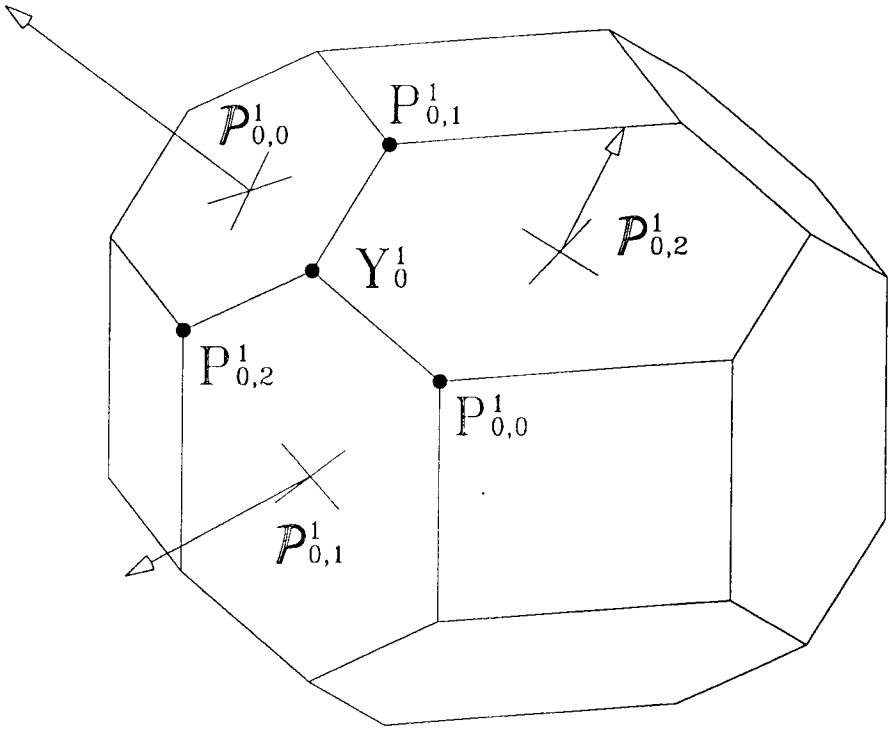

Figure 4.30: Y-Point with Three New Face Points

In general, then, given a vertex on the control polyhedron, $\mathbf{P}^k_i$, and the planes around

it, $\mathcal{P}^k_{i,0}\left(\mathbf{C}^k_{i,0}, \vec{n}^k_{i,0}\right)$, $\mathcal{P}^k_{i,1}\left(\mathbf{C}^k_{i,1}, \vec{n}^k_{i,1}\right)$, and $\mathcal{P}^k_{i,2}\left(\mathbf{C}^k_{i,2}, \vec{n}^k_{i,2}\right)$, we may calculate the new **Y**-point, $\mathbf{Y}^{k+1}_i$, and three new face points, $\mathbf{P}^{k+1}_{i,j}$, that replace $\mathbf{P}^k_i$. [4]

$$\begin{aligned}
\mathbf{Y}^{k+1}_i &= \mathcal{P}^{k+1}_{i,1} \cap \mathcal{P}^{k+1}_{i,2} \cap \mathcal{P}^{k+1}_{i,3} \\
\mathbf{P}^{k+1}_{i,j} &= \mathcal{P}^{k}_{i,j} \cap \mathcal{P}^{k+1}_{i,j+1} \cap \mathcal{P}^{k+1}_{i,j+2} \\
\mathcal{P}^{k+1}_{i,j} &= \left(\mathbf{C}^{k+1}_{i,j}, \vec{n}^{k+1}_{i,j}\right)
\end{aligned}$$

where

$$\begin{aligned}
\mathbf{C}^{k+1}_{i,j} &= (1-t_k)\,\mathbf{P}^k_{p(i,j)} + t_k\left[\frac{1}{2}\left(\mathbf{C}^k_{i,j+1} + \mathbf{C}^k_{i,j+2}\right)\right] \\
t_k &= \frac{1}{1+\cos\theta_k} \\
\theta_k &= \frac{\pi - \cos^{-1}\left(\vec{n}^k_{i,j+1} \cdot \vec{n}^k_{i,j+2}\right)}{2} \\
\mathbf{P}^k_{p(i,j)} &= \mathbf{P}^k_i + \frac{\left\langle \mathbf{P}^k_{i,j} - \mathbf{P}^k_i \right\rangle \cdot \left\langle \frac{1}{2}\left(\mathbf{C}^k_{i,j+1} + \mathbf{C}^k_{i,j+2}\right) - \mathbf{P}^k_i \right\rangle}{\left|\overline{\mathbf{P}^k_{i,j}\mathbf{P}^k_i}\right| \left|\overline{\frac{1}{2}\left(\mathbf{C}^k_{i,j+1} + \mathbf{C}^k_{i,j+2}\right)\mathbf{P}_i}\right|} \left\langle \mathbf{P}^k_{i,j} - \mathbf{P}^k_i \right\rangle
\end{aligned}$$

and

$$\vec{n}^{k+1}_{i,j} = \frac{\left\langle \mathbf{C}^{k+1}_{i,j} \right\rangle}{\left|\left\langle \mathbf{C}^{k+1}_{i,j} \right\rangle\right|}$$

4.4 Ellipsoids

Following the discussion of ellipses in 3.4, we will consider an ellipsoid centered on the origin with its axes aligned with the axes of the coordinate system

$$\frac{x^2}{A^2} + \frac{y^2}{B^2} + \frac{z^2}{C^2} = 1$$

This ellipsoid may be obtained by taking every point, $\mathbf{P}_s(x,y,z)$, on the unit sphere and scaling it to a point on the ellipsoid, $\mathbf{P}_e(xA, yB, zC)$.

In the same manner, we may begin with the cube $(\pm1, \pm1, \pm1)$ and scale it into the rectangular prism $(\pm A, \pm B, \pm C)$. Using the method in section 4.3.4, we may generate a piecewise planar model of the sphere and scale it to a piecewise planar model of the ellipsoid such that every face of the model lies in a plane that is tangent to the ellipsoid at the face's center (Figures 4.31 and 4.32).

[4] subscript j modulo 3

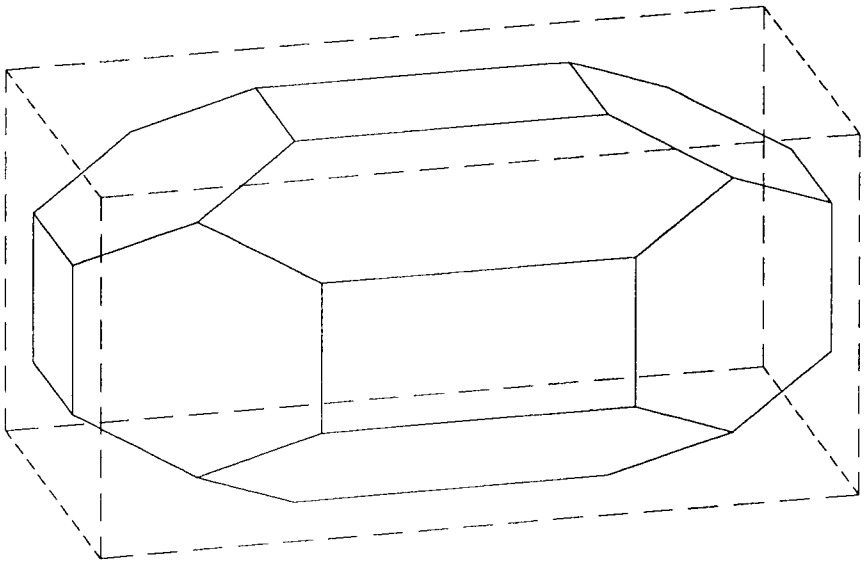

Figure 4.31: Rectangular Prism after First Refinement

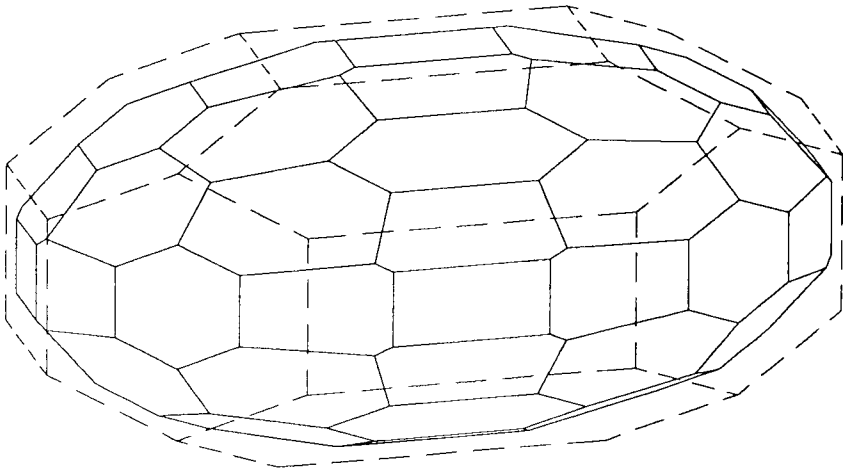

Figure 4.32: Rectangular Prism after Second Refinement

Chapter 5

Conclusions

In this paper, we have presented an algorithm for producing piecewise planar approximations of a sphere. Beginning with a cube, we have produced arbitrarily close approximations of its inscribed sphere by repeatedly bevel-cutting edges. We have shown how this method may generate piecewise planar models for ellipsoids and spheres that are arbitrarily smooth. We have discussed a simple procedure to construct an arbitrarily close piecewise linear approximation of a circle and have adapted this procedure to Chaikin's algorithm. Using this modification of Chaikin's algorithm, we have, in the limit, produced piecewise elliptical curves.

We may measure the smoothness of our models by comparing the angle (ϕ) between adjacent faces, noting that $\phi \rightarrow \pi$ as $k \rightarrow \infty$. It is not necessary to measure each angle in the model to see if it has the smallest ϕ in the model; this may always be found by following the worst case (smallest ϕ) from one refinement to the next. That is, the search for the smallest ϕ is linear. Given a heuristic that associates the prominence of an object in the scene with a minimally acceptable ϕ, we can calculate *a priori* the level of refinement that will contain an acceptable level of detail. Suppose we had a scene that contained several spheres and ellipsoids. We could calculate the minimum and maximum ϕ needed to produce acceptable levels of detail. Using this ϕ, we could calculate the minimum and maximum levels of refinement required. Starting with the unit sphere, we could pre-generate and store models at the levels in this range. When a sphere of radius r with a required level of detail k was needed, we could translate and scale the unit sphere model at level k. For ellipsoids we would first scale the unit sphere along each of its three axes separately, using the A, B,

and C for this ellipsoid, then translate and rotate it into position in the scene.

5.1 Further Work

The model meshes we have used throughout chapter 4 have had a regular topology. We would like to extend this method to more arbitrary, if not completely arbitrary meshes. One problem that must be overcome concerns edges that over-cut neighboring faces. Consider the following level $k = 0$ model.

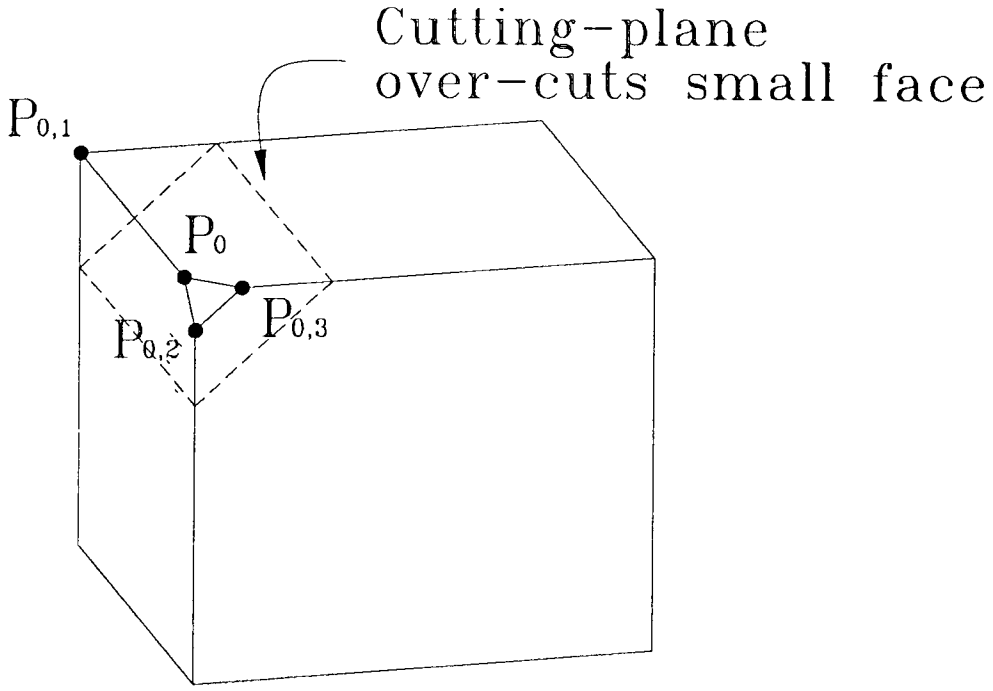

Figure 5.1: Over-cutting Small Face

Here we have a cube that has had one of its corners cut off slightly. Our method only considers the faces adjacent to an edge when deciding how deeply that edge is to be cut. If we cut off edge $\mathbf{e}_{0,1}$, we will completely remove the face formed by points $\mathbf{P}_0, \mathbf{P}_{0,2}, \mathbf{P}_{0,3}$.

The question remains, how will this be done? We have explored two approaches without success.

First, we could attempt to individualize the process to a vertex. The idea is to use only local information to calculate the new **Y**-point and the three new face points at each vertex. To do this, we would no longer retain the center points for each face but would calculate them on-the-fly for each vertex. In pursuing this approach, we noticed that the faces of the cube and all refinements of it had an interesting property. At any level of refinement of the spherical approximation, consider any edge along with its adjacent faces. They will have:

1. The centers of the faces equal distance from the edge.

2. The closest point on the edge to one of the centers is also the closest point on the edge to the other.

We found this property to be suggestive of two-dimensional Vorinori diagrams. Consider a valence-three vertex of a Vorinori diagram where we have the edges, but not the data points (*center points*) from which the tiles were generated. Using only the vertex and the three rays emanating from it, it is possible to calculate *center lines* on which the center points lie. By intersecting the lines from two vertices of the face we may find the tile's data or center point. We were able to adapt this method to our surface tiles and on the spherical model calculate the center points from the information available from the vertices only. However, it is unclear how we can apply this to less uniform models. For instance, the rectangular prism used to model an ellipsoid does not have property 1 above, and its center lines do not necessarily intersect at a unique point. With further research we may be able to find a satisfactory way to combine these differing center points into one center for the face.

Secondly, our algorithm also has the property that all new Type **E** faces are parallel to the edges they replace. We considered the possibility of relaxing this so that the cutting plane used to define this face would not necessarily be parallel to the edge. When we define a new center point for our new Type **E** face, we *blend* the center points of the two adjacent faces. Not only is the new center point at the midpoint of the geodesic from the two adjacent centers , as in section 4.4, but the normal vector at this point is a blend of the two normals. We have explored schemes to make the new center point and the normal at this point not only a combination of the two adjacent points but also the two center points of the faces at the end of the edge.

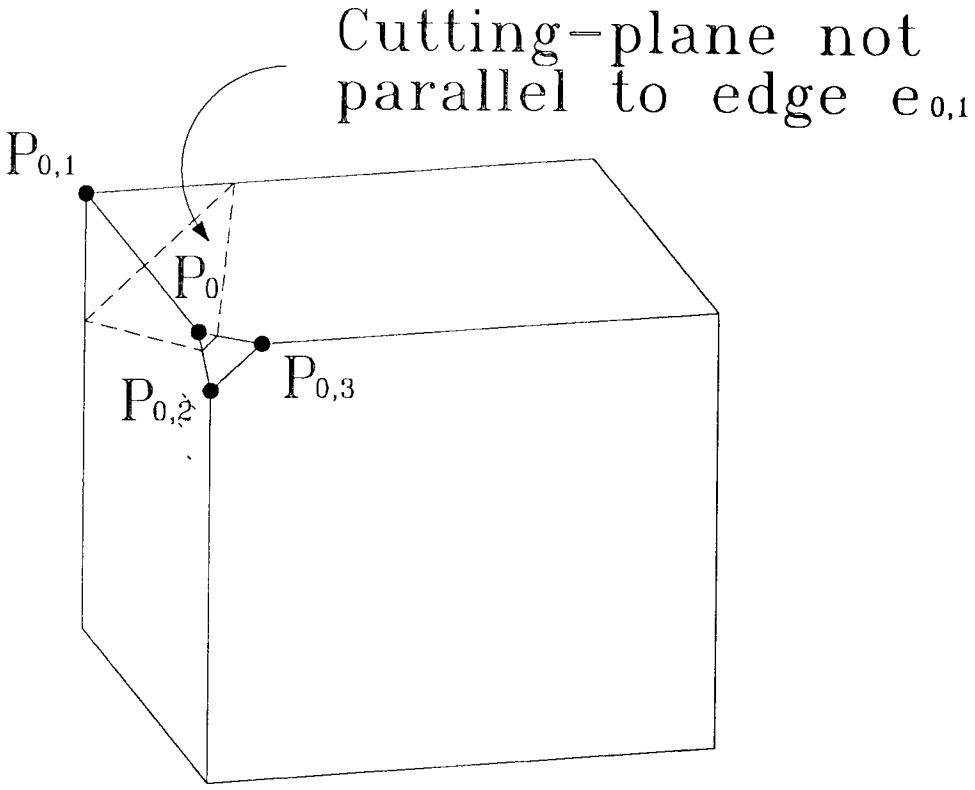

Figure 5.2: Non-parallel Cutting-plane

Bibliography

[1] E. Catmull and J. Clark. Recursively generated B-spline surfaces on arbitrary topological meshes. *Computer-Aided Design*, 10:350–355, September 1978.

[2] G. Chaikin. An algorithm for high speed curve generation. *Computer Graphics and Image Processing*, 3:346–349, 1974.

[3] James E. Cobb. Tiling the sphere with rational bézier patches. Technical Report, Computer Science, University of Utah, July 1988.

[4] C. de Boor. Cutting corners always works. *Computer Aided Geometric Design*, 4(1-2):125–131, 1987.

[5] D. Doo. A subdivision algorithm for smoothing down irregularly shaped polyhedrons. In *Proced. Int'l Conf. Ineractive Techniques in Computer Aided Design*, pages 157–165, 1978. Bologna, Italy, IEEE Computer Soc.

[6] D. Doo and M. Sabin. Behaviour of recursive division surfaces near extraordinary points. *Computer-Aided Design*, 10:356–360, September 1978.

[7] N. Dyn and D. Levin. The subdivision experience. In P. J. Laurent, A. Le Méhauté, and L. L. Schumaker, editors, *Curves and Surfaces II*, pages 0–17. A K Peters, Boston, 1991.

[8] Gerald Farin. *Curves and Surfaces for Computer Aided Geometric Design.* Academic Press, 1993.

[9] James D. Foley, Andries van Dam, Steven K. Fiener, and John F. Hughes. *Computer Graphics Principles and Practice.* Addison-Wesley, Reading, MA, 1990.

[10] Hugues Hoppe, Tony DeRose, Tom Duchamp, Mark Halstead, Hubert Jin, John McDonald, Jean Schweitzer, and Werner Stuetzle. Piecewise smooth surface reconstruction. In Andrew Glassner, editor, *Proceedings of SIGGRAPH '94 (Orlando, Florida, July 24–29, 1994)*, Computer Graphics Proceedings, Annual Conference Series, pages 295–302. ACM SIGGRAPH, ACM Press, July 1994. ISBN 0-89791-667-0.